PREPARATION AND CHARACTERIZATION OF NANOPARTICLES AS CARRIERS FOR GENE DELIVERY

A Thesis Submitted to
the Graduate School of Engineering and Sciences of
İzmir Institute of Technology
in Partial Fulfillment of the Requirements for the Degree of

DOCTOR OF PHILOSOPHY

in Chemical Engineering

by
Metin UZ

June 2014
İZMİR

We approve the thesis of **Metin UZ**

Examining Committee Members:

_____

Prof. Dr. Sacide ALSOY ALTINKAYA
Department of Chemical Engineering, İzmir Institute of Technology

_____

Prof. Dr. Serdar ÖZÇELİK
Department of Chemistry, İzmir Institute of Technology

_____

Prof. Dr. Şermin GENÇ
Institute of Health Sciences, Dokuz Eylül University

_____

Assoc. Prof. Dr. Erol ŞEKER
Department of Chemical Engineering, İzmir Institute of Technology

_____

Assist. Prof. Dr. Hadi M. ZAREIE
Department of Material Science and Engineering, İzmir Institute of Technology

2 July 2014

_____

Prof. Dr. Sacide ALSOY ALTINKAYA
Supervisor, Department of Chemical Engineering, İzmir Institute of Technology

_____

Prof. Dr. Volga BULMUŞ
Co-Supervisor, Department of Chemical Engineering, İzmir Institute of Technology

_____

Prof. Dr. Fehime ÇAKICIOĞLU ÖZKAN
Head of the Department of Chemical Engineering

_____

Prof. Dr. R. Tuğrul SENGER
Dean of the Graduate School of Engineering and Sciences

ACKNOWLEDGEMENTS

I would like to express my deepest gratitude to my advisor, Prof. Dr. Sacide Alsoy ALTINKAYA and my co-advisor Prof. Dr. Volga BULMUŞ and Prof. Dr. Surya MALLAPRAGADA for their guidance, support, motivation and encouragement during my thesis.

I am especially grateful to my laboratory colleagues, Filiz Yaşar MAHLIÇLI, Melda BÜYÜKÖZ and Pelin OYMACI for their support and assistance to my work.

I would also like to thank Handan ACAR, Hüsnü Arda YURTSEVER, Mert TUNÇER, Emre KILIÇ, Özgün DELİİSMAİL, Derya DÜZGÖREN BİLGİNPERK, Özgür YILMAZER, Dane RUSÇUKLU, Yekta GÜNAY OĞUZ, Evrim BALCI PAŞIK, Sanem Ezgi KINAL, Justin ADAMS and Xunpei LIU for their assistance during this study.

I would like to thank İzmir Institute of Technology Biotechnology and Bioengineering Application and Research Center and İzmir Institute of Technology Environmental Development Application and Research Center for providing technical support and help.

Lastly, I offer sincere thanks to my family for their love, continuous support and unlimited patience throughout my education.

This thesis was partially supported by The Scientific and Technological Research Council of Turkey and İzmir Institute of Technology Scientific Research Project Commission (Grant # 2009IYTE01).

ABSTRACT

PREPARATION AND CHARACTERIZATION OF NANOPARTICLES AS CARRIERS FOR GENE DELIVERY

In the first part of this thesis, a comprehensive characterization of polyethylene glycol (PEG) modified AuNPs designed for imaging or diagnostic purposed was carried out to investigate the effect of the size, PEG layer conformation and grafting density on the cellular uptake, toxicity and cell cycle phases against prostate (PC3), colon (CaCo2) cancer cell lines and 3T3 Swiss fibroblast cells. It was noticed that the cellular uptake and toxicity profiles of the particles varied depending on the size, surface properties and cell type. The particles were found to show alterations in cell cycle phases by causing DNA damage without apoptotic behavior at certain doses. In the second part of this thesis, efficient multilayer small interfering RNA (siRNA) delivery systems based on gold nanoparticles (AuNPs), cationic pentablock copolymers or fusogenic peptides were developed using cleavable disulfide bonds and electrostatic interactions. siRNA/Polymer (polyplexes) and siRNA/Peptide (peptideplexes) complexes formed by direct electrostatic complexation between siRNA and the cationic pentablock copolymers or peptides were used as controls, respectively. In addition, a conjugate siRNA delivery system based on the cleavable disulfide bonds between siRNA and fusogenic peptide was also proposed as an alternative system. The siRNA activity, toxicity, cellular uptake and intracellular distribution of the developed systems were investigated against luciferase-expressing SKOV3 ovarian cancer cell line. The use of cationic block copolymers or fusogenic peptides in AuNP based multilayer systems and complex systems, provided efficient siRNA condensation and protection from nuclease enzyme and serum protein degradation, in addition to cellular uptake, endosomal escape and siRNA activity in the cytoplasm.

ÖZET

GEN TAŞINIMI İÇİN NANOTANECİKLERİN HAZIRLANMASI VE KARAKTERİZASYONU

Bu tezin ilk bölümünde, görüntüleme veya tanı amaçlı tasarlanmış polietilen glikol (PEG) modifiye altın nanotaneciklerin, boyut, PEG tabakası yoğunluğu ve konformasyon gibi özelliklerinin, hücre alımı, toksisite ve hücre döngüsü fazları üzerindeki etkileri Prostat (PC3), kolon (CaCo2) kanser hücre hatlarında ve 3T3 İsviçre fibroblast hücrelerine karşı araştırılmıştır. PEG kaplı taneciklerin hücre alımı ve toksisite profillerinin, boyut, yüzey özellikleri ve hücre tipine bağlı olarak değiştiği görülmüştür. Taneciklerin belirli dozlarda apoptotik davranış olmadan DNA hasarına neden olarak hücre döngüsü fazlarında değişikliğe neden olduğu saptanmıştır. Bu tezin ikinci bölümünde, altın nanotanecik (AuNPs), katyonik pentablok kopolimer veya füzyojenik peptit bazlı, kırılabilir disulfit bağları ve elektrostatik etkileşimler ile elde edilen cok katmanlı siRNA tasinim sistemleri geliştirilmiştir. siRNA ve katyonik pentablok kopolimer veya peptit arasındaki doğrudan elektrostatik etkileşimler sonucu elde edilen siRNA/polimer (polipleks) ve siRNA/peptit (peptitpleks) kompleksleri, sırasıyla, kontrol olarak kullanılmıştır. Buna ek olarak, siRNA ve füzyojenik peptit arasında kırılabilir disülfit bağları kullanılarak elde edilen konjuge sistem alternatif bir siRNA taşınım sistemi olarak önerilmiştir. Geliştirilen sistemlerin siRNA aktivitesi, toksisite, hücre alımı ve hücre içi dağılımı gibi özellikleri lusiferaz salgılayan SKOV3 yumurtalık kanseri hücre hattına karşı incelenmiştir. Altın nanotanecik bazlı çok katmanlı sistemlerde ve komplex sistemlerde katyonik pentablok kopolimerlerin veya füzyojenik peptitlerin kullanılması, etkili siRNA yüklemesi ve nükleaz enzimleri ve serum proteinlerinden korunma sağlamasına ek olarak, etkin bir hücre alımı, endozomal kaçış ve sitoplazmada siRNA aktivitesi sağlamıştır. Altın nanotanecik bazlı çok katmanlı sistemlerde kırılabilir disülfit bağlarının mevcudiyeti, bu sistemlerin aynı miktarda siRNA içeren polipleks ve peptitpleks sistemlere oranla herhangi bir toksik etki göstermeden ~% 20 oranda daha etkili bir siRNA aktivitesi gösterdiği saptanmıştır.

TABLE OF CONTENTS

LIST OF FIGURES

Figure **Page**

LIST OF TABLES

Figure **Page**

CHAPTER 1

INTRODUCTION

The application of small interfering RNA (siRNA) has shown great therapeutic potential for cancer treatment. Over the last decade, progress in nanotechnology has led to the development of efficient siRNA delivery systems, proposing new routes to overcome the major challenges and limitations of siRNA delivery (Kesharwani, Gajbhiye, and Jain 2012, Lee, Yoon, and Cho 2013, Li, Wang, et al. 2013). These challenges include siRNA condensation and protection, stability, selective targeting, cellular entry, endosomal escape and efficient siRNA release in the cytoplasm (Bora et al. 2012, Resnier et al. 2013, Scholz and Wagner 2012). In the literature, different siRNA delivery strategies have been developed based on complexation between siRNA and polymers or peptides and multilayer systems composed of polymers, lipids, peptides and inorganic nanoparticles (Dong, Zhou, and Liang 2012, Hoyer and Neundorf 2012b, Liu et al. 2013, Lytton-Jean, Langer, and Anderson 2011, Nakase, Tanaka, and Futaki 2013, Wu et al. 2012).

Most of the existing siRNA delivery systems that have been investigated are based on the self-assembly through the electrostatic interactions between siRNA and cationic polymers. However, these systems resulted in poor siRNA release and activity in the cytoplasm due to excess cationic charge (Ballarin-Gonzalez and Howard 2012, Breunig et al. 2008, Elbakry et al. 2009, Lee, Liu, and Reineke 2008, Varkouhi et al. 2012) . In order to achieve a sufficient siRNA activity, they require high siRNA loadings (Elbakry et al. 2009, Lee et al. 2009) which brings about the use of excessive polymer amounts to provide siRNA condensation and protection. The studies have indicated that some of the siRNA/polymer complex systems are not stable against serum protein mediated aggregation and disassembly and have potential toxic effects through cell membrane disruption due to their cationic nature (Ballarin-Gonzalez and Howard 2012, Buyens et al. 2010, Fischer et al. 2003, Gu et al. 2014, Lee, Liu, and Reineke 2008, Nelson et al. 2013, Prevost et al. 2011, Steele et al. 2012, Troiber et al. 2013, Varkouhi et al. 2012). In order to overcome these drawbacks, different types of responsive block copolymers have been investigated in designing siRNA delivery systems. The advantage of these polymers

comes from the possibility of changing the balance between the blocks with different features, such as electrostatic charge, hydrophilicity, pH and temperature responsiveness, that allows tuning cytotoxicity, siRNA condensation, cellular uptake, endosomal escape and siRNA transfection efficiency (Beyerle et al. 2010, Convertine et al. 2009, Guo, Huang, et al. 2011, Hinton et al. 2012, Merkel et al. 2009, Nelson et al. 2013, Patil, Zhang, and Minko 2011, Sun et al. 2008, Zheng et al. 2012, Zhou et al. 2013).

As an alternative to the responsive block copolymers, cell penetrating and fusogenic peptides have also been used as siRNA delivery vectors (Deshayes et al. 2008, Hoyer and Neundorf 2012b, Lehto, Kurrikoff, and Langel 2012, Morris et al. 2008, Nakase, Tanaka, and Futaki 2013, Wang et al. 2014). These type of peptides are generally composed of 6–30 amino acid residues. The conjugation or stable complex formation of peptides with molecules of interest facilitates the internalization by target cells and endosomal membrane disruption, which yields improved bioactivity. One advantage of peptides is that their sequences can be adjusted in such a way that their toxicity, siRNA loading, cellular uptake and endosomal escape properties can be manipulated (Deshayes et al. 2008, Hoyer and Neundorf 2012b, Lehto, Kurrikoff, and Langel 2012, Morris et al. 2008, Nakase, Tanaka, and Futaki 2013, Wang et al. 2014).

While siRNA/polymer and siRNA/peptide complex systems have been investigated as siRNA carriers, recent studies focused on gold nanoparticles to construct multilayer delivery systems (Lee et al. 2008, Kong et al. 2012, Lee, Lee, et al. 2011, Lee et al. 2009, Elbakry et al. 2009, Lee, Park, et al. 2011) by applying different strategies including chemical and electrostatic layer by layer deposition (Elbakry et al. 2012, Elbakry et al. 2009, Guo et al. 2010, Han et al. 2012, Lee, Park, et al. 2011, Lee, Lee, et al. 2011). Attaching siRNA on the AuNP surfaces through the cleavable disulfide bonds in order to facilitate its release and enhance its activity in cytoplasm became a popular approach. Contrary to the case of complexation between siRNA and polymers or peptides, these approaches make it possible to achieve higher siRNA activities with lower siRNA loadings (Cheng et al. 2011, Giljohann et al. 2009, Gunasekaran et al. 2011, Lee et al. 2009, Lee et al. 2008, Oishi et al. 2006, Takemoto et al. 2010, Varkouhi et al. 2010).

Beside drug/gene delivery, gold nanoparticles (AuNPs) are promising tools for cellular imaging, cancer diagnostics and therapy applications (Cai et al. 2007, Kim et al. 2007, Li et al. 2009, Shukla, Priscilla, et al. 2005, Wang et al. 2011) because of their unique features such as biocompatibility, controllable sizes, easy preparation/modification and strong plasmonic properties (Bhattacharya and Mukherjee

2008, Ghosh et al. 2008, Pissuwan, Niidome, and Cortie 2011). In most of the *in vitro* studies, the surface of the AuNPs was modified with polyethylene glycol (PEG) to enhance colloidal stability in physiological medium, improve biocompatibility (Gu et al. 2009, Simpson et al. 2011, Simpson et al. 2010, Simpson et al. 2013, Walkey et al. 2012) and provide conjugation sites for therapeutic agents and targeting ligands (Lee et al. 2009, Lee, Park, et al. 2011, Lee et al. 2008, Lytton-Jean, Langer, and Anderson 2011, Oishi et al. 2006, Shenoy et al. 2006). The studies in the literature have indicated that the size, shape and surface modification of AuNPs significantly affect their cellular uptake (Chithrani, Ghazani, and Chan 2006, Connor et al. 2005, Tsoli et al. 2005, Kim et al. 2012), intracellular localization (Gu et al. 2009, Shukla, Bansal, et al. 2005) and toxicity (Gu et al. 2009, Pan et al. 2007, Tsoli et al. 2005), however, the potential effects of naked or surface modified AuNPs on cell division and replication along with the possible reasons for these effects have been explored in detail only in a few *in vitro* studies (Austin et al. 2011, Butterworth et al. 2010, Choi et al. 2012, Gu et al. 2009, Kang, Mackey, and El-Sayed 2010, Li et al. 2011, Pan et al. 2007).

This thesis study aims at developing AuNPs for imaging or diagnostic purposes and siRNA delivery systems based on pentablock cationic copolymer and cell penetrating peptide. In the first part of the thesis, detailed characterization of the surface modified AuNPs developed for imaging or diagnostic purposes was presented. In particular; the effects of particle size, PEG layer thickness, PEG conformation and grafting density on the cellular uptake, toxicity and phases of the cell cycle for prostate (PC3), colon (CaCo2) cancer cell lines and 3T3 Swiss fibroblast cells were investigated. These cell lines were specifically selected since their doubling times, therefore, the time required to complete cell cycle, are different from each other, in addition, to the best of our knowledge, this is the first study investigating the intracellular behavior and toxic effect of PEG coated AuNPs against these cell lines.

In the second section of the thesis, a multilayer siRNA delivery system composed of gold nanoparticles (AuNPs) and pH and temperature-responsive pentablock copolymers (PDEAEM-Pluronic F127- PDEAEM) composed of Pluronic F127 (poly(ethyleneoxide)-block-poly(propyleneoxide)-block-poly(ethyleneoxide)(PEO-b-PPO-b-PEO)) and PDEAEM (poly(2-diethylaminoethyl methacrylate) blocks was developed and their toxicity as well as transfection efficiency in terms of luciferase activity were tested against luciferase-expressing SKOV3 ovarian cancer cells for the first time. The AuNPs, constituting the core of the multilayer, can be easily synthesized and

surface modified with different layers. The pentablock copolymer, constituting the outer layer of the system, provides protection of siRNA from the external effects, cellular uptake, endosomal escape and effective siRNA release in cytoplasm. The previous studies clearly indicated that the temperature responsive Pluronic F127 block enables cellular uptake while the pH responsive cationic end blocks, PDEAEM, facilitates DNA condensation and endosomal escape (Zhang and Mallapragada 2011a, b). Moreover, the cytotoxicity of these polymers can be tuned by changing the balance between the cationic and non-ionic blocks (Agarwal, Unfer, and Mallapragada 2008). These pentablock copolymers have the ability to undergo thermoreversible gelation at physiological temperatures (Zhang, Jia, et al. 2012), allowing for a depot of the DNA complexes to be entrapped in the gels, enabling the polymers to facilitate both complexation as well as sustained delivery. The PDEAEM-Pluronic F127-PDEAEM pentablock copolymers have been demonstrated as efficient DNA carriers by forming complexes (Agarwal and Mallapragada 2008, Determan et al. 2005, Zhang et al. 2009), on the other hand, their potential as delivery agents for siRNA has not yet been investigated. Herein, not only AuNP based multilayer system but also the results obtained with siRNA/Copolymer complexes were also reported. In addition, a hydrogel system, as depot for AuNP and cationic pentablock copolymer based siRNA delivery system, was synthesized in order to provide sustained and controlled release of siRNA.

As an alternative to synthesized responsive pentablock copolymers, the commercial TAT-HA2 fusion peptide was used as the outer layer of the AuNP based multilayer system and the results were presented in the third part. The commercial TAT-HA2 peptide was obtained by connecting the first 20 amino acid sequence of influenza A virus hemagglutinin protein (HA2) to a 10 amino acid cell permeable HIV Trans-Activator of Transcription (TAT) protein transduction domain (PTD) (Wadia, Stan, and Dowdy 2004). The TAT PTD provides cellular entry by binding to the cell surface and penetrating the membrane via lipid raft-dependent macropinocytosis (Wadia, Stan, and Dowdy 2004). The HA2 domain, which is a pH-sensitive lipid membrane destabilizing sequence, provides escape from macropinosomes and enhance transduction of the fusion peptide (Wadia, Stan, and Dowdy 2004). siRNA/peptide complex and siRNA/peptide conjugate systems based on the electrostatic interactions and the direct attachment of the siRNA molecules to the peptides through cleavable disulfide bonds, respectively were also developed. Each delivery system was characterized to verify the formation of complexes and conjugates, the adsorption of each layer on the AuNPs, and the siRNA

loading. In addition, their cellular uptake, intracellular distribution, toxicity and transfection efficiencies in SKOV3 cells were evaluated.

This thesis consists of five chapters. After the introduction, in the second chapter the siRNA mechanism, its advantages and challenges of siRNA delivery is explained. Moreover, the current siRNA delivery strategies and type of different delivery systems were mentioned. In the third chapter, the detailed experimental methods used to prepare and test the performances of the developed systems are presented. Chapter 4 includes a detailed discussion of all the obtained experimental results. In chapter 5, brief summary of the study and possible suggestions for further research are presented.

CHAPTER 2

siRNA DELIVERY

2.1. siRNA Mechanism and Pathway

Cancer is a disease that involves several irreversible genetic alterations occuring progressively over time. These gene alterations leading to the transformation of a normal cell into a malignant cell through a multi-step process mediated by the accumulation of successive mutations result in the deregulation of numerous signaling pathways and undesired cell functionalization. (Ambesajir et al. 2012, Bora et al. 2012, Devi 2006, Jones, de Souza, and Lindsay 2004, Shrey et al. 2009). The adverse effects and limited effectiveness of conventional cancer treatment strategies, such as, chemotherapy, surgery, or radiotherapy, have pushed researchers to the development of novel anticancer agents (Gomes-da-Silva, Simoes, and Moreira 2014, Miele et al. 2012, Oh and Park 2009, Resnier et al. 2013). In the last decade, the RNA interference (RNAi) mechanism became popular. This mechanism is mediated by small-interfering RNAs (siRNAs), which are 21–23 nucleotides-long double-stranded (ds) RNA involving sense and antisense strands. The mechanism of siRNA is shown in Figure 1. Upon cellular internalization, siRNAs are incorporated into a multi-protein complex, the RNA induced silencing complex (RISC). The sense strand is then cleaved by Argonaute 2 (AGO 2), which is an endonuclease of the RISC, while the antisense strand guides RISC towards the perfectly complementary target mRNA. Then the target mRNA is further cleaved by AGO 2 into two mRNA fragments. The cleavage takes place between nucleotides 10 and 11 relative to the 5′end of the siRNA antisense strand, leading to the subsequent degradation of the mRNA fragments by cellular exonucleases (Ambesajir et al. 2012, Bora et al. 2012, Devi 2006, Gomes-da-Silva, Simoes, and Moreira 2014, Shrey et al. 2009). Although siRNA is naturally generated from a long dsRNA, synthetic siRNA can also affect RNAi. By the introduction of an artificial siRNA of 21 nucleotides may also trigger the gene silencing in many mammalian cells by blocking the specific expression of endogenous and heterologous genes (Oh and Park 2009). In case of synthetic siRNA use, the mechanism starts with the cleavage of sense strand by AGO 2 upon cellular intermalization.

Therefore, synthetic siRNAs have been extensively used for the treatment of cancer cells, and the development of new therapeutics for various incurable diseases.

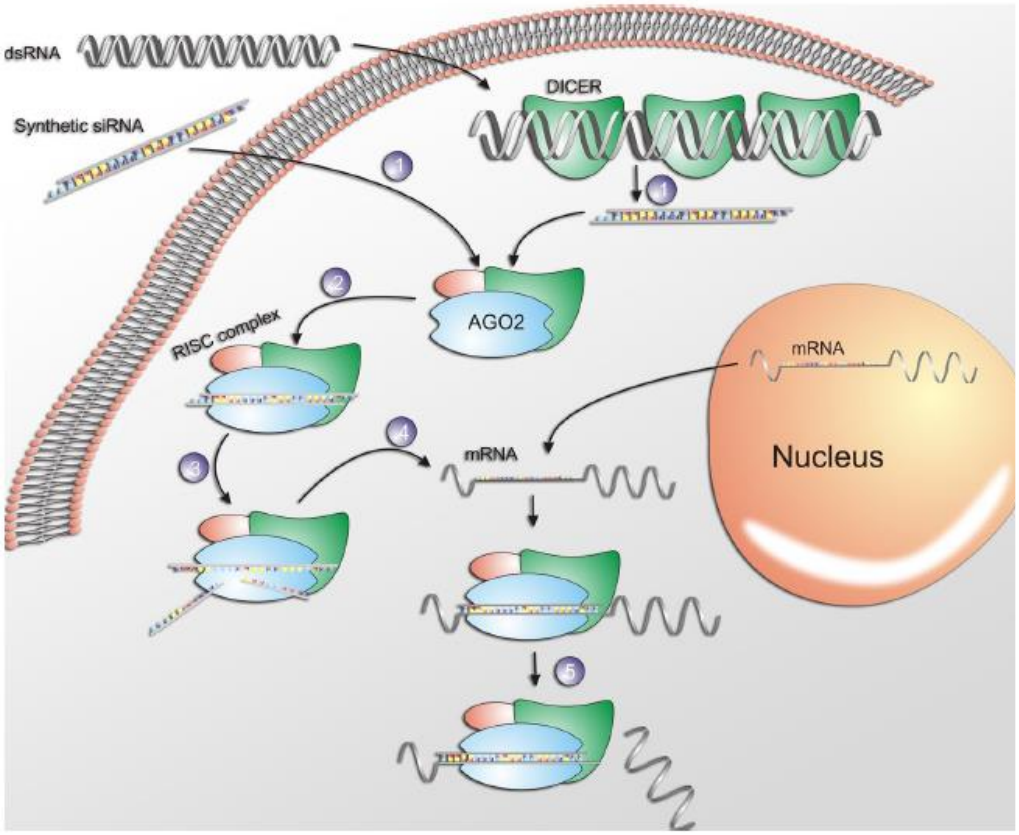

Figure 2.1. Mechanism of RNA interference by siRNA.
(Source: Gomes-da-Silva et al., 2014)

2.2. Advantages and Disadvantages of siRNA

Considering the current obstacles of the conventional cancer treatment methods, siRNAs have an enormous potential to become a novel class of pharmaceutical drugs within different fields of medicine, since they can inhibit the expression of any pathological protein. There are many advantages of siRNA as high potential biopharmaceutical therapeutics. First of all, RNAi directly interferes with translation and it does not interfere with DNA transcription, which, reduce the risk of interaction with chromosomal DNA and therefore, the possible adverse gene alteration. In addition, it is also possible to reduce the production of harmful proteins before synthesis as a result of the interaction of siRNA with mRNA (Oh and Park 2009). The additional degradation of target mRNA molecules and further propagation of the gene silencing activity can also

occur due to the recycle ability of the antisense strand-RISC complex. Another advantage of siRNA is that a wide range of target proteins can be used for gene silencing in order to treat diseases. As opposed to the current biological drugs, siRNA-based drug can target any mRNAs of interest, regardless of their cellular location of the translated proteins. Moreover, siRNA is so active that only a few siRNA molecules per cell are required to produce effective gene silencing leading to the less drug consumption (Gomes-da-Silva, Simoes, and Moreira 2014) (Oh and Park 2009, Resnier et al. 2013, Scholz and Wagner 2012).

Although siRNAs offer several advantages as potential new drugs, there are still some challenges to overcome. One of the challenges is the off-target effect of siRNA. In this situation, siRNA inhibits a gene, the expression of which should not be targeted, because the gene shares partial homology with the siRNA. The silencing of non-targeted genes may lead to toxicity. To avoid this issue, the design and selection of siRNAs should be carefully performed (Gomes-da-Silva, Simoes, and Moreira 2014, Oh and Park 2009, Resnier et al. 2013, Scholz and Wagner 2012, Shrey et al. 2009). Another challenge is immune stimulation which means the recognition of siRNA duplex by the innate immune system. Introduction of too much siRNA is known to result in nonspecific events owing to activation of innate immune responses (Oh and Park 2009). The most important challenge in siRNA therapy is the issue of delivery. siRNA is anionic, hydrophilic, and unable to enter cells by passive diffusion mechanisms. Moreover, delivery of naked siRNA to appropriate disease sites remains a considerable problem due to rapid enzymatic digestion, limited penetration across the capillary endothelium, and inefficient uptake by cells. To overcome these difficulties, the development of effective delivery systems is essential (Gao and Huang 2009, Guo, Bourre, et al. 2011, Lee, Yoon, and Cho 2013, Miele et al. 2012, Singh and Hajeri 2009, Zhang, Zhao, et al. 2012).

2.3. Challenges of siRNA Delivery

The ideal systemic delivery systems for siRNA should have the following characteristics. First, the delivery systems should be biocompatible and non-immunogenic. The system should have high loading of siRNA molecules and provide zero premature release. Second, the systems should provide efficient protection of the active double-stranded siRNA products from attack by serum proteins and nuclease

enzyme. The system should enhance cellular uptake. Finally, after delivery into target cells, the systems should promote the endosomal escape and release of siRNA into the cytoplasm for an efficient siRNA activity (Gao and Huang 2009, Lee, Yoon, and Cho 2013, Malmsten 2013, Miele et al. 2012, Singh and Hajeri 2009, Varkouhi et al. 2011, Zhang, Zhao, et al. 2012). The development of such an ideal system brings many barriers and challenges to overcome.

There are many barriers that should be eliminated by a siRNA delivery system for an efficient siRNA activity. These barriers include siRNA loading and protection, cellular uptake, endosomal escape and efficient release in cytoplasm as indicated in Figure 2.2. The design of a non-toxic siRNA delivery system should possess the following properties to overcome these barriers. An efficient system should include the ability to load the therapeutic genes in desired quantity. Beyond the loading, the strength of the conjugation or complexation between the therapeutic gene and nano-carrier should be optimum for the effective siRNA release at the specific site. Also, the system should provide an efficient protection against serum proteins and nuclease enzymes existing in the extra and intracellular environment in order to prevent nuclease degradation and complex/conjugate dissociation on the way to the cellular entry. The specific molecular sites of the delivery system should facilitate and enhance the entry into cells. Following the cellular entry, the carrier should be capable of providing endo-lysosomal pathway escape in order to prevent the degradation within the cell. After endosomal escape, siRNA delivery system should provide an effective release of cargo (David et al. 2010, Wong, Pelet, and Putnam 2007).

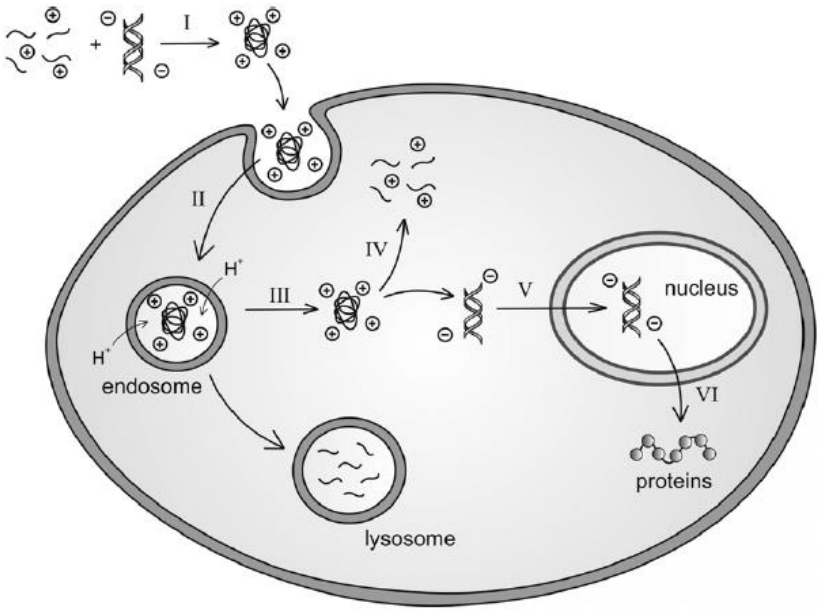

Figure 2.2. Barriers to gene delivery: (I) package therapeutic genes; (II) gain entry into cells; (III) escape the endo-lysosomal pathway; (IV) effect DNA/vector release; (V) traffic through the cytoplasm and into the nucleus; (VI) enable gene expression; and (VII) remain biocompatible (Source: Wong, Pelet, & Putnam, 2007).

2.3.1. siRNA Loading

The siRNA loading to delivery systems is critical in terms of nuclease and serum protein protection, cellular entry, endosomal escape and efficient siRNA activity at desired doses. In order to fulfill these criteria, different loading strategies have been applied in the literature (Figure 2) (David et al. 2010, Wong, Pelet, and Putnam 2007).

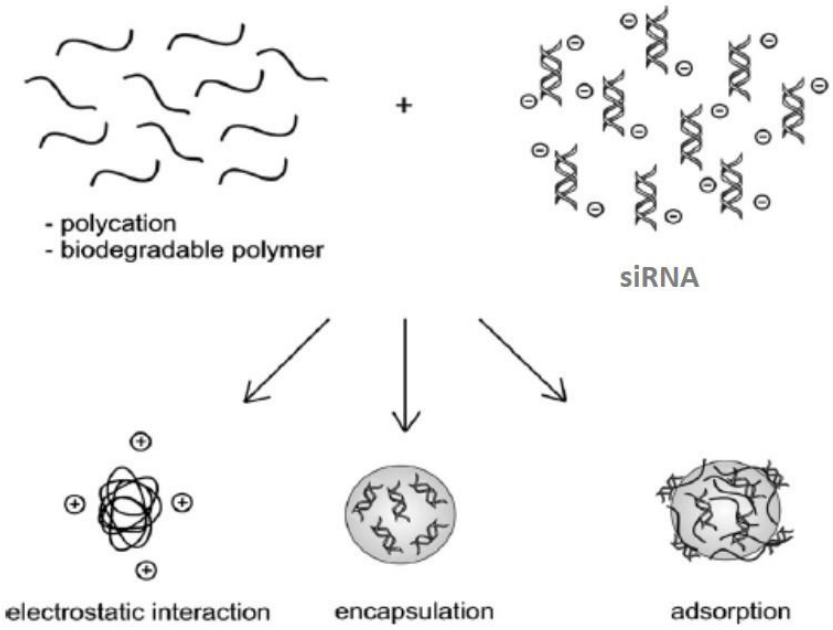

Figure 2.3. Gene packaging: The three main strategies employed to package siRNA are via (1) electrostatic interaction, (2) encapsulation within or (3) adsorption onto nano- or microspheres (Source: David et al., 2010).

2.3.1.1. Electrostatic Complexation

The siRNAs naturally possess negative net charge density due to the negavively charged phosphate backbone existing in their structure. The phosphate groups of nucleic acids play a critical role for the formation of complexes through the direct electrostatic interactions. The interaction between the positively charged groups of carriers (polymers, peptides, liposomes etc.) and negatively charged siRNA enables the formation of gene loaded complexes. By changing the nitrogen to phosphate (N:P) ratio the degree of complexation and therefore, loaded amount of siRNA, strength of complexation and toxicity can be manipulated. This strategy has been succeeded in siRNA protection from nuclease and serum proteins degradation, cellular entry and endosomal escape. However, these systems resulted in poor siRNA release and activity due to strong electrostatic interactions (Ballarin-Gonzalez and Howard 2012, Breunig et al. 2008, Elbakry et al. 2009, Lee, Liu, and Reineke 2008, Varkouhi et al. 2012), consequently, they require high loadings in order to achieve an efficient nucleic acid activity (Elbakry et al. 2009, Lee et al. 2009). This situation brings about the use of excessive polymer amounts to provide efficient condensation and protection. The studies have also indicated that some of the complex systems are not stable against serum protein mediated aggregation and

disassembly and have potential toxic effects through cell membrane disruption due to their cationic nature (Ballarin-Gonzalez and Howard 2012, Buyens et al. 2010, Fischer et al. 2003, Gu et al. 2014, Lee, Liu, and Reineke 2008, Nelson et al. 2013, Prevost et al. 2011, Steele et al. 2012, Troiber et al. 2013, Varkouhi et al. 2012).

2.3.1.2. Encapsulation

siRNA may also be encapsulated by biodegradable spherical structures. Generally these structures involve ester linkages along their backbones and can hydrolytically degrade to shorter oligomeric and monomeric components. As a result of this, their clearance from the body is facilitated (David et al. 2010, Wong, Pelet, and Putnam 2007). One of the advantages of the encapsulation is that siRNA-encapsulating biodegradable agents protect the incorporated genes from enzymatic degradation (Jeon et al. 2007, Wang et al. 1999). However, the genetic material can be degraded due to high shear stresses and exposure to organic solvents and extreme temperatures during processing. Other limitations include low encapsulation efficiency, potential siRNA degradation, and low siRNA bioavailability due to incomplete release from the polymer (Jang and Shea 2006, Jeon et al. 2007, Tahara et al. 2007, Wang et al. 1999).

2.3.1.3. Chemical Conjugation

As an alternative, development of delivery systems based on chemical conjugation have also been investigated. In order to overcome the limitations of electrostatically formed complex systems, the vectors (polymers, peptides etc.) have been modified by some chemical groups in order to facilitate the attachment and release of nucleic acids (Christie et al. 2011, Pittella et al. 2011, Smith, Holley, and McCormick 2011). In one study, the researchers investigated the properties of micellar siRNA delivery vehicles prepared with poly(ethylene glycol)-block-poly(L-lysine) (PEG-b-PLL) comprising lysine amines modified to contain amidine and thiol functionality. Lysine modification was achieved using 2-iminothiolane (2-IT) [yielding PEG-b- PLL(N2IM-IM)] or dimethyl 3,30-dithiobispropionimidate (DTBP) [yielding PEG-b-PLL(MPA)], to impart disulfide cross-linking ability without significantly changing cationic charge (Christie et al. 2011). In another study, green fluorescent protein (GFP) siRNA was conjugated to a

six-arm polyethylene glycol (PEG) derivative via a reducible disulfide linkage (6PEG-siRNA). The 6PEG-siRNA conjugate was also functionalized with a cell penetrating peptide, Hph1 to enhance its cellular uptake property (6PEG-siRNA-Hph1) (Choi et al. 2010). The use of cleavable disulfide linkage in the attachment of nucleic acids has a great potential to facilitate nucleic acid loading and provide efficient release of the cargo. In addition to these type of systems, the nucleic acids can also be attached to the surface of inorganic nanoparticles through chemical bonds in order to develop multicomponent delivery systems based on layer by layer deposition approach (Lee et al. 2008, Lytton-Jean, Langer, and Anderson 2011, Lee et al. 2009, Elbakry et al. 2009). For instance, in one study, the PEG was coated on amine functionalized AuNPs and then siRNA was attached to the PEG molecule through cleavable disulfide bonds (Lee et al. 2008). In another study, thiol modified siRNA was attached to the PEG coated AuNPs through cleavable disulfide bonds and then the outermost surface was covered with the cationic poly(ß-amino ester)s (PBAEs) in order to facilitate the cellular entry and endosomal escape (Lee et al. 2009).

2.3.2. Cellular Entry Path

Most nonviral gene vectors cannot readily cross the plasma membrane due to their large size and hydrophilic nature. Endocytosis (the vesicular uptake of extracellular macromolecules) has been established as the main mechanism for the internalization of nonviral vectors into the cells. Multiple mechanisms for endocytosis have been described to date; clathrin-mediated endocytosis, caveolae, macropinocytosis, and clathrin/caveolae-independent endocytosis.

2.3.2.1. Clathrin-Mediated Endocytosis

Clathrin-mediated endocytosis (CME) is the major endocytic pathway providing continuous uptake of essential nutrients, antigens, growth factors, and pathogens. Generally, the internalization mechanism starts with the binding of a ligand to a specific cell surface receptor leading to the clustering of the ligand-receptor complexes in coated pits on the plasma membrane. Then, the coated pits invaginate and pinch off from the plasma membrane to form intracellular clathrin-coated vesicles (CCVs) which carry

concentrated receptor- ligand complexes into the cells (Conner and Schmid 2003, Dykman and Khlebtsov 2014, Hillaireau and Couvreur 2009, Kettler et al. 2014, Khalil et al. 2006).

In terms of gene delivery, CME can be obtained by using certain ligands (i.e. s transferrin) which can specifically recognize certain receptors on the cell surface. The use of ligands enhance the internalization of the particles and receptor overexpressing specific cell targeting. However, the problem with CME is that the genes internalized are usually trapped in endosomes followed by enzymatic degradation in lysosomes avoiding their access to their target sites. Several strategies have been developed to enhance the cytosolic release of endocytosed genes. This involves the incorporation of vesicular destructive elements to the DNA-carrier complexes, which perturb the integrity of the vesicular membrane and allow the cytosolic release of their contents, while not damaging the DNA. Some cationic polymers, e.g., polyethyleneimine (PEI), and some lipids also have the ability to enhance the cytosolic release of genes through different mechanisms as will be subsequently discussed (Conner and Schmid 2003, Hillaireau and Couvreur 2009, Khalil et al. 2006).

2.3.2.2. Caveolae-Mediated Endocytosis

Caveolae are small, hydrophobic membrane microdomains that are rich in cholesterol and glycosphingolipids. It is generally believed that caveolar uptake does not lead to lysosomal degradation. Therefore, this pathway seems to be advantageous in terms of siRNA delivery. Evidence supporting the existence of a role of caveolae in the uptake of cationic polymer-DNA complexes and the class of protein transduction domains (PTDs), such as the TAT peptide, have appeared (Vandenbroucke et al. 2007). It was suggested that large particles (500 nm) are preferentially taken up through caveolae where they do not suffer lysosomal degradation (Zorko and Langel 2005). However, caveolae are slowly internalized and small in size, and their fluid phase volume is small. Thus, it is unlikely that they contribute significantly to constitutive endocytosis, although the situation is different in endothelial cells in which caveolae constitute 10 to 20% of the cell surface. Caveolae-mediated endocytosis is still a promising strategy for gene delivery especially if the internalization can be increased, possibly through the use of specific receptors for caveolae (Khalil et al. 2006).

2.3.2.3. Macropinocytosis

Macropinocytosis refers to the formation of large endocytic vesicles of irregular size and shape, generated by actin-driven envagination of the plasma membrane. Macropinocytosis usually accompanies cell surface ruffling that is induced in many cell types upon stimulation by growth factors or other signals. A ruffle is formed by a linear band of outward-directed actin polymerization near the plasma membrane, which lengthens into a planar extension of the cell surface. After stimulation by any mitogenic factor, the ruffles become longer and broader and frequently close into large macropinosomes. Macropinosomes have no coat and do not concentrate receptors. They vary in size, sometimes being as large as 5 μm in diameter. Because they are relatively large, macropinocytosis is an efficient route for the nonselective endocytosis of solute macromolecules (Khalil et al. 2006).

Macropinocytosis has recently received attention as an entry route for gene and drug delivery. Recent reports have demonstrated that the uptake of the TAT peptide and its cargos occurs by macropinocytosis. This pathway provides some advantageous such as the increased uptake of macromolecules, the avoidance of lysosomal degradation and the ease of escape from macropinosomes because of their relatively leaky nature (Vandenbroucke et al. 2007, Zorko and Langel 2005).

2.3.2.4. Receptor-Mediated Endocytosis

The use of receptor-mediated endocytosis is a promising approach for the introduction of DNA into defined cell populations. For example, hepatocytes exclusively express large numbers of high-affinity cell surface receptors that bind to and subsequently internalize asialoglycoproteins. Introduction of a galactose moiety into a gene delivery system can produce liver-parenchymal cell-specific gene transfection. Mannose receptor-mediated gene transfection is another approach for targeting macrophages, which overexpress mannose receptors on their surface. Tf, an iron-binding glycoprotein, has been used as a tumor-targeting ligand for gene delivery. Tf receptors are overexpressed in rapidly dividing cells due to the increased cellular need for iron (Tortorella and Karagiannis 2014). The folate receptor is another example of receptors overexpressed in tumor cells, and it can be used for tumor targeting. Although receptor-mediated

endocytosis is a promising approach for drug targeting, most of the currently used ligands are internalized by clathrin-mediated endocytosis, and the poor intracellular trafficking associated with this significantly limits the transfection activities of the systems. Therefore, functional devices that increase the cytosolic delivery of genes are needed. For example, the intracellular fate of Tf-liposomes was improved by adding GALA, a pH-sensitive fusiogenic peptide, which enhances the endosomal escape in response to the low pH in endosomes (Sakurai et al. 2011, Hatakeyama et al. 2009). Exploring and targeting new receptors that can be internalized by clathrin-independent endocytosis are likely to provide more efficient systems because these uptake mechanisms are relatively unaffected by lysosomal degradation.

2.3.3. Endosomal Escape

The endocytic pathway is the major uptake mechanism of cells and any biological agents, such as DNA, siRNA and proteins. These agents become entrapped in endosomes and are degraded by specific enzymes in the lysosome. Thus, a limiting step in achieving an effective biological based therapy is to facilitate the endosomal escape and ensure cytosolic delivery of the therapeutics. After endocytosis, the internalized molecules tend to be trapped in intracellular vesicles and eventually fuse with lysosomes where they are degraded. Therefore, the problem of gene delivery involves not only the cellular uptake of genes but also their intracellular availability at the target sites. Special devices, such as liposomes or peptides, that can enhance the cytosolic release of internalized molecules are essential for achieving successful gene delivery after endocytosis- mediated uptake (Varkouhi et al. 2011).

Different mechanisms such as pore formation in the endosomal membrane, pH-buffering effect of protonable groups and fusion into the lipid bilayer of endosomes have been proposed to facilitate the endosomal escape.

2.3.3.1. Pore Formation in the Endosomal Membrane

Pore formation depends on the interaction between a membrane tension opening the pore and a line tension closing the pore. Some components like peptides have a high affinity for the rim of the pore. Binding of the peptides to the rim leads to reduction of

the line tension which decreases the number of peptides causing the internal membrane tension and keeps the pore radius stable. It has been shown that binding of agents such as cationic amphiphilic peptides (AMPs) to the lipid bilayer leads to internal stress or internal membrane tension that can be sufficiently strong to create pores in the lipid membrane (Varkouhi et al. 2011) (Nakase, Tanaka, and Futaki 2013, Morris et al. 2008).

2.3.3.2. pH-Buffering Effect (The Proton Sponge Effect)

The proton sponge effect is mediated by agents with a high buffering capacity and the flexibility to swell when protonated. Protonation, induces an extensive inflow of ions and water into the endosomal environment which subsequently leads to rupture of the endosomal membrane and release of the entrapped components. Tertiary amine groups that contain a hydrophobic chain, have been shown to accumulate in endosomes which have an acidic pH and become detergents upon protonation resulting in disruption of the membrane. As an example, histidine-rich molecules show a buffering effect upon protonation of the imidazole ring of histidine, resulting in disruption of the endosomal membrane, and poly(amido amine) polymers have a high buffering effect due to the presence of protonatedamine groups in their structure which leads to an increase in osmotic pressure in the endosome that results in disruption of the endosomal membrane (Vicentini et al. 2013, Varkouhi et al. 2011).

2.3.3.3. Fusion in the Endosomal Membrane

Another mechanism for endosomal escape is the destabilization of the endosomal membrane by fusogenic peptides which are used in a number of fusion systems. Membrane fusion plays an important role in cellular trafficking and endocytosis. The majority of viruses have single integral membrane peptides which undergo conformational changes upon a trigger such as a change in pH. These conformational changes allow the protein to induce the fusion in the lipid bilayer. Haemagglutinin, which is a peptide of the influenza virus coat, acts as a fusogenic agent that is converted from an anionic, hydrophilic coil at pH 7.4 to a hydrophobic helical conformation at the acidic endosomal pH. This new α-helical structure leads to fusion of the viral membrane into the cellular membrane (Lee, Johnson, et al. 2011, Liou et al. 2012, Ye et al. 2012).

2.3.3.4. Photochemical Disruption of the Endosomal Membrane

The possibility of photochemically releasing biologicals from endosomal pathway into the cytosol has been described as a technique called photochemical internalization (PCI). Photosensitizers localize primarily in the membrane of the endosomes and lysosomes. After exposure to light, these photosensitizers induce the formation of reactive singlet oxygen which has a short lifetime and destroys the endosomal/lysosomal membrane, whereas the contents of the organelles remain intact and are delivered to the cytosol. This technique has been applied for delivery of several formulations, such as lipid carriers and polymers. Moreover, in some studies photo stimulation has been applied to enhance the endosomal release of the therapeutic complexes containing cell penetrating peptides (Varkouhi et al. 2011).

2.3.3.5. Endosomal Escape Agents

2.3.3.5.1. Virus Derived Agents

Small peptide domains of viral proteins capable of providing endosomal escape have been identified in the literature. For instance, the HA2 subunit of haemagglutinin (HA) protein of the influenza virus with a short chain of an N-terminal amphiphilic anionic peptide has been used as a fusogenic agent for endosomal escape in many studies. The glutamic acid and the aspartic acid existing in the HA2 peptide sequence is protonated at acidic pH leading to a conformational change to a helical structure. The conformational change upon protonation leads to fusogenic activity resulting in destabilization of the endosomal membrane (Lee, Johnson, et al. 2011, Lee, Johnson, and Pellois 2010, Liou et al. 2012, Ye et al. 2012, Wadia, Stan, and Dowdy 2004).

TAT (HIV-1 Trans-activator gene product), which is transcription factor of the integrated human immunodeficiency virus-1 (HIV-1), have been shown as an efficient membrane destabilizing agent in several studies. This protein contains arginine and lysine amino acid residues which are involved in lipid membrane penetration and are able to facilitate and enhance the internalization of large liposomes and large molecules, such as dextran particles encapsulating magnetic beads. For instance, in a study, the sequences of TAT peptide was modified by histidine and cysteine residues in order to promote the

endosomal escape properties and stability of the TAT/DNA complexes, respectively (Lee, Johnson, et al. 2011, Lee, Johnson, and Pellois 2010, Liou et al. 2012, Ye et al. 2012, Wadia, Stan, and Dowdy 2004).

As an alternative, new peptides, KALA, which is a cationic amphipathic peptide, was designed based on the wild type sequence of haemagglutinin subunit (HA-2) from influenza virus. This fusogenic peptide undergoes a conformational change from pH 5.0 to 7.5, resulting in effectively destabilizing the endosomal membranes (Lee, Kim, and Park 2007, Choi et al. 2010, Mok and Park 2008). GALA, which is another synthetic amphipathic peptide obtained by the substitution of glycine for glutamic acid, also undergoes a pHdependent conformational change resulting in formation of a helical structure that induces the leakage of the contents of large unilammellar phosphatidylcholine vesicles. This peptide is soluble at pH 7.5 and destabilizes the lipid bilayers at a pH less than 6.0 (Sakurai et al. 2011, Hatakeyama et al. 2009).

2.3.3.5.2. Chemical Agents

As an alternative to the virus driven peptides, several chemical agents with endosome disruptive properties have also been introduced. It has been noticed that some polymers such as polyethylenimine (PEI) rupture the endosome by the proton sponge effect via their pH buffering features. Most of the poly(amido amine)s possess buffer capacities in the pH range 7.4 – 5.1, a property that may favorably contribute to the endosomal escape. It has been shown that the synthetic pH-sensitive anionic polymer, poly (propylacrylic acid) (PPAA) has been efficient in endosomal escape of non-viral vectors and improved their transfection efficiency. Agents such as ammonium chloride, chloroquine, and methylamine are relatively lipophilic in their unprotonated form and they penetrate the membranes of cells and vacuoles. Upon entering an acidic environment they become protonated and too polar to escape rapidly through the membrane (Lin et al. 2010, Convertine et al. 2010, Mok et al. 2010).

2.4. siRNA Delivery Systems

The application of small interfering RNA (siRNA) has shown great therapeutic potential for cancer treatment. Over the last decade, progress in nanotechnology has led

to the development of efficient siRNA delivery systems, proposing new routes to overcome the major challenges and limitations of siRNA delivery (Kesharwani, Gajbhiye, and Jain 2012, Lee, Yoon, and Cho 2013, Li, Wang, et al. 2013). These challenges include siRNA condensation and protection, stability, selective targeting, cellular entry, endosomal escape and efficient siRNA release in the cytoplasm (Bora et al. 2012, Resnier et al. 2013, Scholz and Wagner 2012). In the literature, different siRNA delivery strategies have been developed based on various systems, composed of different materials such as polymers, lipids, peptides and inorganic nanoparticles (Dong, Zhou, and Liang 2012, Hoyer and Neundorf 2012b, Liu et al. 2013, Lytton-Jean, Langer, and Anderson 2011, Nakase, Tanaka, and Futaki 2013, Wu et al. 2012).

2.4.1. Polymers

Polymers are widely used in the development of siRNA delivery systems. Most of the siRNA/Polymer delivery systems are generally based on homopolymers such as polyethyleneimine and obtained by the electrostatic interactions between siRNA and cationic moieties of the polymers. However, some of these systems suffer from their toxic effects which result from their cationic nature. (Ballarin-Gonzalez and Howard 2012, Breunig et al. 2008, Elbakry et al. 2009, Lee, Liu, and Reineke 2008, Varkouhi et al. 2012). Beside the toxicity, their excessive cationic charge causes condensation of siRNA via strong electrostatic interactions which inhibits the efficient siRNA release, and therefore, activity in cytoplasm. In addition, the systems prepared by electrostatic complexation have a tendency to form aggregates or disassemble in the presence of serum proteins (Ballarin-Gonzalez and Howard 2012, Buyens et al. 2010, Fischer et al. 2003, Gu et al. 2014, Lee, Liu, and Reineke 2008, Nelson et al. 2013, Prevost et al. 2011, Steele et al. 2012, Troiber et al. 2013, Varkouhi et al. 2012). In order to overcome these drawbacks, different types of responsive block copolymers have been investigated to design siRNA delivery systems. The advantage of these polymers comes from the possibility of changing the balance between the blocks with different features or adding some active groups to create effective conjugation sites in the structure (Beyerle et al. 2010, Convertine et al. 2009, Guo, Huang, et al. 2011, Hinton et al. 2012, Merkel et al. 2009, Nelson et al. 2013, Patil, Zhang, and Minko 2011, Sun et al. 2008, Zheng et al. 2012, Zhou et al. 2013). Hinton et al. (2012) synthesized series of ABA tri-block

copolymers from oligo(ethylene glycol) methyl ether methacrylate ($OEGMA_{475}$) and N,N-dimethylaminoethyl methacrylate (DMAEMA) blocks by RAFT polymerization method to investigate the effect of polymer composition on cell viability, siRNA uptake, serum stability and gene silencing activity. The block copolymers were prepared by varying the central cationic block (DMAEMA) length from 38 to 192 monomer units and the outer hydrophilic block ($OEGMA_{475}$) from 7 to 69 units. The siRNA/polymer complexes were formed through electrostatic interactions. Their results indicated that central cationic block significantly affect the cell viability and gene silencing efficiency while the outer hydrophilic blocks contribute to serum stability and overall efficiency of the delivery system. The polymer composition possessing cationic block length of ~120 monomer units and P($OEGMA_{475}$) blocks length with ~15 monomer units on each end showed the most efficient enhanced green fluorescent protein (EGFP) suppression against Chinese Hamster Ovary-GFP and Human Embryonic Kidney 293 cells without showing toxicity at applied dose. In another study, Convertine et al., (2009) developed a new diblock carrier that combines siRNA condensing ability of positively-charged dimethyl aminoethyl methacrylate (DMAEMA) block and pH-responsive endosomal releasing block composed of DMAEMA and propylacrylic acid (PAA), together with butyl methacylate (BMA) using reversible addition fragmentation chain transfer polymerization (RAFT) technique. They synthesized series of diblock copolymers by varying the ratios of DMAEMA, PAA and BMA blocks and prepared electrostatic complexes with siRNA by varying the polymer/siRNA charge ratio. Their results indicated that the polymer composition of 48% BMA, 29% PAA, and 23%DMAEMA with polymer/siRNA charge ratio of 4:1 exhibited the greatest pH-dependent endosomal escape and the most efficient uptake of siRNA over all other polymer carriers examined. Moreover, siRNA delivery using this polymer composition elicited the greatest glyceraldehyde 3-phosphate dehydrogenase (GAPDH) reduction in HeLa cells without showing severe toxicity. With these data, they demonstrated that by changing the ratios of polymer blocks exhibiting different properties and polymer/siRNA charge ratio for complexation, it is possible to manipulate the efficiencies of siRNA delivery systems.

In siRNA delivery systems, obtained by electrostatic interactions with polymers, the formation of micelles in the structure was shown to enhance many properties such as, cellular uptake, endosomal escape, siRNA release and activity. For instance, Convertine et al., (2010) enhanced their previously described diblock copolymer siRNA carriers, composed of BMA, PAA and DMAEMA blocks, by inducing their micelle formation

ability through the incorporation of a longer endosomolytic block with increased hydrophobic content. They obtained siRNA loadings through electrostatic interactions and they found out that the siRNA binding to the cationic shell block did not perturb micelle stability. The presence of micelles triggered the cellular uptake of the systems by 3 fold. The self-assembly of the diblock copolymers into micellar particles was shown to provide a significant enhancement in mRNA knockdown at siRNA concentrations of ~12.5 nM. Their micelle-based systems showed ~89% reduction in GAPDH mRNA levels which was significantly higher than the previously developed nonmicelle system. The increase in siRNA dose upto 25 nM enhanced the reduction in mRNA levels. Yu et al., (2011) reported a novel amphotericin B (AmB)-loaded, dual pH-responsive micelleplex platform for siRNA delivery. Micelles were self-assembled from poly(2-(dimethylamino) ethyl methacrylate)-block-poly(2-(diisopropylamino)ethyl methacrylate) (PDMA-b-PDPA) diblock copolymers. AmB was loaded into the hydrophobic PDPA core, and siRNA was complexed with a positively charged PDMA shell to form the micelleplexes. After cellular uptake, the PDMA-b-PDPA/siRNA micelleplexes dissociated in early endosomes to release AmB, which destabilize the endosome membranes and significantly increased siRNA activity. Their results showed that AmB-loaded micelleplexes resulted in significant increase in luciferase knockdown efficiency over the AmB-free control. In another work, Mao et al., (2011) described a micelleplex system based on an biodegradable, amphiphilic and cationic triblock copolymer, consisting of monomethoxy poly(ethylene glycol), poly(e-caprolactone) and poly(2-aminoethyl ethylene phosphate ($mPEG_{45}$-b-PCL_{30}-b-$PPEEA_{15}$), to deliver the acid ceramidase (AC) gene targeting siRNA for *in vivo* cancer therapy. siRNA was loaded to this system by electrostatic interactions and this triblock copolymer can self-assemble into micellar nanoparticles (MNPs) in aqueous solution. The MNPs were effectively internalized and achieved significant down-regulation of luciferase expression in BT474-luciferase cells. Systemic delivery of a micelleplex carrying specific siRNA targeting the acid ceramidase gene, via intravenous injection, significantly inhibited tumor growth in BT474 xenograft murine model. Similarly, Sun et al., (2008) proposed the use of tri-block amphiphilic copolymer, consisting of a monomethoxy poly(ethylene glycol) (mPEG) block, a poly(3-caprolactone) (PCL) block and a cationic poly(2-aminoethyl ethylene phosphate) (PPEEA) block ($mPEG_{45}$-b-PCL_{100}-b-$PPEEA_{12}$) for siRNA delivery. Their polymer structure is capable of creating self-assembly in aqueous solution to form tri-layered cationic MNPs. They selected PCL block to induce the micellar core formation

and stabilize the nanoparticles through hydrophobic interactions, while they used hydrophilic poly- (ethylene glycol) (PEG) to protect siRNA and extend blood circulation and positively charged degradable poly(2-aminoethyl ethylene phosphate) (PPEEA) as siRNA binding block. The properties of the developed system were changed by varying the N/P ratio. Their results demonstrated that the green fluorescence protein (GFP) siRNA loaded nanoparticles can be effectively internalized and subsequently release siRNA, resulting in significant decrease in GFP expression up to 40–70% in HEK293 cells. They proposed that higher N/P ratio resulted in more effective silencing activity due to better cell internalization. Besides, they hypothesized that the disassociation of siRNA from the micellar nanoparticles may be due to the loss of stability of particles resulting from the dilution in cytoplasm, leading to the release of siRNA. Other than that, degradation of positively charged PPEEA component of MNPs may cause the deprotonation of polyphosphoester block and lose siRNA binding ability, resulting in siRNA release in cytoplasm. Lin et al., (2010) designed degradable, pH-sensitive, membrane destabilizing, comb-like polymers based on a diblock polymer backbone. The first block is a copolymer of pH-sensitive ethyl acrylic acid (EAA) monomers and hydrophobic butyl methacrylate (BMA) or hexyl methacrylate monomers while the second block is a homopolymer of N-acryloxy succinimide (NASI) or ßbenzyl L-aspartate N-carboxy-anhydride (BLA-NCA) monomers. This second block are functionalized to allow controlled grafting of hydrophobic hexyl methacrylate (HMA) and cationic trimethyl aminoethyl methacrylate (TMAEMA) copolymers via acid-labile hydrazone linkages. These comb-like polymers were complexed with siRNA via electrostatic interactions by changing N/P ratio to form pH-sensitive particles that fragment upon exposure to acidic endosomal environment due to hydrolysis of the hydrazine linkages connecting poly(HMA-co-TMAEMA) grafts to the polymers backbone. Their results indicated that the membrane-destabilizing backbone and the hydrophobic monomers embedded in the comb-like grafts of poly(EAA-co-BMA)-b-NASI-g-(HMA-co-TMAEMA) block copolymer with 100 nM of anti-GAPDH siRNA molecules at N/P ratio of 2.5 synergistically disrupt the endosomal membrane and release siRNA into the cytoplasm to achieve ~50% knockdown of GAPDH gene expression against MCF-7 breast cancer cell line without severe toxicity. This combination also provided high cellular uptake and efficient siRNA protection against serum proteins and nuclease enzymes.

The studies mentioned above indicated that the use of block copolymers instead of homopolymers in the design of siRNA/polymer complex systems is capable of

compensating the disadvantages resulting from the cationic nature and strong electrostatic interactions. On the other hand, the use of chemical conjugation alone or in combination with electrostatic interactions may further enhance the efficiencies of polymeric siRNA delivery systems. For this purpose, different siRNA delivery systems designed by chemical conjugation strategy have been proposed. Breunig et al., (2008) hypothesized that disulfide cleavable carrier systems are favorable for the release of siRNA into the cell cytoplasm. For this purpose, they tested various PEI derivatives (linear PEI, disulfide cross-linked PEI and branched PEI) electrostatically complexed with siRNA by changing N/P ratio as carrier system. They found that the cellular uptake of siRNA was more efficient with branched PEI rather than with the linear PEI. The increase in N/P ratio enhanced the uptake rate. However, an efficient siRNA release and therefore, a significant reduction in EGFP expression against CHO-K1 cells, was achieved by cleavable disulfide cross-linked PEI. Hence, they suggested a combination of a high branching density and reductively cleavable bonds within the PEI-based carrier system as a potential siRNA delivery system. In another study, York, Huang, and McCormick (2010) developed N-(2-hydroxypropyl) methacrylamide-s-N-(3-aminopropyl) methacrylamide (HPMA-s-APMA) copolymer, for the design of multiconjugate delivery system containing both siRNA and cell targeting folate receptor. The copolymer consists of a biocompatible poly(HPMA) and a primary amine, APMA, portion. A multifunctional cross linker, N-succinimidyl 3-(2-pyridyldithio)-propionate (SPDP), was linked to a fraction of the APMA in order to attach thiolated siRNA through a disulfide exchange reaction while the unmodified APMA portion were coupled to amine reactive folates. These modifications resulted in the formation of a multifunctional copolymer both capable of cellular targeting and providing easy siRNA release.

In some studies, the use of polymeric micelles in combination with chemical conjugation strategy were also proposed to enhance the efficiency of the systems. For instance, Christie et al., (2011) investigated the micellar siRNA delivery system composed of poly(ethylene glycol)-block-poly(Llysine) (PEG-b-PLL) block copolymer. They applied lysine amine modification to provide amidine and thiol functionality using 2-iminothiolane (2-IT) [yielding PEG-b-PLL(N2IM-IM)] or dimethyl 3,3'-dithiobispropionimidate (DTBP) [yielding PEG-b-PLL(MPA)] to impart disulfide cross-linking ability without compromising cationic charge. However, these two lysine modification reagents affected micelle formation behavior and stability along with in vitro and in vivo performance differently. Their results indicated that a high degree of PEG-b-

PLL modification with 2-iminothiolane reduced the polymer charge density at pH 7.4, which in turn shifted the optimal conditions of micelle formation to favor higher molar ratios of polymer/siRNA compared to a highly charged block copolymer. Despite lower free thiol content and disulfide cross-linking efficiency, micelles formed with PEG-b-PLL(N2IM-IM) and siRNA were more stable in buffer and in the bloodstream compared to those formed with PEG-b-PLL(MPA) and siRNA. However, higher micelle stability and loss of sensitivity to disulfide reducing conditions resulted in lower siRNA activity (10% decrease in luciferase expression); thus, reversible micelle stability is critical to achieve high gene silencing at the target site. On the other hand, PEG-b-PLL(MPA), possessing cleavable disulfide bonds, was complexed with siRNA and provided 60% decrease in luciferase expression at dose of 200 nM siRNA against B16F10-luc cells. Lundy et al., (2013) described a neutral, ampholytic conjugatable diblock polymer micelles. The first segment of this copolymer contains a hydrophilic poly[N-(2-hydroxypropyl)methacrylamide-co-N-(2-(pyridin-2-yldisulfanyl)ethyl)methacrylamide) (poly[HPMA-co-PDSMA]) block to promote aqueous stability and facilitate thiol−disulfide exchange reactions while a second segment involves ampholytic block consisting of propylacrylic acid (PAA), dimethylaminoethyl methacrylate (DMAEMA), and butyl methacrylate (BMA). These diblock copolymers are capable of forming self-assembly under aqueous conditions to form polymeric micelles. The endosomal escape was obtained by the neutral hydrophilic micelles possessing membrane destabilizing activity at acidic pH values. The attachment of thiolated siRNA, targeting glyceraldehyde 3-phosphate dehydrogenase (GAPDH), occurs via the disulfide exchange reaction with the pyridal disulfide groups present in the micelle corona. This system showed 90% mRNA and 65% protein knockdown at the end of 48h against HeLa cells at siRNA/polymer molar ratio of 1:10 without severe toxicity. However, the polymeric micelles lacking a pH responsive endosomalytic segment demonstrated negligible mRNA and protein knockdown under these conditions. Matsumoto et al., (2009) reported a micellar siRNA delivery system based on the core-shell-type polyion complex (PIC) micelle with a disulfide cross-linked core. For this purpose, PEG-b-PLL copolymer was reacted with 2-iminothiolane to obtain poly(ethyleneglycol)-block-poly[L-N-(1-imino-4-mercaptobutyl)lysine] [PEG-b-(PLL-IM)] with a portion of lysine residues bearing both mercaptopropyl and amidine groups. This thiolated copolymer was subsequently used to prepare disulfide cross-linked PIC micelles incorporating siRNA. The system was prepared through the assembly of iminothiolane-modified poly(ethylene glycol)-block-

poly(L-lysine) [PEG-b-(PLL-IM)] and siRNA. They found that the combination of disulfide cross-links and cationic amidine groups enhanced the stability and dissociation of micelles in the intracellular environment. Their results also indicated that PIC micelles with disulfide linking achieved 90% decrease in luciferase expression in Huh7 cells at 100nM dose which was comparatively higher than that achieved with unmodified PEG-b-PLL. The same group reported a new PIC based siRNA delivery system based on chemically modified siRNA and poly(aspartic acid) (PAsp). siRNA was grafted to PAsp via a disulfide linkage. Besides forming more stable PICs, the presence of cleavable disulfide linkage facilitates siRNA release. This system managed to provide 80% decrease in luciferase expression against B16F10-Luc cells at the end of 48h of incubation (Takemoto et al. 2010).

siRNA is a very efficient therapeutic that even small amount is enough to reach high silencing efficiencies. Because of this, most of the systems was designed to target siRNA delivery to the cytoplasm, providing burst siRNA release instead of controlled one. However, some studies aimed to achieve long term activity of siRNA with controlled manner. For this purpose, they proposed the encapsulation of siRNA by block copolymers to provide sustained release. Patil and Panyam (2009) investigated the formation of nanoparticles using polyethylenimine (PEI) incorporated biodegradable poly(d,l-lactide-co-glycolide) (PLGA) polymer using double emulsion-solvent evaporation technique for siRNA encapsulation and delivery. They prepared PLGA nanoparticles containing siRNA, PLGA-PEI nanoparticles containing siRNA and PLGA nanoparticles containing previously prepared siRNA-PEI complex. The PLGA loaded with siRNA-PEI complex showed enhanced, cellular uptake and ~50% decrease in luciferase expression at the end of 3 days. Moreover, their study put an emphasis on the sustained and controlled release problem of siRNA. With this system, they achieved around 2 weeks of controlled release of siRNA. By changing molecular weight of polymers or amount of PEI they managed to manipulate the siRNA release. Liu et al., (2012) snynthesized amphiphilic block copolymer composed of conventional monomethoxy (polyethylene glycol)-poly (D,Llactide-co-glycolide)-poly (L-lysine) (mPEG-PLGA-b-PLL) for siRNA delivery. The siRNA was loaded on this system by double emulsion method. Their study focused on the cellular uptake and controlled release of siRNA. The results indicated that the developed system enhanced cellular uptake and provided sustained release of siRNA during 5 days.

2.4.2. Hydrogels

The current siRNA delivery systems have a great potential to deliver siRNA to cytoplasm, however, most of them suffer from providing sustained release at the specified site (Smith and Lyon 2012). In order to resolve this problem, hydrogel systems have been proposed by researchers. Krebs, Jeon, and Alsberg (2009) proposed three different biodegradable, injectable hydrogel systems involving; calcium crosslinked alginate, photocrosslinked alginate, and collagen for localized and sustained delivery of siRNA. The siRNA was uniformly distributed and encapsulated into these biopolymer hydrogel systems via cross-linking for sustained release. The siRNA loading potential of these hydrogels are considerably high between 5 to 10 µg. They manipulated the release rate by changing siRNA/hydrogel ratio or adding cationic polymers like chitosan and PEI. Their results indicated that the mechanism of siRNA release over the time period examined is likely a combination of diffusion through the biopolymer pores as well as biopolymer degradation. They monitored GFP expression level on day 3 and 6 in HEK293 cells incubated with siRNA loaded hydrogel. The results indicated that siRNA-collagen hydrogel system exhibited sustained release of siRNA and provide ~95% decrease in the GFP level during 6 days. Nguyen, Dang, and Alsberg (2013) designed a functionalized, biodegradable siRNA delivery system based on covalent incorporation of cationic linear polyethyleneimine (LPEI) into photocrosslinked dextran (DEX) hydrogels through a biodegradable ester linkage. They controlled the sustained release of siRNA through the degradation of the covalent ester linkages between the LPEI, which electrostatically condense siRNA to form LPEI/siRNA complexes, and the hydrogels. They manipulated the release of siRNA by varying the concentrations of LPEI and DEX in the hydrogel. The increase in PEI in the hydrogel slowed down the release rate causing complete release of siRNA in 9 days for 8% w/w DEX hydrogels and in 17 days for 12% w/w DEX hydrogels. During this period, the 12% w/w DEX hydrogels with PEI managed to keep the GFP expression levels around 5% during 14 days against HEK293 cells without showing toxicity. Nuhn et al., (2012) demonstrated covalently stabilized hydrogel superstructures by cross-linking the hydrophobic reactive inner core with amine-containing cross-linker molecules using amphiphilic reactive ester precursor polymers for siRNA delivery purposes. They synthesized amphiphilic reactive ester block copolymers of P(PFPMA)-b-P(MEO_3MA) and P(MEO_3MA)-b-P(PFPMA) by RAFT polymerization

of pentafluorophenyl methacrylate as reactive ester monomer together with tri(ethylene glycol)- methyl ether methacrylate. In polar aprotic solvents, they observed a self-assembly of these polymers leading to the formation of nanometer-sized polymer aggregates. The resulting superstructures were used to convert the reactive precursor block copolymers with amine containing cross-linker molecules into covalently stabilized hydrogel particles. Therefore they managed to synthesize precise nanohydrogels of different size starting from various block copolymers and further modified via reactive ester approach.

2.4.3. Peptides

Peptides, which are generally composed of 6–30 amino acid residues, have also been used to develop novel siRNA delivery systems. Since the conjugation or stable complex formation of peptides with molecules of interest facilitates the cellular internalization and endosomal disruption, they yielded improved bioactivity. Also, the adjustment of the peptide sequence depending on the desired properties and ease of conjugation or modification also enhance the development of peptide based siRNA strategies.

Peptides may be directy complexed with siRNA through the electrostatic interactions. For instance, Cantini et al., (2013) examined the design of a peptide, named 599, consisting of a synthetic influenza virus-derived endosome disruptive fusogenic peptide sequence (HA-2) and a stretch of cationic cell-penetrating nona(D-arginine) residues, to deliver siRNAs into oral cancer. They electrostatically condensed siRNA to the positively charged nona(D-arginine) residues by changing the peptide to siRNA molar ratio. Their results indicated that the increase in peptide to siRNA ratio up to 50:1 led to a higher siRNA loadings (100 nM) and therefore enhanced siRNA activity against oral cancer cells with no significant long-term cytotoxic effects.

In addition to the direct electrostatic complexation of peptides with siRNA, the peptides were also combined with polymers by using chemical conjugation. Considering this approach, Lee et al., (2007) conjugated vascular endothelial growth factor (VEGF) siRNA to poly(ethylene glycol) via a disulfide linkage (siRNA-PEG) and electrostatically condense this conjugate with cationic fusogenic peptide KALA by changing the N/P ratio to prepare polyelectrolyte complex micelles (PECMs). The charge neutralized

siRNA/KALA complex constitute the inner core of the PECMs while the PEG layers surround the core providing siRNA protection and stability. KALA, which is an amphipathic peptide undergoes conformational change from pH 5.0 to 7.5, resulting in effectively disrupting an endosomal membrane and providing endosomal escape. The PECMs with N/P ratio of 6 and possessing 200 pmol/ml siRNA loading resulted in ~80% reduction in VEGF expression in PC3 cells without toxicity. Choi et al., (2010) developed a siRNA delivery system composed of polymers and peptides. In their design, siRNA was conjugated to a six-arm PEG derivative via a reducible disulfide linkage (6PEG-siRNA). The 6PEG-siRNA conjugate was also functionalized with a cell penetrating peptide, Hph1, which was tethered to the residual thiol end group, to enhance its cellular uptake property (6PEG-siRNA-Hph1). The 6PEG-siRNA-Hph1 conjugate was electrostatically complexed with cationic self-crosslinked fusogenic KALA peptide (cl-KALA), which was obtained by the disulfide linkage between its two terminal cysteine residues, by changing the siRNA/cl-KALA ratio in order to form multifunctional polyelectrolyte complex micelles. According to their results, the formed systems provided superior physical stability and resistance to enzymatic degradation due to the polymeric arms. The peptide moieties on the other hand enhanced the cellular uptake and endosomal escape. The 6PEG-siRNA-Hph1/cl-KALA complexes exhibited 70% decrease in GFP expression at siRNA/cl-KALA ratio of 16 against for MDA-MB-435 cells. Segura and Hubbell (2007) reported the synthesis of ABC triblock copolymer composed of poly(ethylene glycol) (PEG), poly(propylene sulfide) (PPS), and a positively charged peptide (PEG-PPS-peptide) for siRNA delivery applications. They synthesized the diblock copolymer PEG_{45}-$PPS_{5,10}$ through the anionic polymerization of propylene sulfide upon a PEG macroinitiator. The hydrophobic portion of this polymer facilitates the self-assembly having hydrophilic core. Following this, the TAT or oligolysine peptide was coupled to the PPS terminus via disulfide exchange reaction using N-terminal cysteine residue on the peptide. The peptide was designed to interact electrostatically with siRNA to both condense siRNA and enhance cellular entry. The proposed triblock was able to decrease GAPDH expression upto ~10% in HeLa cells without severe toxicity. Zhao et al., (2012) developed a biodegradable amphiphilic tri-block copolymer ($mPEG_{2000}$-PLA_{3000}-b-R_{15}) composed of monomethoxy poly(ethyleneglycol), poly(d,l-lactide) and polyarginine peptide. This amphiphilic tri-block copolymer is capable of making self-assembly into cationic micellar nanoparticles, which are able to bind siRNA to form micelle/siRNA complexes, by changing the N/P ratio. The PEG corona helps to reduce the aggregation

of the micelleplexes. The peptide arginine is responsible from the siRNA binding and cellular entry enhancement. Depending on their hemolysis results, they claimed that the primary and secondary amines from the R15 segment may facilitate endosomal rupture. Their results indicated that the micelleplexes exhibited ~70 percent decrease in EGFP expression in MCF-7 cells with 200 nM siRNA loading at the end of 48h.

Hatakeyama et al., (2009) developed a multifunctional envelope-type nano device (MEND) for efficient delivery of siRNA. In order to further modify the MENDS, they developed a PEG-peptide-DOPE (PPD) that can be cleaved in a matrix metalloproteinase (MMP)-rich environment. Following this, to further improve the silencing activity of encapsulated siRNA, they modified the PPD-MEND with a pH-sensitive fusogenic GALA peptide (GALA/PPD-MEND). They demonstrated that the introduction of both of a pH-sensitive fusogenic GALA peptide and PPD into the MEND facilitates nanoparticle endosomal escape, thereby enhancing the efficiency of siRNA delivery and gene silencing. A 30 amino acid GALA contains a glutamic acid-alanine-leucine-alanine sequence that is repeated 4 times. Since the carboxyl groups of glutamic acid are negatively charged at a physiological pH, electric repulsion between these groups results in GALA with a random coil structure. In contrast, at an acidic pH (around 5.5) protonation of the side chain of carboxyl groups of the glutamic acids dissipates electric repulsion. As a result, the GALA structure changes into an α-helix, a structure that tends to induce membrane fusion. They tried to optimize the siRNA activity by changing the GALA and PPD contents. The results indicated that the most efficient siRNA activity was obtained in case of equimolar use of GALA and PPD. The same group then noticed that the GALA-modified PEG-MEND (GALA-MEND) was eliminated rapidly when injected into the blood circulation. To circumvent this, they developed a new shorter version of GALA (shGALA), which would be masked by the aqueous layer formed by PEG-modification of the MEND and which would result in avoiding this type of recognition (Sakurai et al. 2011).

Peptides have also been used as part of multilayer siRNA delivery systems. For instance, Li et al., (2013) described a magnetic mesoporous silica nanoparticles (M-MSNs)-based, polyelectrolyte (polyethylenimine, PEI) and fusogenic peptide (KALA)-functionalized siRNA delivery system. The construction of this delivery system involves the encapsulation of siRNA within the mesopores of M-MSNs, followed by the coating of PEI on the external surface of siRNA-loaded M-MSNs and the chemical conjugation of KALA peptides.

2.4.4. Gold Nanoparticle Based siRNA Delivery Systems

While synthetic and natural polymers and peptides have been investigated as siRNA carriers, recent studies have focused on gold nanoparticles to construct multilayer siRNA delivery systems (Lee et al. 2008, Kong et al. 2012, Lee, Lee, et al. 2011, Lee et al. 2009, Elbakry et al. 2009, Lee, Park, et al. 2011). Gold colloids are bioinert, nontoxic, easily synthesized and functionalized, in addition, they can be used for both therapeutic and diagnostic purposes (Ghosh et al. 2008, Pissuwan, Niidome, and Cortie 2011). In the construction of multicomponent siRNA delivery systems involving AuNPs, different strategies have been applied, including chemical and electrostatic layer by layer deposition of cationic polymers (Elbakry et al. 2012, Elbakry et al. 2009, Guo et al. 2010, Han et al. 2012, Lee, Park, et al. 2011, Lee, Lee, et al. 2011).

Elbakry et al., (2009) proposed the use of gold nanoparticles as template and obtained the siRNA delivery systems with the layer by layer deposition of oppositely charged polyelectrolyte layers for the first time. They used 11-mercaptoundecanoic acid (MUA) as first layer around the gold surface to facilitate the binding of the subsequent layers. Thereafter, the consecutive deposition of PEI, double stranded 21-mer siRNA and PEI as the outer layer took place. They conducted a very detailed characterization and their system showed a great stability and achieved a 70% decrease in EGFP expression against CHO-K1 cells without showing toxicity. However, LbL system required high amount of PEI and siRNA loading due to the strong electrostatic interactions between siRNA and PEI layers avoiding the efficient release of siRNA into cytoplasm. The similar siRNA activity was also achieved with siRNA/PEI complex system having 100 nM siRNA loading which was much lower than the LbL system. Therefore, their study showed the potential use of LbL approach for AuNP based siRNA delivery systems while emphasizing the disadvantage of strong electrostatic interactions in siRNA activity.

Target-specific intracellular delivery of siRNA is regarded as an important challenge for the development of siRNA therapeutics since the positive surface charge of nanoparticles might induce nonspecific binding with blood serum components resulting in aggregation or induced nonspecific delivery of siRNA. The use of LbL technique make it possible to attach such components on the AuNPs. Lee et al., (2011) designed a cysteamine modified gold nanoparticle (AuCM) based siRNA delivery system (AuCM/siRNA/PEI/HA) composed of subsequent layers of siRNA, polyethyleneimine

(PEI) and hyaluronic acid (HA) using a layer-by-layer approach. Following the formation of AuCMs, each layer was deposited on the previous one through the electrostatic interactions. HA was used as receptor specifying the target cell (B16F1 cells with HA receptors) and mediate endocytosis. Also, the presence of HA at the outer surface enhanced the serum stability of the system. Following the target cell entry the system showed excellent target-specific gene silencing efficiency causing 70% decrease in luciferase expression in B16F1 cells with a negligible cytotoxicity. The success of this system was attributed to the presence of selective targeting layer in the system.

In addition to the target specificity, the endosomal escape properties of these systems is also important for an efficient siRNA delivery. Especially the polymers capable of shifting their charge nature between negative and positive depending on the pH of the environment are widely used to enhance endosomal disruption. Some of these polymers were adapted to the AuNP based systems prepared by LbL approach. Zhao, et al., (2012) constructed siRNA delivery system based on the LbL modification of bovine serum albumin (BSA) stabilized AuNP. The poly(allylamine hydrochloride) (PAH) and siRNA were alternately assembled on the surface of AuNPs to sandwich siRNA between the PAH layers by electrostatic self-assembly. PAH at the outer surface of the system was used to provide cellular entry and endosomal escape due to the primary amine groups in its structure. This system provided 50% decrease in epidermal growth factor receptor (EGFR) expression in MCF-7 cells without toxicity. The same system prepared by PEI proposed same siRNA activity, however, depicted severe toxicity. Guo et al., (2010) proposed a charge reversal polymer and AuNP based siRNA delivery system to facilitate endosomal ecape and enhance the siRNA activity. Charge-reversal copolymer is capable of shifting their charge between positive and negative depending of the pH of the environment. Therefore, the charge conversion of the polymer in the acidic medium of endosome helps the endosomal membrane disruption. They developed charge-reversal siRNA delivery system of PEI/PAH-Cit/PEI/MUA-AuNPs with cationic PEI, charge-reversal PAH-Cit, and MUA-AuNPs by layer-by-layer assembly technique. The chemical modification of AuNPs with 11-mercaptoundecanoic acid (MUA) was followed by subsequent polyelectrolyte layer deposition of PEI, siRNA and PAH-Cit through electrostatic interactions. They used PEI layer for siRNA condensation and PAH-Cit layer to facilitate siRNA release. They proved that the charge conversion of PAH-Cit enhances the siRNA release and, hence, the activity. Their results showed that their system managed to silence the expression of lamin A/C protein in HeLa cells efficiently. Han et

al., (2012) developed similar siRNA delivery system using layer-by-layer assembly by replacing the inner PEI layer with chitosan (CS), which is a natural, biocompatible, and biodegradable polymer. Also, they obtained the same system with less number of layers. AuNPs were directly reduced and stabilized by CS, forming a positively charged AuNP-CS core. Charge reversible PAH-Cit and polyethylenimine (PEI) were sequentially deposited onto the surface of AuNP-CS through electrostatic interaction, forming a PEI/PAH-Cit/AuNP-CS shell/core structure. Then, the siRNA was electrostatically complexed with the developed core/shell structure. Their results indicated that the complex disassembled to release as much as 79% of the loaded siRNA during 4 h incubation time at pH 5.5.

As an alternative to the LbL systems constructed through the electrostatic interactions, the use of chemical conjugations, especially cleavable disulfide bonds, has been proposed for such systems. The disulfide bonds, obtained mainly by thiol chemistry, may be easily cleaved under the reductive environment of cytosol. This property is used to facilitate the siRNA release, which was strongly restricted in most of the systems obtained by electrostatic interactions. The disulfide bonds were generally used in combination with electrostatic interactions to build AuNP based LbL systems. Lee et al., (2008) demonstrated the use of amine-functionalized gold nanoparticles (Af-AuNPs) for intracellular siRNA delivery. siRNA was conjugated to polyethylene glycol (PEG) via a di-sulfide linkage that can be cleaved to allow and efficient release under a reductive environment in the cytoplasm. The positively charged gold nanoparticles formed stable polyelectrolyte complexes through electrostatic interactions with negatively charged siRNA–polyethylene glycol (PEG) conjugates having a cleavable di-sulfide linkage. Therefore, the Af-AuNPs constitute the core of the system facilitating siRNA attachment while PEG micelles oriented outside to generate PEG shell layer. They manipulated the green fluorescence protein (GFP) level in PC3 cells by changing the Af-AuNP:siRNA-PEG molar ratio and applied siRNA dose. Their best results indicated that the system with Af-AuNP:siRNA-PEG molar ratio of 20 and possessing 60 nM siRNA dose managed to decrease the GFP expression up to 20% in PC3 cells without showing any toxic effect. Lee et al., (2009) developed a new nanoparticulate siRNA delivery system based on AuNPs and biodegradable polycationic poly(α-aminoester)s (PBAEs). They modified the AuNPs with the hydrophilic polymer poly(ethylene glycol) (PEG), which stabilize the particles and facilitate the sequential surface modification, and then, siRNA was conjugated to the PEG modified nanoparticles via cleavable disulfide linkages by using

cross linker. The siRNA loaded particles were then electrostatically coated with different PBAEs. They clearly demonstrated the advantage of using disulfide bonds to enhance the siRNA release and activity. According to their results, the system provided almost 95% decrease in luciferase expression in HeLa cells with significantly lower siRNA loadings, 3 nM. They hypothesized that the swelling and degradation of PBAEs facilitate the disulfide bond cleavage leading to the efficient siRNA release and activity. Conde et al., (2012) developed a nanocarrier for siRNA delivery based on AuNPs functionalized with multiple biomolecules: PEG, cell penetration and cell adhesion peptides. They applied two different approaches; covalent approach, use of thiolated siRNA for gold-thiol binding to the nanoparticle and ionic approach, interaction of the negatively charged siRNA to the modified surface of the AuNP through ionic interactions. AuNPs were first functionalized with two types of thiolated poly(ethylene glycol) (PEG) spacers: SH-EG(8)-$(CH_2)_2$-COOH, and an azide-containing spacer, SH-$(CH_2)_3$-CONH-EG(6)-$(CH_2)_2$-N_3. The carboxylated spacer provides the anchoring moieties for the covalent binding of amine-containing molecules through carbodiimide chemistry, while the azide containing spacer confers positive charge. Combined functionalization of the AuNPs with both spacers was finely tuned by controlling both specific spacer composition and degree of saturation. In order to elucidate the most efficient strategy to bind siRNA to AuNPs, two types of AuNPs stabilized by different degrees of PEG saturation were selected and siRNA attachment was achieved using either ionic interaction (ION) or covalent binding (COV). The quaternary ammonium groups (R_4N^+) were bound to AuNPs through carbodiimide chemistry between the carboxylated spacer and (2-aminoethyl)trimethylammonium hydrochloride. Ionic interactions between the negatively charged siRNA backbone and both the azide and quaternary ammonium positively charged groups ensured binding of siRNA onto the NP surface. On the other hand, the thiolated siRNA was bound via a disulfide bonds to AuNPs with a nonsaturated PEG layer. The TAT peptide was attached to the outer surfaces of both system by EDC/NHS coupling between the carboxylated spacer and the amine terminal group of the KKK-TAT peptide. The TAT peptide and R_4N^+ was used to enhance siRNA activity by providing cellular uptake and endosomal escape. Their overall results indicated that the efficient siRNA activity of the system with covalent bonding was due to the efficient cytoplasmic release of siRNA compared to the system with electrostatic interactions.

Another approach in the development of AuNP based siRNA delivery systems is the formation of AuNPs by the direct reduction of gold precursor via polymers. Therefore,

positively charged AuNPs may be achieved to create complexes with siRNA through electrostatic interactions. Lee et al., (2011) demonstrated synthesis of polyethyleneimine (PEI)-coated gold nanoparticles (AuNPs) using catechol-conjugated PEI (PEI-C) for siRNA delivery. Reductive and hydrophobic cathechol groups formed spherical multi-cored micelles and served as reductive templates for the synthesis of spherical AuNPs. PEI-C was stably anchored on the surface of growing crystal gold seeds with crosslinking, resulting in the formation of cationic AuNPs. The PEI coated AuNPs created stable complexes with siRNA through electrostatic interactions by changing the PEI-C-AuNP to siRNA ratio. The PEI-C-AuNP-siRNA complexes with the ratio of 50 lowered the GFP expression down to 27.8±4.3% against MDA-MB435 cells. They noted that the complexes with lower size and moderate positive surface charge, which could be adjusted by the degree of catechol substitution of PEI-C, depicted a better siRNA activity, probably due to the enhanced cellular uptake and less toxicity. Kirkland-York et al., (2010) prepared AuNPs, reduced by poly(N-2-hydroxypropyl methacrylamide$_{70}$-block-N-[3-(dimethylamino)propyl] methacrylamide$_{24}$) [P(HPMA$_{70}$-b-DMAPMA$_{24}$)] block copolymer, to develop neutral and sterically stable complexes with siRNA. The amine-containing cationic block (DMAPMA) was utilized to promote the in situ reduction of Au^{3+} to AuNPs and create binding sites for siRNA, while the nonimmunogenic, hydrophilic block (HPMA) provided steric stabilization. Their results indicated that system provided moderate release of siRNA and 50% decrease in luciferase expression in KB cells with 100 nM siRNA loading.

As a brief conclusion, these multilayer approaches have shown the added advantage of making it possible to achieve higher siRNA activity with lower siRNA loadings and lower polymer concentrations, thereby significantly reducing toxicity (Cheng et al. 2011, Giljohann et al. 2009, Gunasekaran et al. 2011, Lee et al. 2009, Lee et al. 2008, Oishi et al. 2006, Takemoto et al. 2010, Varkouhi et al. 2010). In addition, the LbL technique using either electrostatic interactions or chemical conjugations or both of them in combination, makes it possible to bring different properties of various components together to design an efficient system capable of providing, siRNA protection, cellular entry, endosomal escape and efficient siRNA release in cytoplasm with smaller amounts of siRNA and other components, i.e. polymers, peptides etc.

CHAPTER 3

EXPERIMENTAL

3.1. Materials

1-propylamine, 2-pyridinecarbaldehyde, N,N-(diethyl amino)ethyl methacrylate (DEAEM), 2-bromoisoburyryl bromide, copper(I) bromide (CuBr 99.99%), Pluronic F127 (MnZ12600, 70% PEO) and copper powder (99) for organic synthesis were purchased from Sigma-Aldrich. Triethylamine, tetrahydrofuran (THF) and toluene were purchased from Fisher Scientific and all chemicals were used with no further purification. N-Propyl-pyridynyl methanimine (NPPM) was prepared by reacting 1-propylamine with 2-pyridinecarbaldehyde. Hydrogen tetrachloroaurate (III)trihydrate (99.9%), sodium citrate, and sodium borohydrate used in the preparation of gold nanoparticles were purchased from Sigma-Aldrich. Thiol and amine end group-modified PEG (SH-PEG-NH_2: MW1000) used for gold nanoparticles surface modification was purchased from Creative PEGworks. SPDP (N-Succinimidyl 3-(2-pyridyldithio)-propionate) cross linker was obtained from Fisher Thermo Scientific. The luciferase suppressing siRNA and thiol modified siRNA sequences (sense: 5' HS-GAUUAUGUCCGGUUAUGUA-UU 3'; antisense: 5' UACAUAACCGGACAUAAUC-UU 3') were obtained from IDT-DNA Technologies. Fluorescein isothiocyanate (FITC), used to stain AuNP-PEG conjugates, was from Sigma-Aldrich. Alexafour488 and NHS-FITC fluorescence dyes were purchased from Invitrogen to prepare dye attached polymers and peptides respectively. Cell penetrating peptide, TAT-HA2, was obtained from Anaspec. The cell lines, colon cancer, CaCo-2 (ATCC number HTB-37), prostat cancer, PC-3 (ATCC number CRL-1435) and 3T3-Swiss albino (ATCC number CCL-92), were obtained from American Type Culture Collection. The luciferase expressing ovarian cancer cell line, SKOV3 (AKR-232), was purchased from Creative Biogene. The cell culture media, Dulbecco's Modified Eagle Medium (DMEM) and RPMI Media 1640, and cell culture medium additives, fetal bovine serum (FBS), penicillin streptomycin and nonessential amino acids were obtained from Invitrogen. Annexin V staining kit for apoptosis detection and 3-(4,5-dimethythiazol- 2-yl)-2,5-diphenyl tetrazolium bromide (MTT) toxicity assay dye were

obtained from Sigma Aldrich. The fluorescence dyes, Lysotracker Red and Hoechst and DAPI, used in staining lysosome and nucleus respectively, were obtained from Invitrogen. Cell titer96 and Luciferase assay kits were obtained from Promega. The Ribogreen siRNA detection kit was purchased from Invitrogen. Polyacrylamide gel desalting columns (MWCO: 1800) were obtained from Invitrogen. All the buffers were prepared by using sterile RNase free water according to standard laboratory procedures.

3.2. Synthesis of Pluronic F127 Macroinitiator

The difunctional 2-bromo propionate Pluronic F127 was synthesized as illustrated in Figure 3.1. Pluronic F127 (40 g) was dissolved in 800ml of tetrahydrofuran (THF) during 15 min under continuous stirring in ice bath. Then, 20ml of triethylamine and 3ml of 2-bromoisobutyryl bromide was added and the solution was stirred overnight. After that, the excess solvent was removed with a rotary evaporator, the product was precipitated in n-hexane (at -72 ºC) and dried under vacuum.

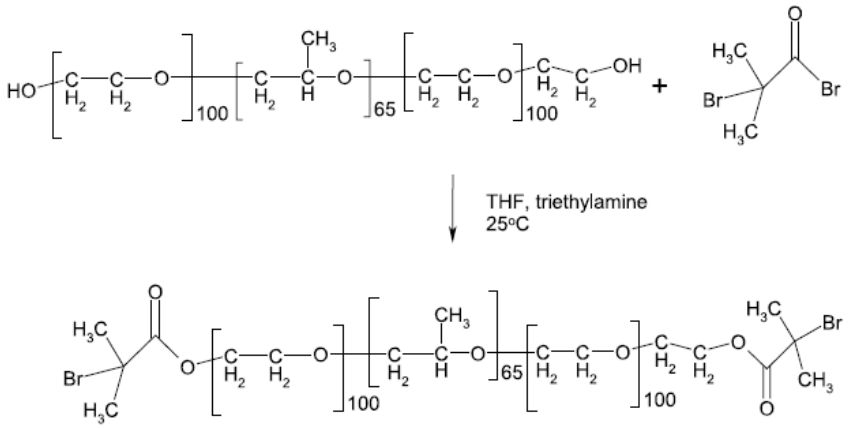

Figure 3.1. Synthesis of difunctional Pluronic F127 macroinitiator.
(Source: Determan et al., 2005)

3.3. Synthesis of Pentablock Copolymers

The pentablock copolymers used in this study, PDEAEM-PEO-PPO-PEO-PDEAEM, were synthesized by atom transfer radical polymerization (ATRP), as explained in detail elsewhere (Determan et al. 2005). A typical synthesis, as depicted in Figure 3.2., was carried out as follows. The macroinitiator (10g) was dissolved in toluene

(50ml) in an argon flushed round bottom flask under continuous stirring during 10 min. Then, 0.24g of catalyst copper (I) bromide (99.99%), 0.5ml of ligand N-propylpyridynyl methanimine (N-PPM) and 4 ml of DEAEM monomer were added to the round bottom flask and degassed via 3 freeze–pump–thaw cycles. A small quantity of copper (0) powder (~1 mg) was added to the reactions in order to enhance the stability of the Cu(I)/Cu(II) equilibrium. Then, the reaction mixture was left overnight under continuous stirring (300rpm) at 70 ºC in oil bath. The reaction mixture was diluted with 50ml of toluene and passed through a column of basic alumina and sand. The excess solvent of the obtained product was removed by rotary evaporator and precipitated in n-hexane, yielding light brown solid. The final product was collected and dried overnight under vacuum. The pentablock copolymers possessing different molecular weights were prepared by changing the DEAEM monomer amount (6ml and 10ml) and following the same procedure mentioned above.

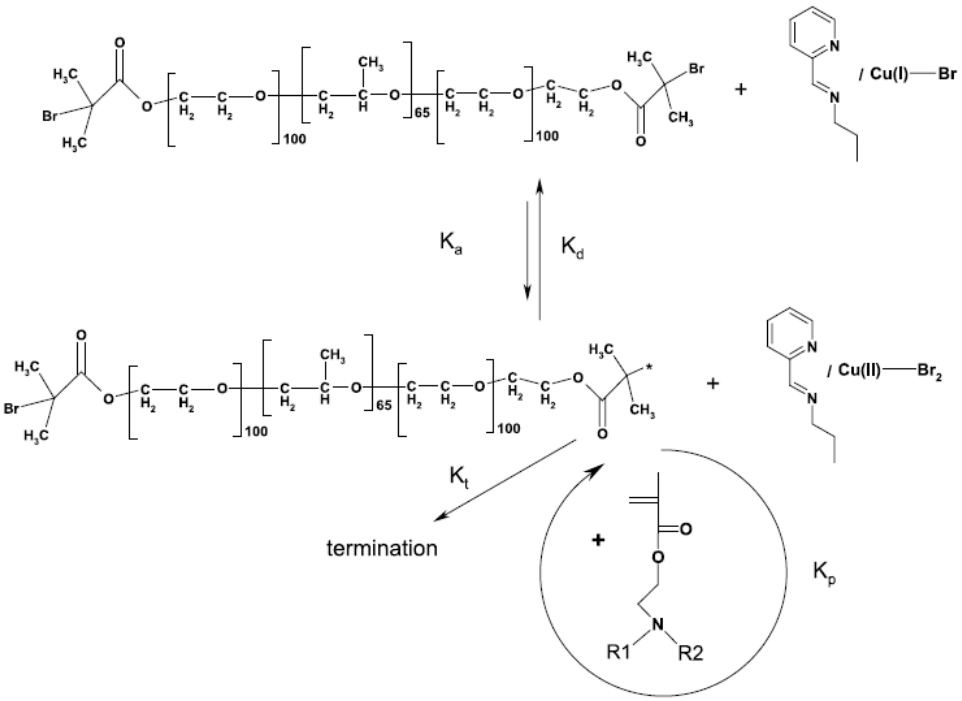

Figure 3.2. Synthesis of pentablock copolymers.
(Source: Determan et al., 2005)

3.4. Characterization of Pluronic F127 Macroinitiator and Pentablock Copolymers

All ^{1}H NMR spectra were collected using a Varian VXR400 (400 MHz) spectrometer, and chemical shifts are given in ppm. Chloroform-d (98%, Fisher) was used as solvent. The copolymer molecular weight and polydispersity index (PDI) were determined using gel permeation chromatography (GPC). The GPC system consisted of a Waters 510 pump, Waters 717 autosampler, a Wyatt Optilab DSP refractometer, and a Wyatt Dawn EOS light scattering detector. The mobile phase was THF at a flow rate of 1 ml/min in the column.

3.5. Preparation of siRNA/Polymer and siRNA/Peptide Complex Systems

siRNA/Polymer complexes at various N/P ratios (N/P : molar ratios of nitrogens (N) in the pentablock copolymer to phosphates (P) in siRNA : 100, 75, 50, 25, 10, 5, 2.5) (siRNA: sense: 5' GAUUAUGUCCGGUUAUGUA-UU 3'; antisense: 5' UACAUAACCGGACAUAAUC-UU 3') were prepared by adding appropriate quantities of pentablock copolymer solution in Hepes Buffer at pH 7.0 to siRNA solution (1µl of 100µM siRNA stock solution). The mixture was briefly vortexed and allowed to incubate at room temperature for 30 min to ensure complexation.

siRNA/Peptide complexes were also obtained by changing the N/P ratio (N/P: 10, 7.5, 5, 2.5, 1.25). The proper quantity of peptide solution in PBS at pH7.4 was added to the siRNA solution (1µl of 100µM siRNA stock solution). After brief vortexing, the mixture was allowed for incubation for 30 min at room temperature.

3.6. Preparation of Multilayer Systems

3.6.1. Preparation of AuNPs

The ~5nm gold nanoparticles were prepared by applying classical sodium borohydrate ($NaBH_4$) reduction method as explained elsewhere (Yang et al. 2006).

Basically, 20 mL aqueous solution containing $2.5x10^{-4}$ M $HAuCl_4$ and $2.5x10^{-4}$ M tri-sodium citrate was prepared. Next, 0.6 mL of 0.1 M $NaBH_4$ solution was added to the solution drop wise while stirring. The reaction was carried out during 6h under stirring at room temperature. The ~13nm gold nanoparticles were prepared by applying the classical citrate reduction method (Turkevich, Stevenson, and Hillier 1951). In a typical experiment, 2 ml of 38.8 mM sodium citrate was quickly injected into 20 ml of 1 mM boiling $HAuCl_4$ solution under vigorous stirring. The heating was continued for 10 min, then, the solution was kept stirred for another 15 min without heating.

3.6.2. PEG Modification of Gold Nanoparticles

The surface of AuNPs were modified by heterobifunctional PEG molecules in order to facilitate subsequent surface modifications. Different amounts of thiol-PEG-amine (HS-PEG-NH2) (0.2 and 1mg/ml) were added to the 5ml of prepared 5nm and 13nm sized AuNP solutions (10 nM). The reaction was carried out under continuous stirring in the dark at room temperature during 24h. The thiol group (-HS) of PEG molecules attach to the AuNP surface through gold-sulfur interactions (Hakkinen 2012). At the end of the reaction, the formed complex was centrifuged under 20000g for 15 min and washed with phosphate buffer (PBS) at pH 7.4 four times to eliminate weakly bound PEGs. For the construction of multilayer siRNA delivery systems, the 13 nm sized AuNP coated by 1 mg/mL PEG was used for further surface modification steps.

3.6.3. SPDP Modification

The PEG coated AuNPs were further modified by SPDP (N-Succinimidyl 3-(2-pyridyldithio)-propionate), which is an amine- and sulfhydryl-reactive heterobifunctional cross linker, in order to facilitate the attachment of siRNA through thiol-disulfide exchange reaction (Figure 3.3.). Freshly prepared SPDP solution (1 mM, 10% DMSO in PBS-EDTA) was mixed with AuNP-PEG solution (10 nM, in PBS-EDTA) in equal amounts and incubated at room temperature under mild stirring during 6 h. At the end of 6 h, the modified particles were centrifuged, washed with PBS for four times in order to remove excess amount of unreacted SPDP.

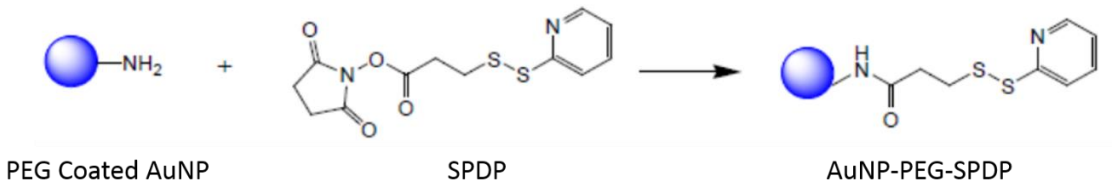

Figure 3.3. SPDP attachment mechanism to PEG-AuNP.

3.6.4. siRNA Loading

Before reacting with SPDP modified AuNPs, the thiol groups attached to the 5' end of the siRNA were deprotected. In order to do that, 400 µl of siRNA (sense: 5' HS-GAUUAUGUCCGGUUAUGUA-UU 3'; antisense: 5' UACAUAACCGGACAUAAUC-UU 3') was reacted with 0.5mM 10 µl TCEP at pH7.4 and incubated 1h at room temperature. At the end of 1h, 50 µl of 3mM sodium acetate at pH5.2 and 1.5 mL of 200 proof ethyl alcohol was added to siRNA solution and the mixture was incubated 2h at -80 ºC. Then, the ethanol precipitated siRNA was centrifuged (20000g, 10min), supernatant was discarded and precipitated SH-siRNA was re-suspended in borate buffer (2.5 M NaCl, 30 mM borate, pH 8, 0.01 % Tween 20). The deprotected thiol modified siRNA (SH-siRNA) was attached to the SPDP-PEG-AuNP conjugate through the thiol-disulfide exchange reaction as indicated in Figure 3.4. Following deprotection, the precipitated SPDP modified AuNPs were resuspended in 500 µl borate buffer containing 15 µM siRNA. The mixture was incubated at room temperature during 48h under continuous shaking. At the end of the incubation, the siRNA loaded AuNPs were precipitated by centrifugation and washed with PBS 3 times in order to remove excess siRNA. The loaded amount of siRNA was determined by Quant-iT™ Ribo Green siRNA detection kit.

Figure 3.4. siRNA attachment mechanism through thiol-disulfide exchange reaction.

3.6.5. siRNA Quantification

The re-suspended siRNA loaded AuNPs were treated with DTT in order to break the disulfide bonds between the siRNA and SPDP cross linker and the quantity of free siRNA was detected by RiboGreenTM RNA reagent kit following the manufacturer's protocol. Basically, the siRNA sample was diluted in 1X TE buffer to a final volume of 100 µl in 96 well plate and 100 µl of the aqueous working solution of the Quant-iT™ Ribo Green reagent was added to each sample. The plate was incubated for 2 to 5 minutes at room temperature in the dark and the fluorescence of the sample was measured at excitation ~480 nm, emission ~520 nm in microplate reader. The calibration curve, theoretical and experimental siRNA loading calculations were shown in Appendix A.1.

3.6.6. Polymer and Peptide Coating

The AuNP-siRNA-Polymer system was prepared through the direct electrostatic complexation between the positively charged pentablock co-polymer and siRNA attached AuNPs. The molar ratios of AuNP/Pentablock copolymers were varied as 1/100, 1/50 and 1/10. The polymer solution in 1x Hepes buffer was added to the 20 nM siRNA-AuNP conjugate and incubated 20 min at room temperature to ensure the complexation. Similarly, for the AuNP-siRNA-Peptide system, the surface of siRNA attached AuNPs were electrostatically coated by positively charged peptide. An appropriate amount of peptide was mixed with 20 nM siRNA-AuNP conjugate in PBS buffer and incubated 20 min at room temperature The molar ratios of AuNP/Peptide were varied as 1/1000, 1/750 and 1/500. Then, the excess polymers and peptides were removed by centrifugation.

3.7. Preparation of Hydrogel System and *in vitro* siRNA Release

To simulate extracellular matrix environment for the in vitro studies, a hydrogel system was created. To each well in a 24-well plate, 75 mg of PEG-DA, 100 µl of photo initiator (0.2 wt.% solution in water), 200 µl of deionized water and appropriate amount of Pluronic F127 were added with the final pluronic concentration of 15% in well. The plate was then placed in a refrigerator overnight and gently vortexed before exposure to

UV light. The solution was photo crosslinked under UV beam of 50 MW/cm^2 for 2 min. After gel formation, they were carefully scraped out using a spatula and soaked in 50 ml of DI water for 3 days at −4 °C with water changed every day. Appropriate amount of pluronic was added to the AuNP and polymer based multilayer system solution at 4 °C to make the final PL concentration around 20 wt %. At this concentration, the delivery system solution can be injected as liquid and can form a solid gel in response to the change in surrounding temperature (37 °C). The pre-warmed PEG-DA gels were placed in the Transwell inserts equipped on the 6-well plates. Each well contained 1.5 ml of PBS with 5% of DTT. The plate was then placed on an incubator shaker and shaken with 100 rpm at 37 °C for 3 days. In predetermined time intervals the samples were collected and the released siRNA amount was determined by siRNA detection kit.

3.8. Preparation of siRNA/Peptide Conjugate System

For an efficient siRNA release, the siRNA was attached to the peptide through cleavable disulfide bonds. For this purpose, first, the peptide was modified by the amine reactive portion of SPDP cross linker (Figure 3.3.). The peptide solution (115 µM) was reacted with 25 µL of SPDP solution (20 mM, 10% DMSO in PBS-EDTA) during 3h under continuous stirring at room temperature. At the end of the reaction the unreacted SPDP was removed from the mixture through polyacrylamide gel desalting column. The SPDP modified peptides collected from the column were concentrated in speed vacuum evaporator and reacted with DTT in order to reveal pyridine-2-thione group. The SPDP modification degree was calculated through determining pyridine-2-thione group the concentration of which can be determined by measuring the absorbance at 343nm Appendix A.3.. Following the SPDP modification, the deprotected thiol modified siRNA was attached to the peptide through the disulfide exchange reaction (Figure 3.4.). For this purpose, different amounts of peptide solution (115 µM) was reacted with 20 µM siRNA solution in borate buffer (2.5 M NaCl, 30 mM borate, pH 8.5, 0.01 % Tween 20) during 48h at room temperature. The siRNA/Peptide molar ratio was changed as 5, 2.5, and 1.25.

3.9. Agarose Gel Electrophoresis

The siRNA condensation and formation of the complex, conjugate and multilayer systems was visualized on a 2% (w/v) agarose gel containing 0.5 µg/mL ethidium bromide (EtBr) for 30 min at 100 V in a 1xTAE buffer solution (40 mM Tris–HCl, 1% (v/v) acetic acid, and 1 mM EDTA). To investigate the protective effect and stability of the systems against RNase and serum proteins, the systems were incubated with 0.25% RNase and 50% serum containing HEPES buffer at 37°C for 1 h and 6 h, respectively. Then, the samples were loaded in wells and their electrophoretic mobility was visualized under the same conditions mentioned above using a UV-trans illuminator.

3.10. Characterization of the AuNPs besed Multilayer Systems

The size, size distribution and zeta potential of the multilayer system were determined by Dynamic Light Scattering (DLS) (Malvern Zetasizer Nanozs90).

The shift in specific wavelengths at which maximum absorption was observed for bare AuNPs (520nm for ~13nm AuNPs and 512nm for ~5nm AuNPs) was used to verify the adsorption of each layer.

The stabilities of the siRNA loaded polymer or peptide coated AuNPs were determined by measuring the changes in their size and zeta potential after 24h of incubation with serum supplied cell culture medium at 37 °C in a 5% CO_2 humidified atmosphere. Following the incubation, the samples were centrifuged, washed with PBS in order to remove the medium and the size and zeta potential of the samples resuspended in PBS were measured in DLS.

The naked and PEG coated AuNPs were visualized by Transmission Electron Microscopy (TEM) (FEI-Tecnai 2-F20). Samples were prepared by dipping a carbon-coated copper grid (Ted Pella 400 mesh Cu Holey Carbon) in 20 µL colloidal nanoparticle solution and air-dried before taking images. For visualization of PEG layer around AuNPs, a copper grid, prepared as described above, was deposited in a uranyl acetate (2% v/v) aqueous solution for 5 min. Excess solution on the grid was wiped off using a filter paper and residual solution was air-dried. X-ray photoelectron spectroscopy (XPS) was also used to confirm the presence of PEG layer on AuNPs. Samples were prepared by adding a small drop of an aqueous solution of gold nanoparticles onto a silicon wafer and

air dried. Analyses were performed using a monochromatic Al KX-ray source (1486.6 eV) with an Omni Focus III small area lens and multichannel detector. Measurements were taken at an electron take-off angle 45º from a normal sampling surface depth of ~50 Å. The binding energy scale was calibrated prior to analysis by the Au4f7/2 peak at 83.9 eV. Survey scans were collected from 10 eV to 1100 eV with a pass energy of 187.85 eV. All spectra were referenced by setting the C 1s peak to 285.0 eV to compensate for residual charging effects.

3.11. Cell Culture

The luciferase-expressing SKOV3 cells (Creative Biogene CSC-RR0061) were grown in high glucose Dulbecco's Modified Eagles Medium (DMEM, Invitrogen) supplemented with 10% (v/v) fetal bovine serum (FBS, heat inactivated, GIBCO), 0.1 mM MEM Non-Essential Amino Acids (NEAA), 2 mM L-glutamine and 1% Pen-Strep. PC-3 cells and 3T3 cells were cultured in high glucose DMEM supplemented with 10% FBS, while CaCo-2 cell line was cultured in RPMI medium supplemented with 20% FBS. Cells were incubated at 37°C under a humidified atmosphere containing 5% CO_2. Cells were passaged approximately every 2–3 days.

3.12. Cellular Uptake of AuNP based Conjugates and Multilayer Systems by ICP-MS

To measure the cellular uptake of PEG coated AuNPs, PC-3, CaCo-2 and 3T3 cells (2×10^5 cell/well) were plated in each well and incubated with the samples at 37 °C in a 5% CO_2 humidified incubator for 24h. In order to determine the cell uptake of AuNP-siRNA-Polymer and AuNP-siRNA-Peptide multilayer systems, the SKOV3 cells (2×10^5 cell/well) were plated in each well and incubated with the developed systems at 37 °C in a 5% CO_2 humidified incubator for 24h. After incubation, the cell culture medium was removed and the exposed cells were further washed with PBS to remove nanoparticles existing in the medium or adhering to the outer cell membrane. The cells were then harvested, dispersed into culture medium and collected by centrifugation. After removal of supernatant, the cell pellet was treated with 500 μL of concentrated nitric acid (HNO_3) at 70 °C for 4 h to digest AuNPs (Gu et al. 2009). Following serial dilutions, the quantity

of Au was analyzed by Inductively Coupled Plasma Mass Spectroscopy (ICP-MS) (Agilent 7500ce). The number of AuNPs per cell was calculated as described in Appendix A.2.

3.13. Cytotoxicity Tests

For the toxicity evaluation of PEG coated AuNPs, the PC-3, CaCo-2 and 3T3 cells (95 µl) were plated at a density of 1×10^4 cells/well in 96-well plates. After 24 h incubation at 37 °C in a 5% CO_2 humidified incubator, the cells were exposed to different concentrations of 5nm and 13 nm AuNPs (5µl) (50, 25, 12.5 µM) coated by different PEG concentrations (0.2 and 1 mg/mL) and incubated for 24 h. In order to evaluate the toxicities of the developed siRNA/Polymer, siRNA/Peptide complexes, siRNA/Peptide conjugates and AuNP based multilayer siRNA delivery systems, SKOV3 cells (95 µl) were plated at a density of 1×10^4 cells/well in 96-well plates. After the cells reached confluency at the end of 24h, the systems were applied at different doses and cells were further incubated for 24h. Following incubation, the cell culture medium in the well plates was removed and 100 µL of MTT dye (0.5 mg/mL in PBS at pH 7.4) was added to each well and incubated for further 4 h. At the end of incubation, the 96-well plate was centrifuged and the medium was removed. Then, the precipitated formazan crystals were solubilized with 100 µL of DMSO and the absorbance was measured spectrophotometrically at 570 nm in microplate reader (Thermo Scientific, Varioskan Multimode Microplate Reader).

3.14. Luciferase Activity Test

The SKOV3 cells (100 µl) were plated at a density of 2×10^4 cells/well in separate 96-well plates and incubated 24h at 37 ºC in a 5% CO_2 atmosphere. Then, the siRNA/Polymer, siRNA/Peptide complexes, siRNA/Peptide conjugates and multilayer siRNA delivery systems were administered to the wells at various concentrations and further incubated for 24h under same conditions. Following incubation, the growth medium was removed and the cells were washed with PBS. 20 µl of 1X lysis buffer was added to the cells and the plate, containing 20 µl of cell lysate per well, was placed into

the luminometer (Veritas Microplate Luminometer). Following the instant injection of 100 µl Luciferase Assay Reagent into each well, the luminescence values were recorded.

3.15. Synthesis of Fluorescent Dye-Attached Pentablock Copolymers

The previously synthesized pentablock copolymer (Polymer A) was modified by alkyne attached fluorescence dye AlexaFluor 488 through the azide-alkyne click reaction for intracellular trafficking studies. Pentablock copolymer was amine functionalized by transforming the bromine group into azide. For this purpose, 3 g of pentablock copolymer was reacted with 300 mg of sodium azide in 15 mL dimethylformamide (DMF). The reaction was carried out at 50 ºC under continuous stirring (300 rpm) during 24 h and the excess DMF was removed by rotary evaporation. The remaining polymer was dissolved in water, the excess sodium azide was removed by dialysis and the modified polymer was freeze-dried. The AlexaFluor 488 alkyne dye was attached to the azide modified polymer via copper-catalyzed azide alkyne click reaction. The azide-modified polymer (20 mg/ml) was reacted with 100 µg dye in DMF with 4.7 mg ascorbic acid and 3.325 mg copper II sulphate under continuous stirring during 2 h in the dark. The excess dye was removed by dialysis during 24 h and the purified polymer was freeze-dried. siRNA/Polymer complexes and AuNP-siRNA-polymer conjugates were prepared using the dye-attached polymers by following the same procedure used for the polymer not attached to the dye.

3.16. Synthesis of Fluorescent Dye-Attached Peptides

The peptides were labelled by NHS-Fluorescein dye through the reaction between the NHS esters existing in the dye structure and primary amino groups present in the peptide structure. 1 mg/mL peptide solution in 50 mM borate buffer at pH 8.5 was reacted with 1 mg/mL FITC in DMSO during 3h. Then, the unreacted dye was removed through polyacrylamide gel desalting column and the collected samples were concentrated in speed vacuum evaporator. The labelling degree of the peptide was calculated in Appendix A.4.

3.17. Cellular Uptake of siRNA/Polymer and siRNA/Peptide Complexes by Flow Cytometry

The cellular uptake rates of the siRNA/Polymer and siRNA/Peptide complexes were evaluated through the flow cytometer analysis. The SKOV3 cells were seeded ($2x10^5$ cell/well) and grown to 80% confluency. Then, the complexes with different N/P ratios, prepared by using fluorescence dye attached polymer and peptide, were applied to the cells. After 24 h of incubation at 37°C under 5% CO_2 atmosphere, the cells were harvested and washed with PBS and kept cold until the analysis. Then, the fluorescence intensity of the complexes within the cells were measured by flow cytometer (BD Biosciences Facs Canto).

3.18. Visualization of siRNA/Polymer, siRNA/Peptide and AuNP Based Multilayer Systems through Confocal Microscopy

The SKOV3 cells (2 mL) were plated at a density of 2×10^5 cells/well in cell culture petri dishes and incubated 24 h at 37 ºC in a 5% CO_2 atmosphere. Then, the siRNA/Polymer, siRNA/Peptide and AuNP based multilayer systems prepared using the dye-attached polymers and peptides were administered to the wells and further incubated with cells during 24 h under same conditions. For live cell imaging, first, the growth medium was removed and cells were washed 3 times with PBS. Then, 2 mL of serum free medium was added to wells and 250 nM Lysotracker Red was added. The petri dishes were incubated 30min at 37 ºC in a 5% CO_2 atmosphere. For the nucleus staining with Hoechst, the growth medium with Lysotracker Red was removed and washed 3 times with PBS. Following this, 2 mL of serum free medium was added to petri and 1 µM of Hoechst dye was applied. The dye applied petri dish was incubated 30 min at 37 ºC in a 5% CO_2 atmosphere for nucleus staining. At the end, the cells were washed again and analyzed through confocal microscopy.

3.19. Cell Cycle and Apoptosis Analysis of PEG coated AuNPs with Flow Cytometry

PC-3, CaCo-2 and 3T3 cells were grown ($2x10^5$ cell/well) in 6-well plates at 37 °C in a 5% CO_2 humidified incubator for 24 h and then further incubated under same conditions with PEG coated AuNPs (50, 25 and 12.5 µM) in culture medium for another 24 h. After incubation, cells were harvested, centrifuged at 1200 rpm for 10 min and supernatant was discarded. The precipitated cells were suspended in 1ml PBS solution, fixed with cold ethanol (at −20 °C, 70%) under continuous vortex and stored at -20 °C until analysis. On the day of experiment, the fixed cell suspensions were washed by centrifugation (1200 rpm for 10 min) three times and precipitate was suspended in 1ml of PBS containing 0.1% Triton X-100. The cells were further treated with 200 µg/mL RNase for 30 min at 37 °C and then, DNA staining with 100 µg/mL of propidium iodine was conducted at room temperature for 15 min. Samples were analyzed through flow cytometer (BD Biosciences Facs Canto) and data were analyzed using Modfit flow cytometry analyzing software.

For the apoptosis test, the same NPs with the same doses were applied to the cells and incubated as in cell cycle analysis. Then, the cells were harvested, washed with cold PBS and centrifuged. The cell pellet was resuspended in annexin-binding buffer and 5 µl of Annexin V FITC Conjugate and then, Propidium Iodide solution was added to the sample in order to detect apoptotic and necrotic cell populations, respectively. Finally, the cells were incubated at room temperature for 15 minutes and measurement was conducted by flow cytometer.

3.20. Evaluation of DNA Damage caused by PEG coated AuNPs with Comet Assay

The cells grown in 6-well plates ($2x10^5$ cell/well) were exposed to PEG coated AuNPs for 24 h at 37°C in a 5% CO_2 humidified incubator. Then, they were harvested, washed with PBS for two times and re-suspended in PBS. 5 µl cell suspension was embedded in 75µl of 1% low melting agarose and spread on previously prepared comet slides and lysed in prechilled lysis solution (1.2 M NaCl, 100 mM Na_2EDTA, 0.1% sodium lauryl sarcosinate, 0.26 M NaOH (pH > 13)) during 24 h. Cells were then

subjected to denaturation solution (0.03 M NaOH, 2 mM Na_2EDTA (pH 12.3)) for 45 min in the dark at room temperature. After denaturation, electrophoresis was performed at 25 V and 90 mA for 20 min. The slides were immersed in dH_2O for neutralization for 15 min. Subsequently, they were stained with propidium iodide (PI) dye (10µg/ml) during 20 min and washed with water to remove excess dye (Olive and Banath 2006). Hydrogen peroxide (H_2O_2) was used as positive control. The images were taken by using fluorescence microscopy and analyzed using image analysis software.

3.21. Preparation of Dye Attached PEG coated AuNPs

For the fluorescence microscopy imaging, the PEGylated AuNPs were reacted with fluorescein isothiocyanate (FITC) dye. For this reaction, 1 mg of FITC was dissolved in 200 µL of anhydrous dimethylformamide (DMF) and added to 50µM nanoparticle solution. The suspension was vortexed and placed on a shaker for 24 h. Free FITC molecule was removed by centrifugation and washing with PBS.

3.22. Visualization of Dye Attached PEG coated AuNPs by Fluorescence Microscopy

PC-3, CaCo-2 and 3T3 cells (2×10^5 cell/well) were plated in each well and grown on a microscope slide at 37 °C in a 5% CO_2 humidified incubator for 24 h. The cells were further incubated with the FITC attached conjugates for 24h under same conditions. After incubation, the cell culture medium was removed and the exposed cells were further washed with PBS. Then, the cells were fixed with 4% paraformaldehyde (PFA) in PBS for 20 min at room temperature. The cells were then washed with PBS for three times and they were permeabilized with 1 mL 0.1% tritonx100 in PBS for 15 min at room temperature. Following this, the cells were blocked with 0.5ml 3% BSA in 0.1% tritonx100/PBS for 30 min. Finally, the cells were incubated with 300µl 4',6-diamidino-2-phenylindole (DAPI) dye (300 nM) for 3 min in the dark. At the end of incubation, the cells were washed with PBS and mounted on a microscope slide with 1:1 PBS:Glycerol before taking fluorescence images.

3.23. Statistical Analysis

The significant difference between the groups were evaluated by ANOVA analysis by Tukey's method with 95% confidence interval. The results were presented as mean ± standard deviations which were calculated from at least three independent experiments.

CHAPTER 4

RESULTS AND DISCUSSIONS

4.1. PEG Modified AuNPs for Imaging Purposes

4.1.1. Characterization of PEG Modified AuNPs

Two different sized (~5 nm and ~13 nm) bare AuNPs were synthesized and modified with varying amounts of heterobifunctional PEG (HS-PEG-NH_2: 0.2 and 1 mg/mL) in order to prepare PEG coated AuNPs with different surface properties. The code of the nanoparticles along with the preparation conditions are shown in Table 4.1.

Table 4.1. The codes of the prepared PEGylated AuNPs.

Code of the Nanoparticles	**Bare AuNP Size (nm)**	**PEGConcentration (mg/mL)**
Particle A	5	0.2
Particle B	5	1.0
Particle C	13	0.2
Particle D	13	1.0

Successful coating of AuNPs with PEG was first shown with DLS data by an increase in the cumulative size of the bare AuNPs (Table 4.2). The results in Table 4.2 have shown that with the increased PEG concentration , the thickness of the PEG layer on the 5 nm sized nanoparticles changed significantly whereas the layer on the 13 nm sized AuNPs became thicker (the thickness increased from 5.16 nm to 7.04 nm). The PEG layer coated on the AuNPs was also observed in TEM images (Figure 4.1.). The thicknesses of layers determined from the images (~4nm for the layers on all 5 nm sized particles and ~2 nm and ~3 nm for the coatings on 13 nm sized particles when they were modified with 0.2

mg/ml and 1 mg/mL PEG concentration, respectively) were found slighly lower compared to the values calculated from the DLS data. Due to higher surface area and curvature allowing more PEG attachment, the PEG layer formed on the 5 nm sized AuNPs is thicker than that on the 13nm sized particles (Rahme et al. 2013).

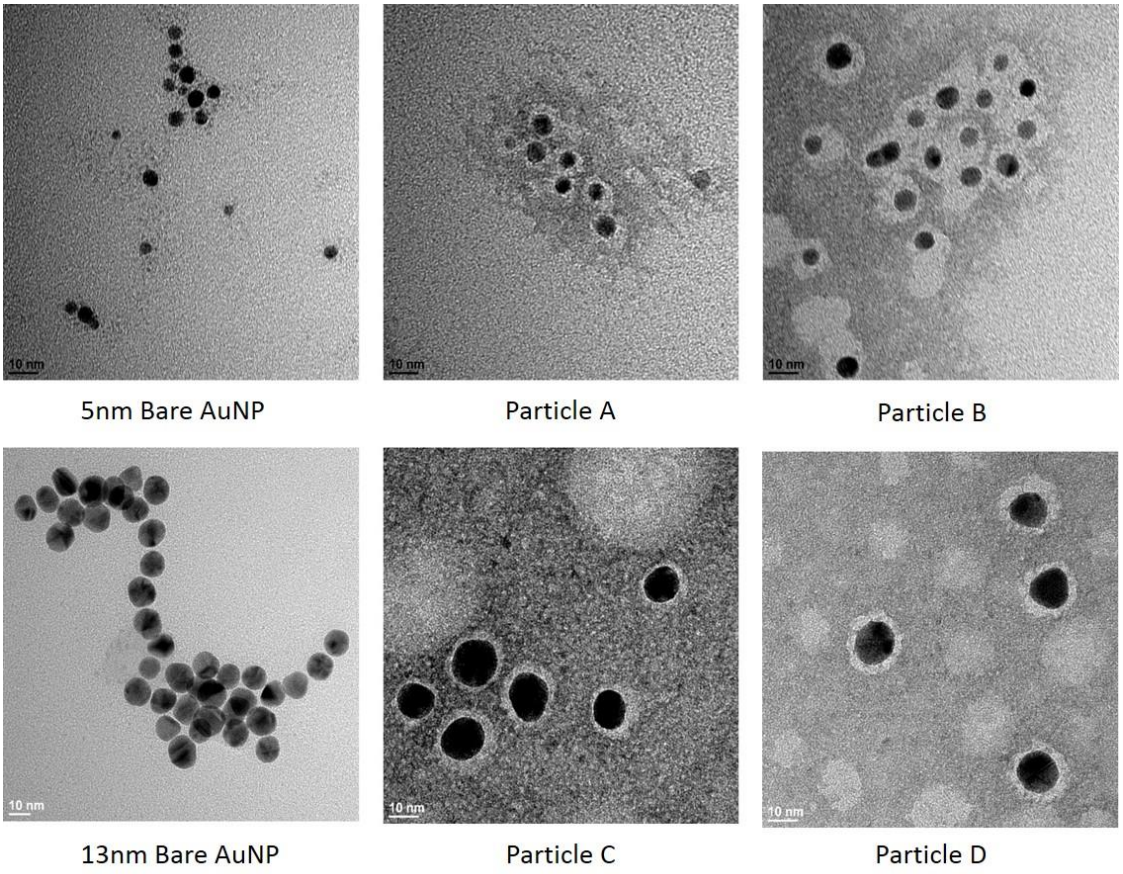

Figure 4.1. TEM images of bare and PEG coated AuNPs. AuNP size: 5 nm and 13 nm. Applied PEG concentration: 0.2 and 1 mg/mL.

The change in zeta potential values was another indication of successful PEG coating. Upon PEG attachment, the negatively charged surfaces of the bare AuNPs become positively charged due to the presence of $–NH_2$ groups at the open end of the PEG (Table 4.2). The PEG concentration did not cause a significant change in the zeta potential of the particles formed from 5 nm AuNPs while the surface of the 13 nm sized nanoparticles became more positively charged by increasing the PEG concentration from 0.2 to 1 mg/ml. The XPS data and the change in the UV-vis spectra of the particles can also give clues about the success of the surface modifications. According to the XPS data (Figures C.1. and C.2. in Appendix C), the formation of C-O bond at 286.5 eV corresponds to the presence of PEG layer on the AuNP surface (Damodaran et al. 2010). Maximum

absorption in the UV-Vis spectra for the 5 nm and 13 nm sized bare AuNPs are observed at 512 nm and 520 nm, respectively (Figures 4.2 and 4.3). In the case of 5 nm AuNPs, the absorbtion maximum shifted from 512 nm to 517 and 518 nm upon attachment of 0.2 mg/ml and 1mg/ml PEG on the surface, respectively. Similarly, when the 13 nm AuNPs were modified with the same PEG concentrations, the shift from 520 nm to 525 nm and 526 nm was observed. Compared to bare AuNPs, there was a slight broadening in UV-spectra for the particles indicating that they did not form aggregates. The stabilities of the particles in serum supplemented cell culture medium were evaluated through the changes in the size and zeta potential values (Table 4.2). In general, most of the particles prepared were stable in the medium since the incubation with the medium did not cause significant change in the size of the particles. However, their positively charged surfaces turned to negative, most probably due to the attachment of negatively charged medium components.

Table 4.2. Size and zeta potential values of prepared particles before and after serum supplemented cell culture medium incubation. *represents statistically insignificant difference (p>0.05).

		Before Serum Incubation		After Serum Incubation	
	5 nm Bare AuNP	**Particle A**	**Particle B**	**Particle A**	**Particle B**
Size (nm)	5.5 ±1.2	13.09 ±0.35	15.35 ±1.34	13.5 ±0.24	20.9 ±1.34
Zeta Potential (mV)	-34.4 ±0.9	11.2 ±0.28*	12.6 ±1.03*	-7.7 ±0.24	-21.5 ±1.15
PEG Layer Thickness (nm)		7.59 ±0.53	9.85 ±1.34	8 ±0.24	15.35 ±1.34
	13 nm Bare AuNP	**Particle C**	**Particle D**	**Particle C**	**Particle D**
Size (nm)	11.78 ±1.34	16.94 ±0.26	18.83 ±0.07	16.39 ±0.59	19.5 ±1.5
Zeta Potential (mV)	-32.5 ±1.67	16.1 ±0.67	21.6 ±0.23	-10 ±0.19	-21.1 ±1.3
PEG Layer Thickness (nm)		5.16 ±0.26	7.04 ±0.07	4.6 ±0.59	7.7 ±1.5

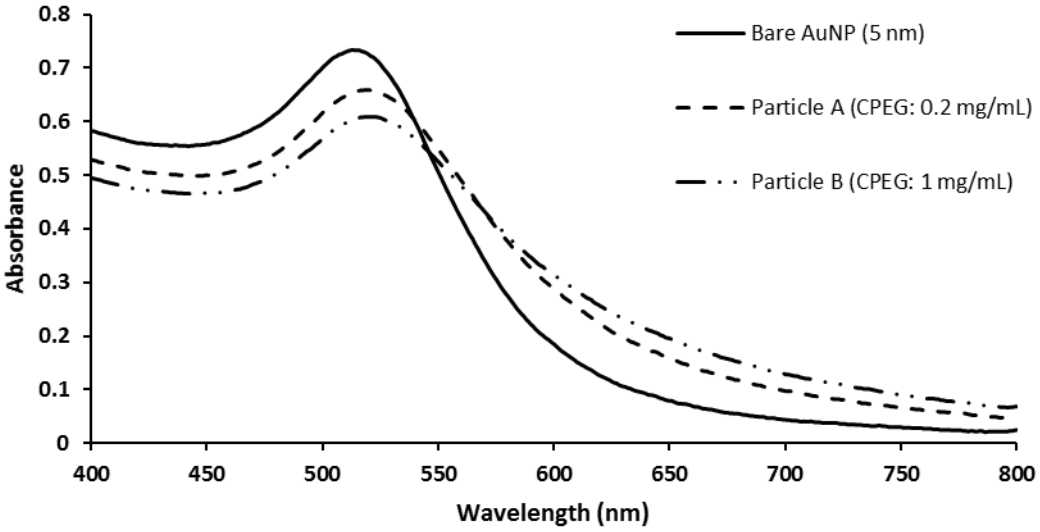

Figure 4.2. UV-vis spectra of 5 nm sized AuNPs modified with 0.2 and 1 mg/mL PEG.

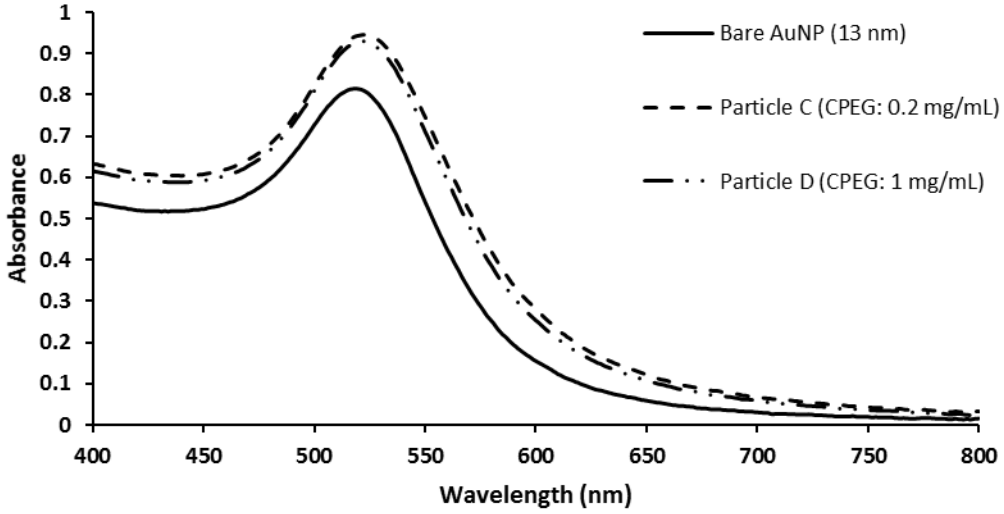

Figure 4.3. UV-vis spectra of 13 nm sized AuNPs modified with 0.2 and 1 mg/mL PEG.

The conformation of PEG chains attached to the nanoparticles was calculated from the Flory Radius (*Rf*). As shown in Eq. 4.1., Flory radius is a function of the PEG size (*a* = 3.5 Å) and the number of monomer units (*N*) (Rahme et al. 2013, Damodaran et al. 2010).

$$Rf = a\,N^{3/5} \tag{4.1.}$$

The PEG chains can acquire either 'mushroom' or 'brushed' configurations. The 'mushroom' conformation mainly occurs when the distance, *D*, between the attachment points of PEG to the surface is larger than *Rf* (*D* > *Rf*); however, the 'brush' conformation is observed when *D* < *Rf* (Rahme et al. 2013) (Damodaran et al. 2010). Using the thickness of the PEG layer obtained from DLS measurements after incubation with serum supplemented culture medium (*t*) and the density of PEG (ρ=1.09 g/ml), the surface concentration (Γ, g/nm^2), and the average distance between grafted PEG chains (*D*, nm) were calculated using Eq. 4.2. and 4.3., respectively.

$$\Gamma = \rho t \tag{4.2.}$$

$$D = \left(\frac{M}{\Gamma N_A}\right)^{1/2} \tag{4.3.}$$

In Eq. 3, *M* is PEG molecular weight (Da) and N_A is Avogadro's number (6.02 x 10^{23} mol^{-1}).

Finally, the grafting density (σ) was calculated from Eq. 4.4. and the results are represented in Table 4.3.

$$\sigma = \left(\frac{a}{D}\right)^2 \tag{4.4.}$$

Table 4.3. Conformation, PEG layer thickness and grafting density of AuNP-PEG particles.

Particle **Type**	**Conformation**	**PEG Layer Thickness (nm)**	**Grafting Density (g/nm^2)**
Particle A	Brushed (R_F > D)	7.59 ±0.24	0.67 ±0.02
Particle B	Brushed (R_F > D)	9.85 ±1.34	0.92 ±0.1
Particle C	Brushed (R_F > D)	5.16 ±0.59	0.36 ±0.05
Particle D	Brushed (R_F > D)	7.04 ±1.5	0.62 ±0.12

The theoretical calculations indicated that the PEG layers deposited on each particle possessed brushed like conformation. This could be due to utilizing excess amount of PEG concentration to completely cover the surface of the nanoparticles. Although all particles have the same conformation, their grafting density increased with respect to increased PEG concentration. It was observed that 5 nm sized AuNPs have higher grafting density due to their higher surface area than the 13 nm sized ones and this result is in agreement with the findings in the literature (Rahme et al. 2013). The influence of PEG grafting density on the serum protein adsorption levels can be qualitatively evaluated from the the zeta potential values measured before and after serum incubation. Upon incubating the nanoparticles with the cell culture medium, the PEG coated AuNPs prepared from smaller AuNPs (5 nm) exhibited lower reduction in zeta potential values ($\Delta\Phi$) ($\Delta\Phi$=18.9 mV for Particle A prepared from 5 nm AuNPs and $\Delta\Phi$=26.1 mV for Particles C prepared from 13 nm AuNPs). This result suggests that less serum protein adsorption occurred on the 5nm AuNP based PEG coated AuNPs than on the 13 nm AuNP based PEG coated AuNPs due to their higher PEG grafting densities, i.e., increasing PEG density decreases total serum protein adsorption.

4.1.2. Cellular Uptake of PEG Modified AuNPs

The cellular uptake of particles by CaCo2, PC3 and 3T3 cells at the end of 15, 30 and 60 minutes was estimated by measuring the internalized Au concentration with ICP-MS (Figure 4.4.).

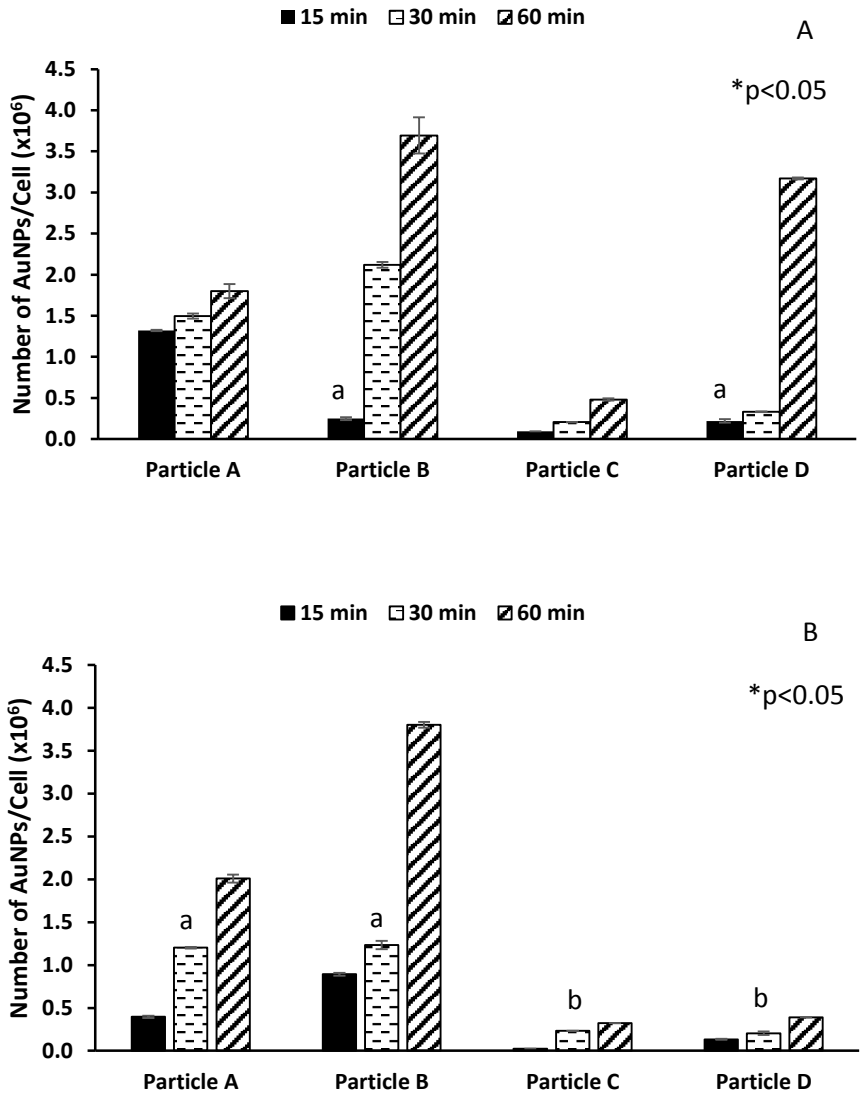

Figure 4.4. Time dependent cellular uptake of PEG modified AuNPs in A) CaCo2 cells, B) PC3 Cells C) 3T3 Cells. Applied dose: 50 µM. Incubation times: 15, 30 and 60 min. Same letters indicate the statistical indifference: a, b $p>0.05$. * indicates statistical difference for all cases: $*p<0.05$

(Cont. on next page)

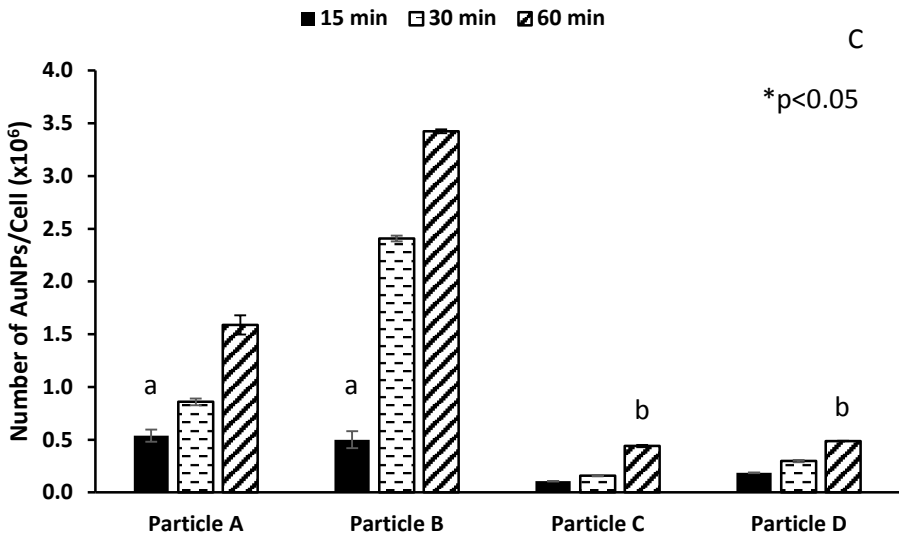

Figure 4.4. (Cont.)

Although both bare and PEG modified nanoparticles are negatively charged, they are uptaken by the cells. The cellular uptake of negatively charged nanoparticles with different core materials has also been reported in other studies (Cho et al. 2010). The published data in general showed lower levels of internalization for the negatively charged nanoparticles as compared to the positively charged ones (Cho et al. 2010).The internalization of negatively charged particles is thought to take place through nonspecific binding and clustering of the particles on cationic sites on the plasma membrane (Verma and Stellacci 2010). As shown in Figure 4.4., the uptake of the nanoparticles by all cell types is highly dependent on the size of bare AuNPs and PEG concentration used for coating. The uptake is higher for the PEG coated AuNPs prepared from 5 nm sized AuNPs than for those synthesized from 13 nm sized AuNPs (Particle A > Particle C or Particle B> Particle D). Similarly, the internalization of AuNPs PEGylated with 1 mg/ml PEG is higher than that of the nanoparticles coated with 0.2 mg/ml PEG (Particle B> Particle A or Particle D> Particle C). The results clearly indicate that the PEG grafting density is the primary factor in determining the cell uptake by regulating the interaction of nanoparticles with the cell surface. Higher cellular uptake of the AuNPs coated with 1 mg/ml PEG compared with those modified with 0.2 mg/ml PEG and the higher cellular uptake of the PEG coated AuNPs prepared from 5 nm sized AuNPs compared to the PEG coated AuNPs synthesized from 13 nm AuNPs can be attributed to their higher grafting densities as shown in Table 4.3. The cellular uptake of the bare AuNPs seemed to be determined by their size. According to the results shown in Table 4.2, the size of bare AuNPs

increased significantly after incubation in cell culture medium as a result of adsorption of serum proteins. Consequently, at least 10 times larger size of the uncoated AuNPs than those of PEGylated ones significantly reduced their internalization into the cells. In previous studies, the shape and size of the nanoparticles has been found to significantly affect binding and activation of membrane receptors and subsequent cellular uptake (Chithrani, Ghazani, and Chan 2006, Chithrani et al. 2009). Chithrani et al. (2006) investigated the uptake of 14, 30, 50, 74 and 100 nm AuNPs and observed the highest cell uptake with 50 nm sized AuNPs. Their results indicate that there might be an optimum nanoparticle size for efficient uptake of nanoparticles into the cells.

The amount of nanoparticles in the cells accumulated at the end of 24 hour was also measured. According to the results in Table 4.4, the accumulation of the bare AuNPs in all cell types is lower than the PEG modified particles. This indicates the advantage of PEG coated AuNPs since the accumulation inside a cell for an extended period of time can lead to improvements in diagnostic sensitivity and therapeutic efficiency. The accumulation of nanoparticles in the cells was found to depend upon the size of the bare AuNPs. Regardless of the PEG concentration used for coating, the PEGylated nanoparticles prepared from 5 nm AuNPs (Particles A and B) accumulated more in the cells than the modified nanoparticles synthesized from 13 nm AuNPs (Particles C and D). In addition, the coating of both 5 and 13 nm AuNPs with higher PEG concentration (1 mg/ml instead of 0.2 mg/ml) enhanced cellular accumulation of the nanoparticles. These results show the importance of PEG grafting density on the accumulation of the nanoparticles in the cells. Higher nanoparticle concentration in the all cell types is a consequence of higher PEG grafting densities on the 5 nm AuNPs than on the 13 nm ones or higher PEG grafting densities of the nanoparticles prepared from 1 mg/ml PEG as compared to the nanoparticles modified with 0.2 mg/ml PEG (Table 4.3.).

Table 4.4. Cellular accumulation of AuNP-PEG particles with respect to particle and cell type. The applied dose: 50 μM. Incubation time: 24h.

	Number of AuNPs per Cell (x10^6)		
	CaCo2	**PC3**	**3T3**
Particle A	4.81 ±0.02	1.17 ±0.007	9.45 ±0.14
Particle B	4.33 ±0.113	1.23 ±0.0018	11.4 ±0.19
Bare 5nm AuNP	0.16 ±0.027	0.86 ±0.038	0.21 ±0.005
Particle C	0.27 ±0.015	0.10 ±0.0018	0.54 ±0.017
Particle D	0.32 ±0.016	0.13 ±0.0007	0.73 ±0.0035
Bare 13nm AuNP	0.02 ±0.0002	0.05 ±0.0002	0.02 ±0.00095

4.1.3. Cytotoxicity of PEG Modified AuNPs

The results shown in Figures 4.5 through 4.7 indicate that the toxic effect of the particles may change depending on the cell type, applied dose, size and surface properties of the nanoparticles. The dose of the applied particle influenced the cell viability significantly. For almost all PEG coated AuNPs, the increase in the applied dose resulted in a decrease in viability of all cell lines as expected. The PEG grafting density plays a significant role on the toxicity of the nanoparticles. The particles with higher PEG grafting densities (Particle B> Particle A and Particle D) exhibited lower toxicities on two cancer cell lines, $CaCO_2$ and PC3. This comes from the stealth effect of the PEG as reported in previous studies (Zhang et al. 2011, Zhang, Wu, et al. 2012, Cho et al. 2010)**.** The impact of the PEG grafting density was found to be insignificant for 3T3 cell line. In addition to grafting density, the zeta potential values of the nanoparticles also influenced their toxicities. Decreased negative charge on the surface caused higher toxicity. After incubating with serum proteins, the zeta potential of Particle A was -7.7 mV while that of Particle B was three times higher (-21.5 mV). Among the cell lines tested, PC3 was most significantly influenced by the surface charge and PEG grafting density of the nanoparticles. The difference in the toxicity of the same particles in different cell lines may be due to different characteristics of the cells or intracellular behaviors of the particles. The toxicities of the particles did not increase with their cell uptake or

accumulation levels in the cells. Indeed, the particles internalized and accumulated at higher rates in the cells showed less toxic effect.

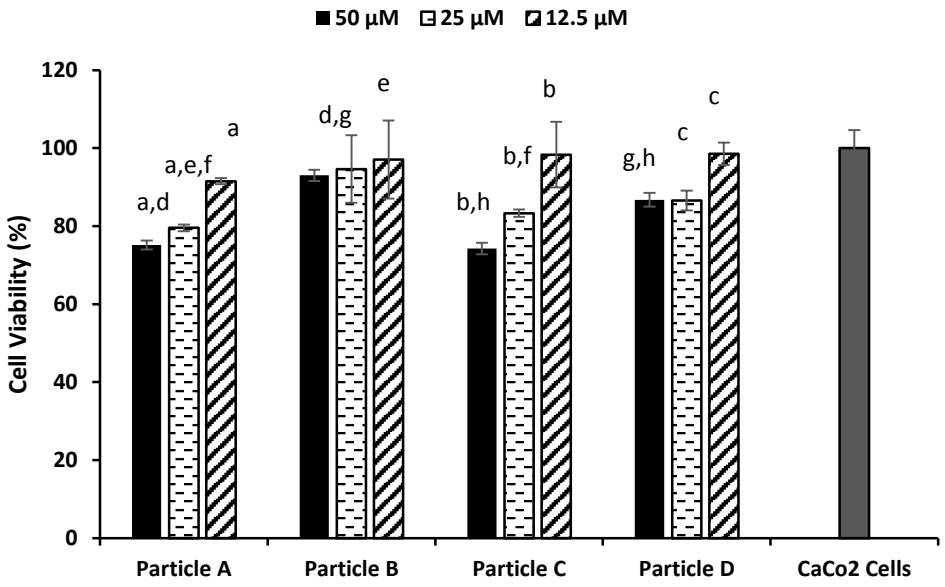

Figure 4.5. Cell viability of CaCo2 cells transfected with AuNPs-PEG particles. Incubation time: 24h. a, b, c: represent doses of particles which caused significant difference in cell viability. d,e: represents PEG coating concentration which caused significant difference in cell viability for Particles A and B at dose of 25 and 12.5 µM respectively. h: represents PEG coating concentration which caused significant difference in cell viability for Particles C and D at the dose of 50 µM. f, g: represents the significant difference in the effect of bare AuNP size on cell viability for Particles A and C at the dose of 12.5 µM and Particles B and D at the dose of 50 µM, respectively ($p<0.05$).

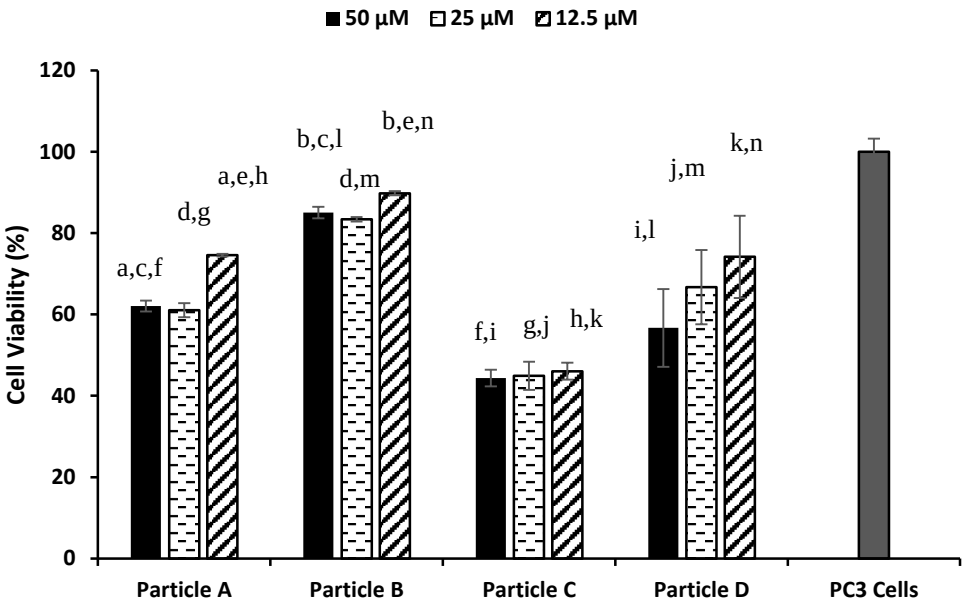

Figure 4.6. Cell viability of PC3 cells transfected with AuNPs-PEG particles. Incubation time: 24h. a, b: represent doses of particles which caused significant difference in cell viability. c,d,e: represents PEG coating concentration which caused significant difference in cell viability for Particles A and B at dose of 50, 25 and 12.5 µM respectively. f,g,h: represents the effect of bare AuNP size which caused significant difference in cell viability for Particles A and C at all doses. i,j,k: represents the significant difference in the effect of PEG concentration on cell viability for Particles C and D at all doses. l,m,n: represents the significant difference in the effect of bare AuNP size on cell viability for Particles B and D at all doses ($p<0.05$).

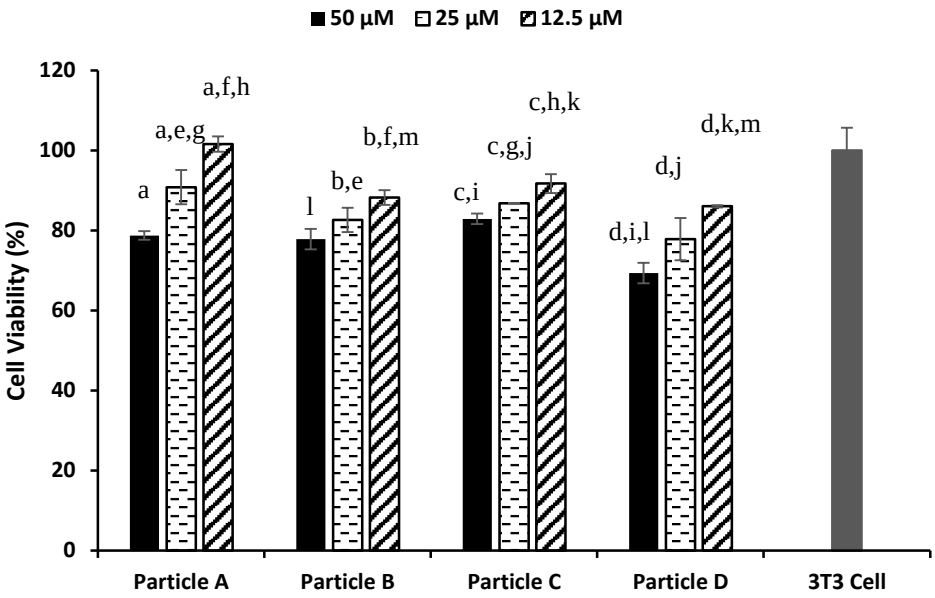

Figure 4.7. Cell viability of 3T3 cells transfected with AuNPs-PEG particles. Incubation time: 24h. a,,b,c,d: represent doses of particles which caused significant difference in cell viability. e,f: represents PEG coating concentration which caused significant difference in cell viability for Conjugates A and B at dose of 25 and 12.5 µM, respectively. g,h: represents the effect of bare AuNP size which caused significant difference in cell viability for Particles A and C at dose of 25 and 12.5 µM, respectively. i,j,k: represents the significant difference in the effect of PEG concentration on cell viability for Particles C and D at all doses. l,m: represents the significant difference in the effect of bare AuNP size on cell viability for Particles B and D at doses of 50 and 12.5 µM, respectively ($p<0.05$).

4.1.4. Effect of PEG Modified AuNPs on Cell Cycle

Literature studies have demonstrated that the action of nanoparticles is mediated by apoptosis induction or cell cycle delay, depending on cell type and cellular context. Therefore, the influence of the particles on the cell cycle was considered. It was observed that the nanoparticles altered cell cycle phases significantly by causing an arrest at different checkpoints (Figures 4.8 through 4.10.). It is not possible to establish a direct link between the toxicity results and cell cycle tests. For instance, Particles A and B showed different cell viabilities (Particle A:~60% and Particle B:~80%, respectively) against PC3 cells in Figure 4.9, however, they caused insignificant difference on cell cycle phases (G1, S and G2) in Figure 4.9.. Based on this comparison, it can be said that the

influence of the nanoparticles on the cellular level should be checked not only with cell viability tests but also with the cell cycle results.

The cell cycle disruption by the particles was investigated through flow cytometry measurements. The change in the G1, S and G2/M phases for all the cells treated with the particles is shown in Figures 4.8 through 4.10. Most of the conjugates resulted in alteration cell cycle steps. In particular, all of the PEGylated nanoparticles caused an increase in S phase following a decrease in G2/M phase of the CaCO2 cells (Figure 4.8.) while completely opposite trend was observed when the PC3 cells were exposed to the modified nanoparticles (Figure 4.9.). In the case of 3T3 cells, only the Particles B and C possessing the .PEG grafting densities of 1.23 g/nm^2 and 0.37 g/nm^2 increased the S phase and subsequently decreased the G2/M phase (Figure 4.10.). The results in Figures 4.8 through 4.10. illustrate that it is possible to minimize alteration in cell cycle upon exposure to nanoparticles by changing the surface properties of the nanoparticles. It is noted that among four types of PEG coated AuNPs prepared, Particle C carrying the lowest PEG grafting density (0.37 g/nm^2) showed the most significant alteration in cell cycle of all cell lines. This result proves that the PEG grafting density is important not only on the cell uptake and cell viability but also on cell cycle phases.

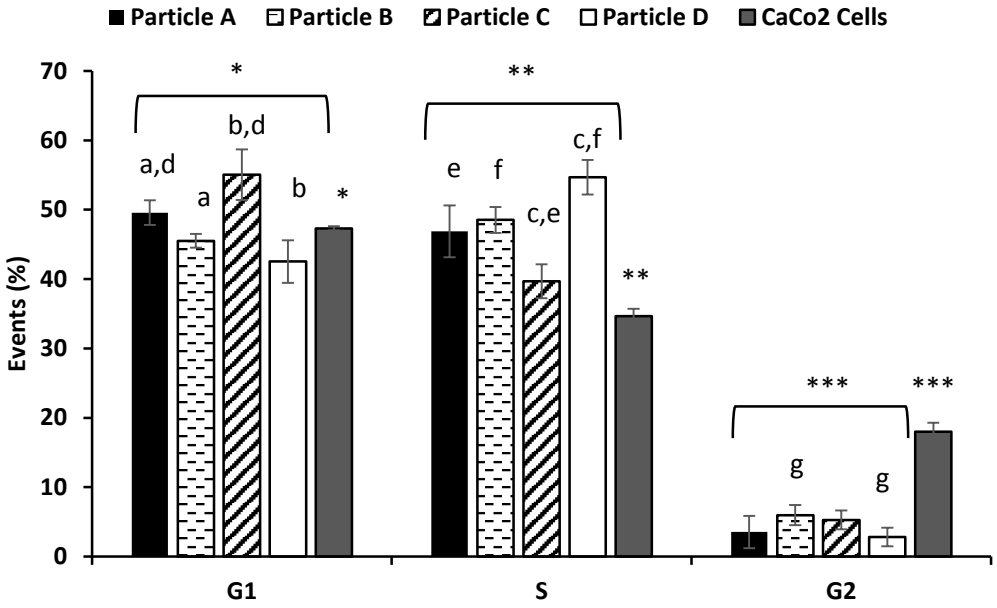

Figure 4.8. Complete cell cycle analysis of AuNP-PEG particles (50 µM) exposed CaCo2 cells. Incubation time: 24h. a,b: represent the significant difference in G1 phase of cell cycle caused by the effect of PEG concentration and d: represent the significant effect of size on the G1 phase. c: represents the significant difference caused by PEG layer in S phase of cell cycle while e,f: represent the effect of the size significantly altering the S phase. g: represents the significant difference in G2 phase of cell cycle caused by the effect of PEG layer. *, **, *** represent the significant difference of AuNP-PEG particles with respect to control groups for G1, S and G2 phases respectively ($p<0.05$).

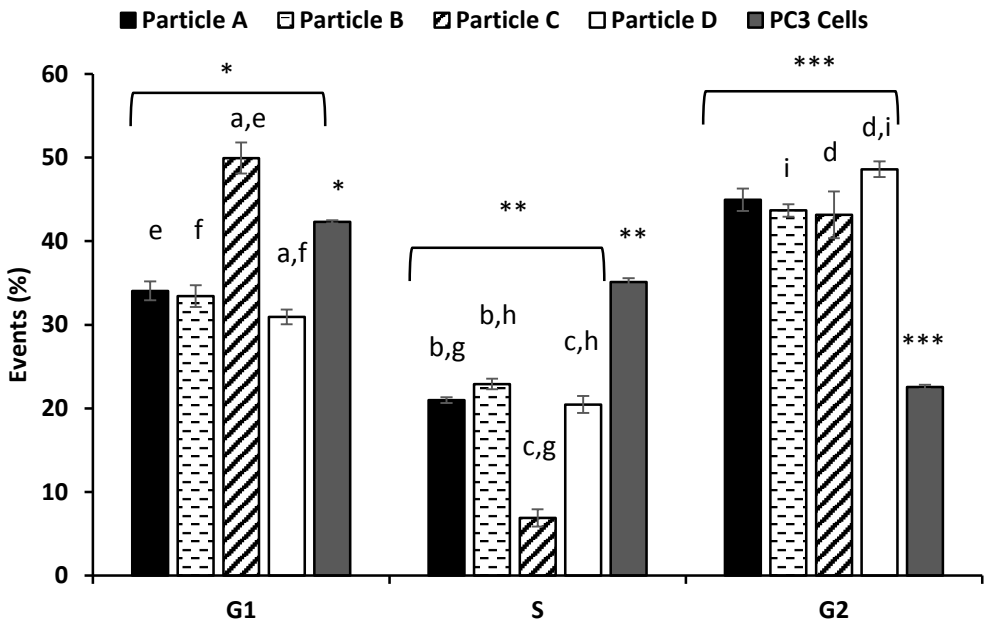

Figure 4.9. Complete cell cycle analysis of AuNP-PEG particles exposed (50 µM) PC3 cells. Incubation time: 24h. a: represents the significant difference in G1 phase of cell cycle caused by the effect of PEG concentration and e,f: represent the significant effect of size. b,c: represents the significant difference caused by PEG layer in S phase of cell cycle while g,h: represent the effect of the size significantly altering the S phase. d: represents the significant difference in G2 phase of cell cycle caused by the effect of PEG layer while i: represents the significant difference due to the effect of size. *, **, *** represent the significant difference of AuNP-PEG particles with respect to control groups for G1, S and G2 phases respectively ($p<0.05$).

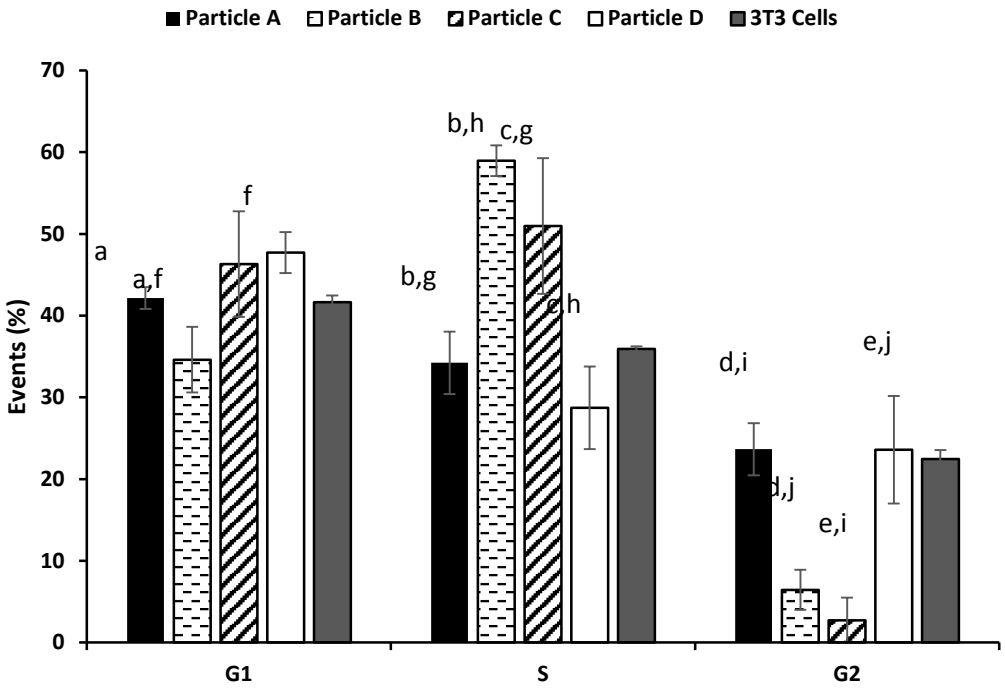

Figure 4.10. Complete cell cycle analysis of AuNP-PEG particles (50 µM) exposed 3T3 cells. Incubation time: 24h. a: represents the significant difference in G1 phase of cell cycle caused by the effect of PEG concentration and f: represent the significant effect of size. b,c: represents the significant difference caused by PEG layer in S phase of cell cycle while g,h: represent the effect of the size significantly altering the S phase. d,e: represent the significant difference in G2 phase of cell cycle caused by the effect of PEG layer while i,j: represent the significant difference due to the effect of size ($p<0.05$).

4.1.5. Effect of PEG Modified AuNPs on Apoptosis

The cells can be arrested at cell cycle checkpoints temporarily in order to repair cellular damage, dissipate exogenous cellular stress signal or provide essential growth factors, hormones, or nutrients. Besides, in case the cellular damage is too severe to be repaired, activation of pathways leading to apoptosis (programmed cell death) occurs through checkpoint signaling (Pietenpol and Stewart 2002). Because of this reason, the apoptotic effect of the particles on the selected cell lines was investigated. In previous section, it was demonstrated that almost all of the particles resulted in a significant G1, S and G2 phase delays against all cell lines. However, although the particles caused significant cell cycle phase arrests, the apoptosis results indicated that they did not depict apoptotic effect against CaCo2 and PC3 cells while they slightly caused apoptotic behavior against 3T3 cells (Figure 4.11.). This deduction implies that the particles acted

through pathways other than the apoptosis to inhibit cell growth or they caused retarded cell proliferation without accompanied massive apoptosis (Chuang et al. 2013).

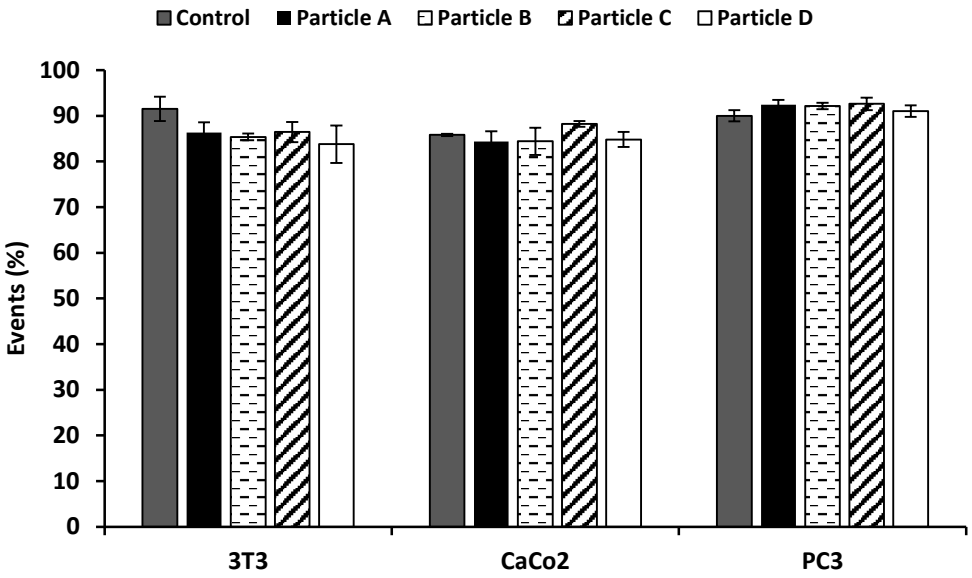

Figure 4.11. Apoptosis and programmed cell death analysis of AuNP-PEG particles (50 µM) exposed 3T3, CaCo2 and PC3 cells by using flow cytometry. Incubation time: 24h.

4.1.6. DNA Damage and Visualization of Particles by Fluorescence Microscopy

Previous studies have shown that cells are arrested at different phases of cell cycle due to DNA damage caused by external or internal effects (Pietenpol and Stewart 2002, Malumbres and Barbacid 2009, Kastan and Bartek 2004). Basically, DNA damage triggers a signaling network that induces phosphorylation and consequent activation of ATM (Ataxia telangiectasia mutated) which functions in DNA repair, apoptotic death and cell cycle arrest (Malumbres and Barbacid 2009, Kastan and Bartek 2004). Possible DNA damage caused by the PEG coated AuNP particles against the selected cell lines were investigated by conducting Comet assay which detects single and double-strand DNA breaks at individual cells. Cells that have broken DNA fragments or damaged DNA migrate much further and appear as fluorescent comets with tails of DNA fragmentation, whereas undamaged DNA moves minimally due to its large size (Wan et al. 2012). The

results in Figure 4.12. indicated that for CaCo2 and PC3 cell lines, all particles caused significant DNA damage almost at the same level. On the other hand, in the case of 3T3 cells, Particles A and D did not induce any DNA damage. This result is in accordance with the cell cycle alterations indicated in Figure 4.10. for 3T3 cells.

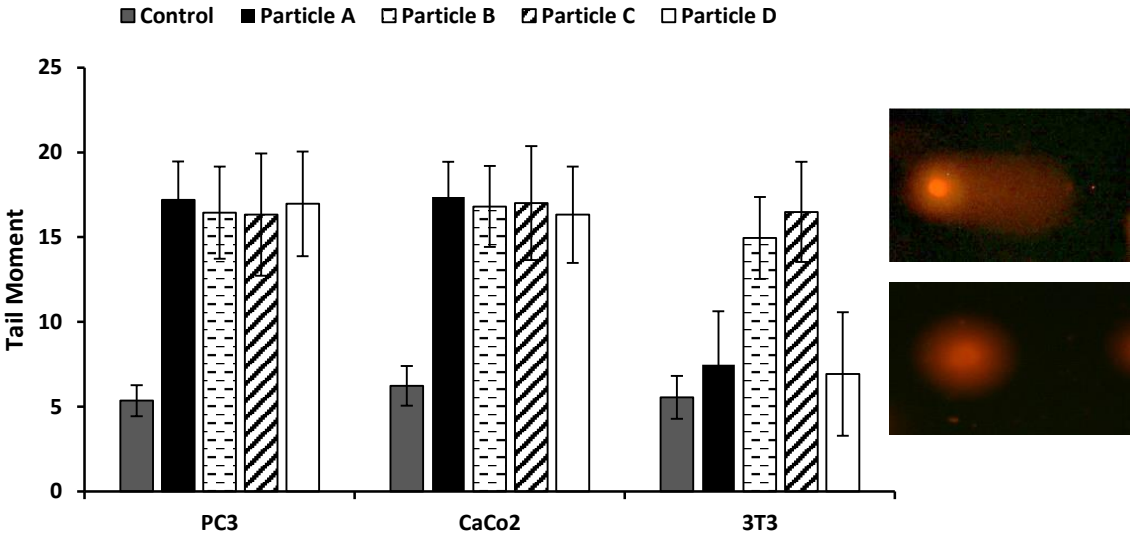

Figure 4.12. Tail moments of the cells exposed to AuNP-PEG particles (50 µM). Incubation time: 24h.

The reason for DNA damage is generally explained by the accumulation of the particles around nucleus where the DNA content is high. To support this hypothesis, the fluorescence images of the Particle C in all cells were taken. This particle was selected since it caused highest toxicity and most significant alteration on the cell cycle phases. The images in Figure 4.13. clearly indicated that the nanoparticles have a tendency to end up in nucleus, which was also mentioned in literature (Kang, Mackey, and El-Sayed 2010).

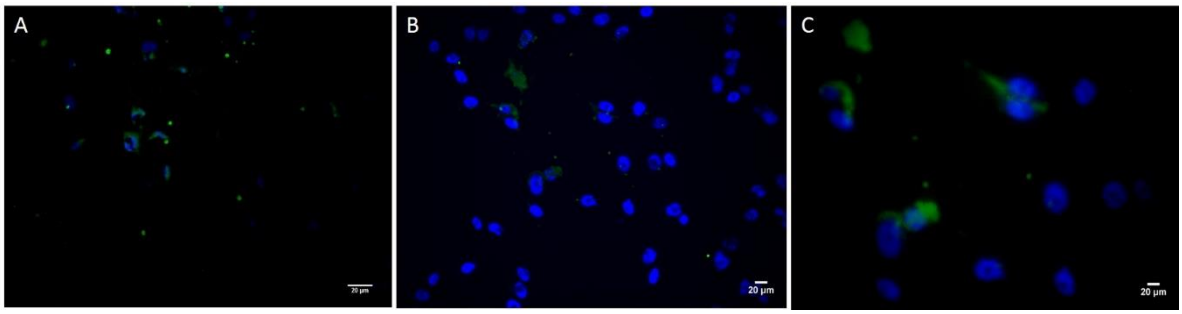

Figure 4.13. Merged fluorescence images of Particle C (13nm sized AuNP with 0.2 mg/ml PEG coating) in A) CaCo2, B) PC3 and C) 3T3 cells. Incubation time: 24h. Blue color: Nucleus staining with DAPI. Green color: Particle staining with FITC.

4.2. Development of AuNP and Pentablock Copolymer Based siRNA Delivery Systems

In this section, AuNP and pentablock copolymer based multilayer siRNA delivery system was developed by using disulfide bonds and electrostatic interactions through layer by layer approach. In addition, a siRNA/polymer polyplex system, obtained by direct electrostatic complexation of negatively charged siRNA and positively charged pentablock copolymer, was used as control. The efficiencies of both systems were tested in terms of siRNA protection, cellular uptake, endosomal escape, siRNA activity and cytotoxicity against SKOV3 cell line.

4.2.1. Synthesis of Pluronic F127 Macroinitiator and Pentablock Copolymers

The reaction mechanism for bromide modification of difunctional Pluronic F127 macroinitiator and ATRP reaction initiated by this macroinitiator to form pentablock copolymers were previously illustrated (Determan et al. 2005). The conversion of hydroxyl end groups to bromides was confirmed by ^{1}H NMR spectra (Figure 4.14.).

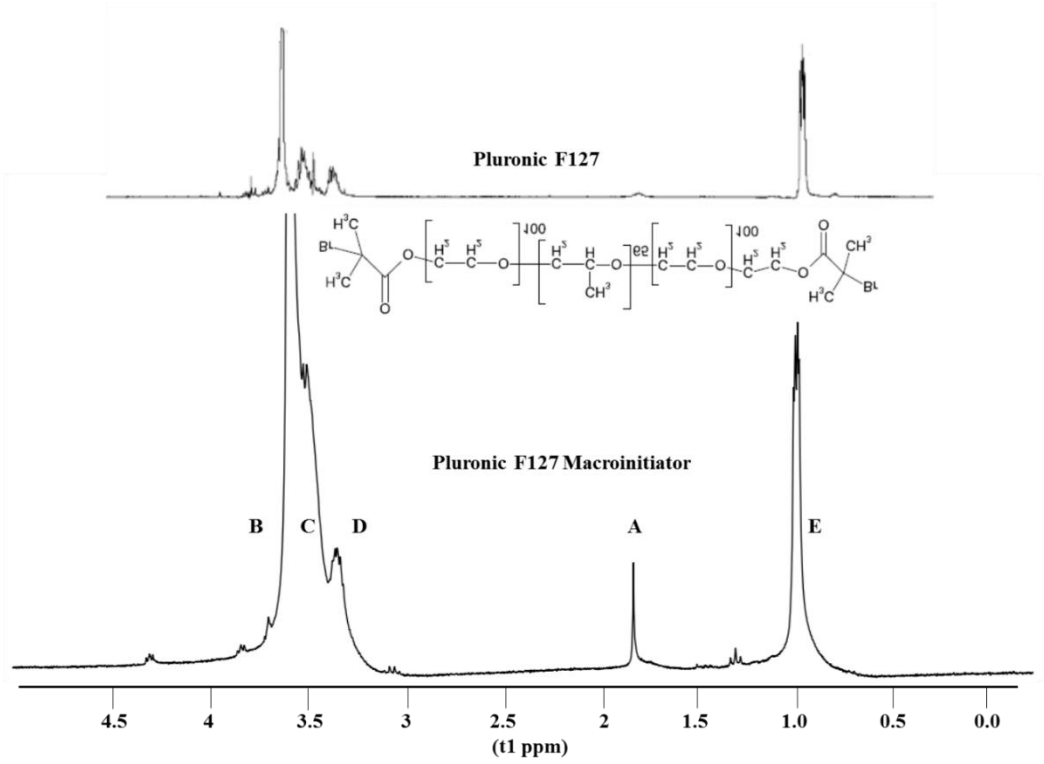

Figure 4.14. ^{1}H NMR of Pluronic F127 and Pluronic F127 ATRP macroinitiator.

The peak at 1.9 ppm in the spectra given for the macroinitiator corresponds to the methyl groups in the alpha position relative to the bromide. In order to calculate conversion of initiating end groups, this specific peak was integrated relative to the peaks arising from the F127 backbone protons. The reaction of amine methacrylate blocks with the macroinitiator results in the formation of pentablock copolymers. This was proved by the presence of the bonds A, E, F, G, I, J in the ^{1}H NMR spectra shown in Figures 4.15 and 4.16. as reference to the ^{1}H NMR of Pluronic F127 macroinitiator (Figure 4.14.).

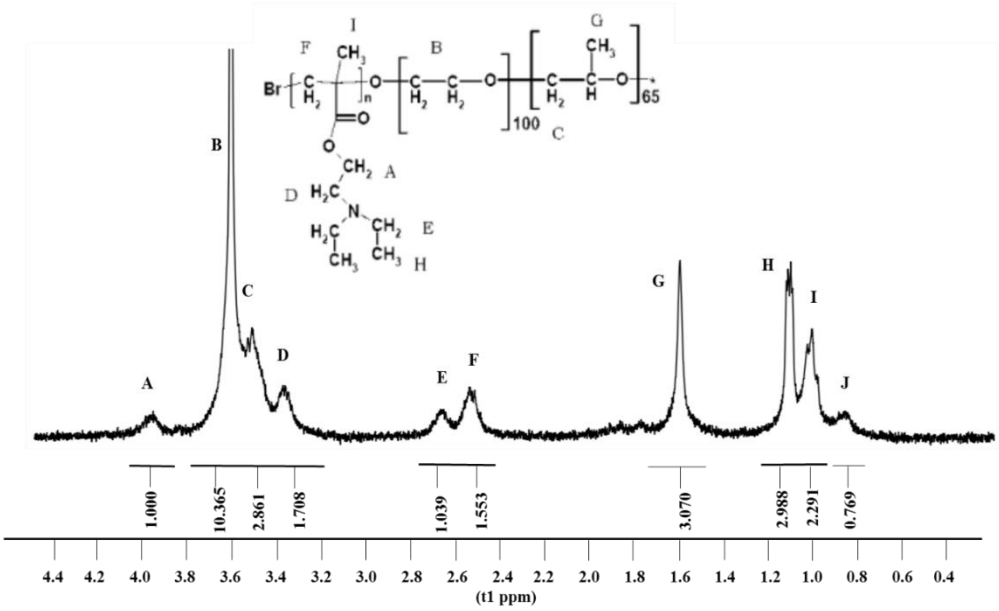

Figure 4.15. ^{1}H NMR of pentablock copolymers PDEAEM-PluronicF127-PDEAEM, Polymer A.

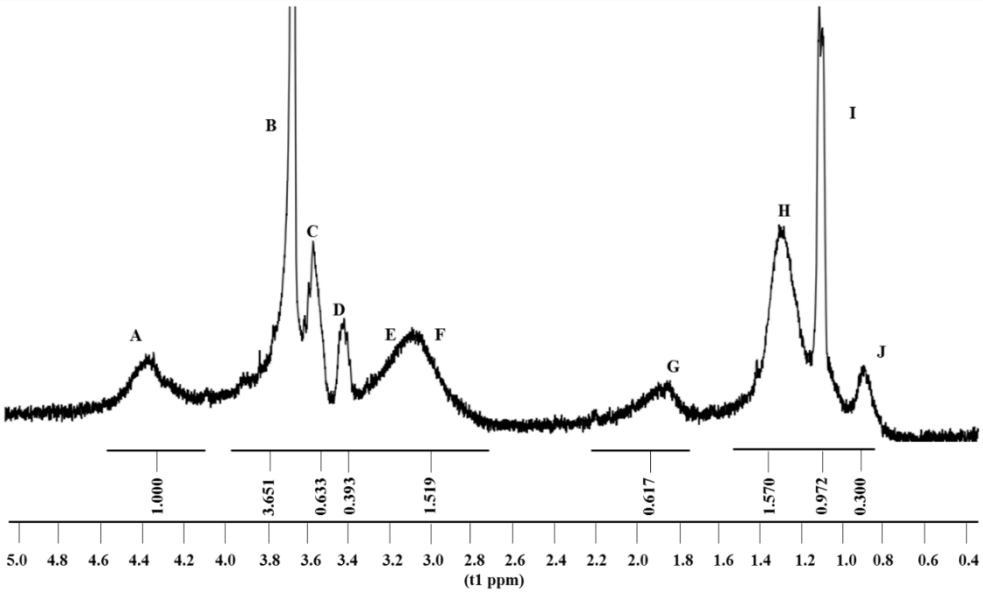

Figure 4.16. ^{1}H NMR of pentablock copolymers PDEAEM-PluronicF127-PDEAEM, Polymer C.

The formation of pentablock copolymer was also demonstrated with gel permeation chromatography through the faster elution time as compared to the macroinitiator (Figure 4.17.).

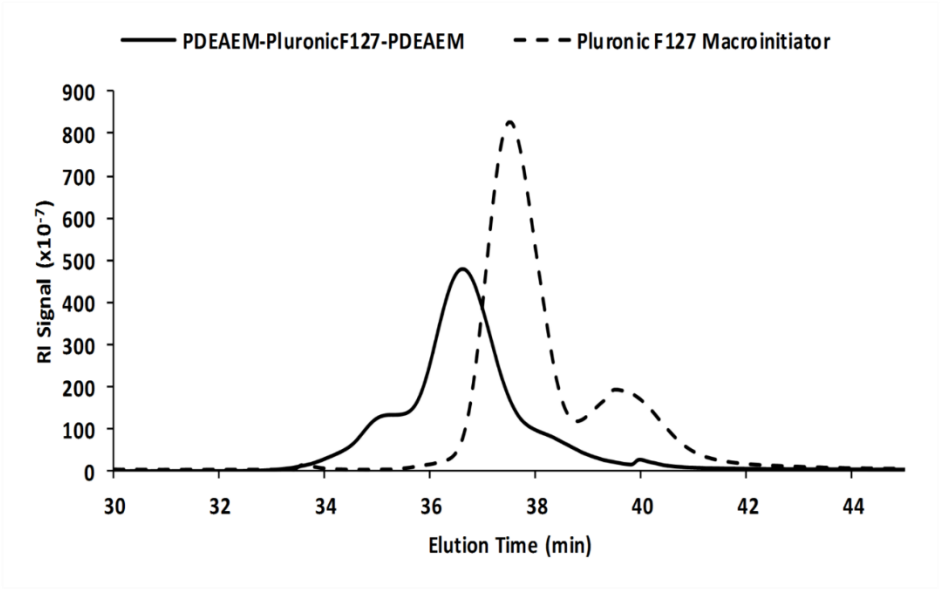

Figure 4.17. GPC chromatograph of Pluronic F127 macroinitiator and a pentablock copolymer.

The number and weight average molecular weight of the polymers synthesized are summarized in Table 4.5. The average polymer molecular weight can be controlled in a relatively low polydispersity range by manipulating the macroinitiator to monomer ratio. By keeping the macroinitiator amount constant and increasing the monomer amount, the increase in molecular weight was achieved.

Table 4.5. Molecular weight data for the Pluronic F127 and PDEAEM-based pentablock copolymers synthesized by ATRP.

	GPC			NMR
	M_w (g/mol)	M_n (g/mol)	M_w/M_n	M_n (g/mol)
Pluronic F127	13560	12540	1.081	
Pluronic F127 Macroinitiator	14810	13150	1.126	
PDEAEM-Pluronic F127-PDEAEM (Polymer A)	32240	26650	1.2	15650
PDEAEM-Pluronic F127-PDEAEM (Polymer C)	72450	36050	2.01	18522

4.2.2. The siRNA/Polymer Polyplex System

4.2.2.1. siRNA/Polymer Complexation

The siRNA/polymer polyplex system formed mainly by electrostatic interactions between negatively charged siRNA and positively charged polymers is illustrated in Figure 4.18 A.

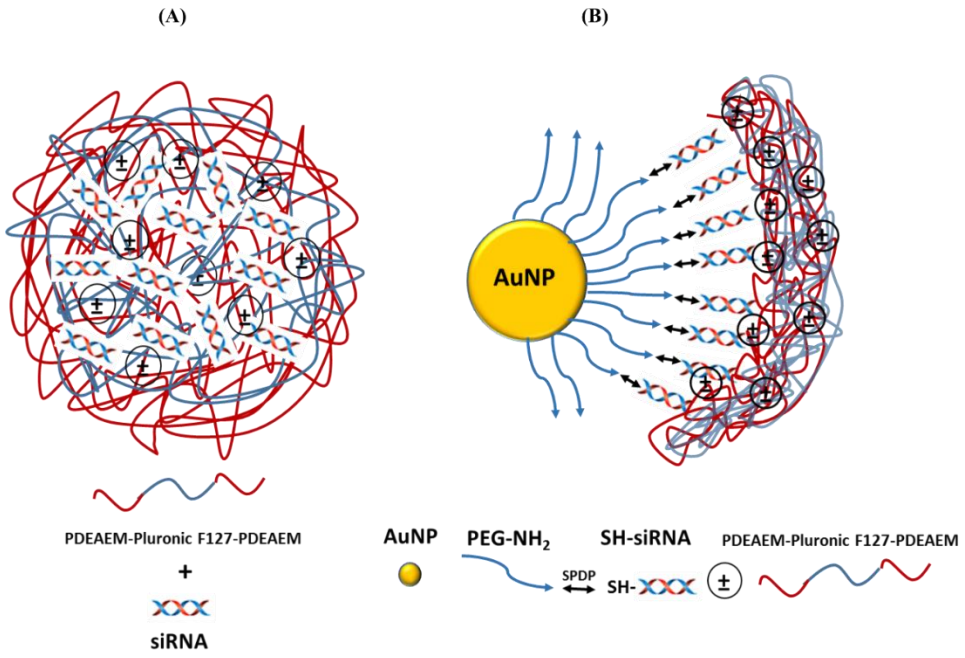

Figure 4.18. (A) PDEAEM / Pluronic F127 / PDEAEM - siRNA polyplexes. (B) PDEAEM / Pluronic F127 / PDEAEM -siRNA-PEG-AuNP multilayer delivery system.

The polyplex formation was determined through gel retardation as shown in Figure 4.19 A. Complete complexation of siRNA with Polymers A and C was observed at N/P ratios of 100, 75 and 50. On the other hand, the decrease in the polymer amount resulted in incomplete condensation of siRNA as demonstrated by similar mobilities of the naked siRNA with that of the siRNA condensed on the polymers when the N/P ratio was 1.25. Figure 4.19 A also indicated that there was no significant difference in the amount of condensed siRNA for the different polymer types.

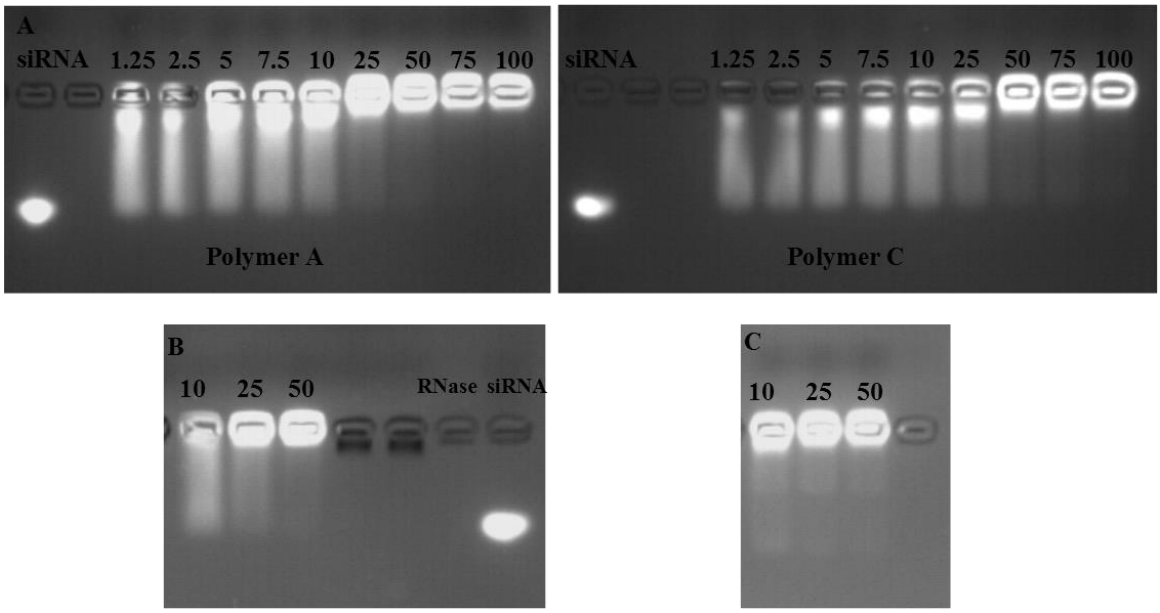

Figure 4.19. A) Gel electrophoresis of siRNA/Polymer polyplexes with Polymer A and Polymer C at various N/P ratios: 1.25, 2.5, 5, 7.5, 10, 25, 50, 75, 100. Control: Naked siRNA. B) RNase stability of the polyplexes prepared by Polymer A at N/P ratios of 10, 25 and 50. Control: Naked siRNA and RNase exposed naked siRNA. C) Serum protein stability of the polyplexes prepared by Polymer A at N/P ratios of 10, 25 and 50.

Preliminary screening tests for luciferase expression activity in SKOV3 cells indicated that the polyplexes prepared by Polymer A and C possessing N/P ratios of 100 and 75 caused a significant decrease in luciferase expression at applied doses. However, the toxicity tests showed that the actual reason for the decrease in the luciferase expression was due to severe toxic effect of the applied dose (Figure 4.20.).

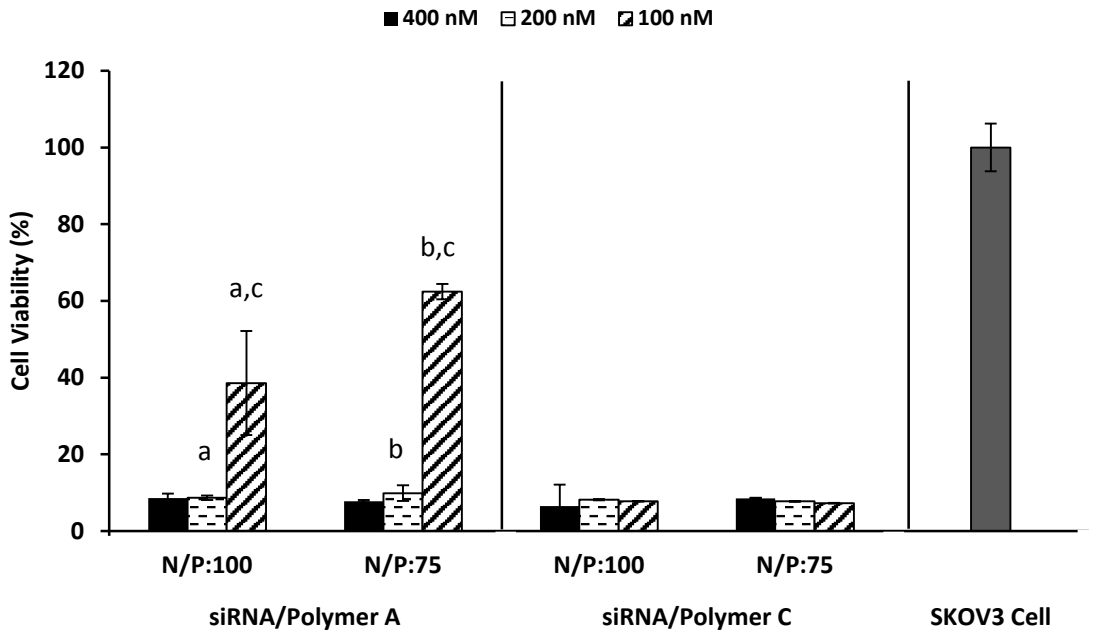

Figure 4.20. Cell viability of siRNA/Polymer A and siRNA/Polymer C complexes administered SKOV3 cells. N/P: 100, 75. Applied siRNA dose: 400, 200, 100 nM. Initial SKOV3 cell density: $2x10^4$ cell/well. Incubation time: 24h. a, b: represent doses of siRNA/Polymer A complexes which caused significant difference in cell viability ($p<0.05$) for N/P ratios of 100 and 75, respectively.

On the basis of these results, we decided to use N/P ratios of 50, 25 and 10, at which the siRNA activity can be observed without severe toxicity. The stabilities of selected polyplexes against degradation of RNase and serum proteins have also been evaluated by gel electrophoresis. Polyplexes did not show a significant sign of disassembly or dissociation in the presence of RNase or serum proteins as illustrated in Figures 4.19 B and C. The results suggest that in addition to complete siRNA condensation, the polymers may function as effective siRNA stabilizing agents.

The time dependent stabilities of the polyplexes were also investigated by monitoring the change in size and zeta potential. The polyplexes were incubated in HEPES buffer during 72h at 4°C. Figure 4.21 A indicated that there is slight agglomeration in polyplex with N/P ratio of 50 while there was not a significant change in the size for other polyplexes. The zeta potential values of the polyplexes did not change significantly except for the one with N/P ratio of 25 which showed a slight decrease in zeta potential value (Figure 4.21 B). In addition, the stabilities of the polyplexes in serum containing growth medium were also observed. The polyplex size in the presence of serum medium increased due to the agglomeration tendancy or deposition of serum

proteins on the surface (Figure 4.22 A). Moreover, the net positive charges of the polyplexes turned to negative due to the attachment of negatively charged moieties present in growth medium (Figure 4.22 B).

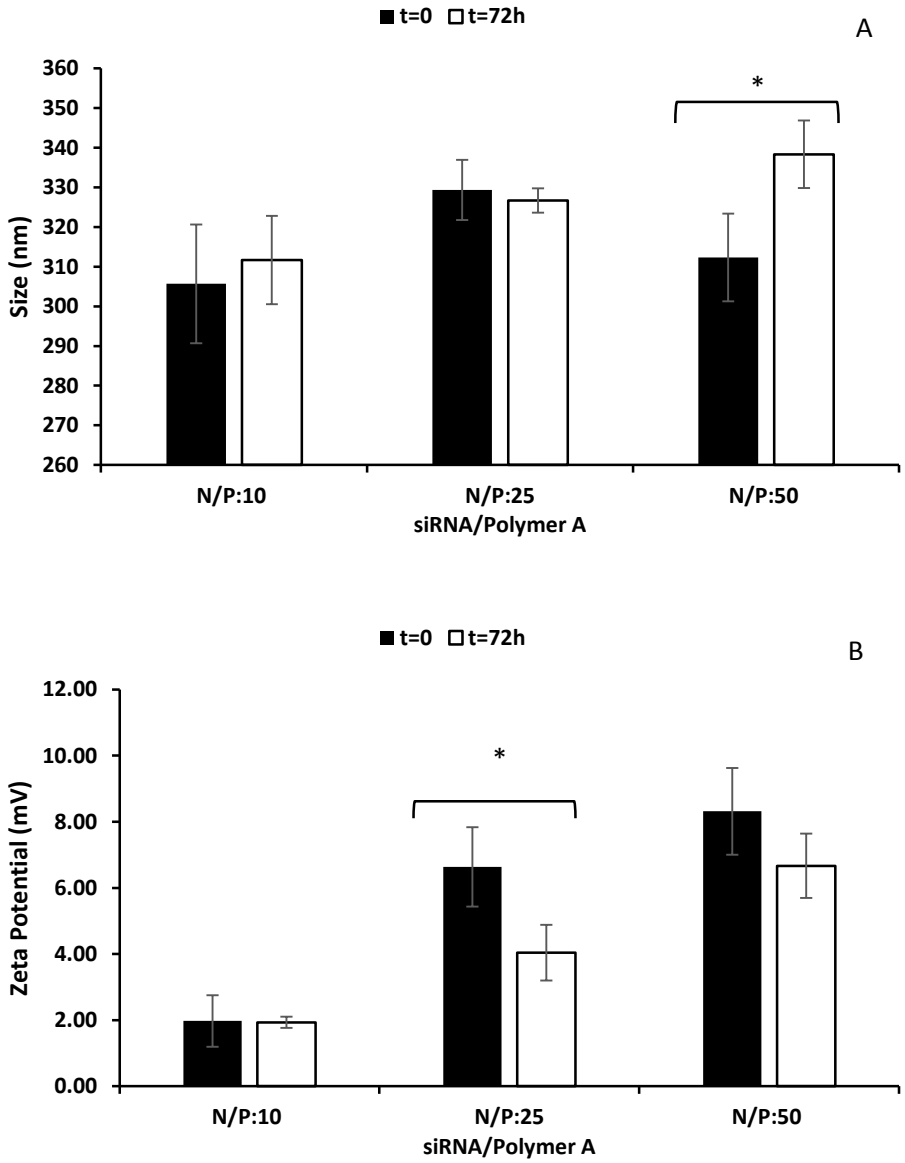

Figure 4.21. The change in the size (A) and zeta potential (B) values of siRNA/PolymerA polyplex systems (N/P ratio: 10, 25 and 50). After preparation (t=0) and after 72h of incubation in HEPES buffer at pH 7.4 at +4°C (t=72h). * represents statistically significant difference ($p<0.05$).

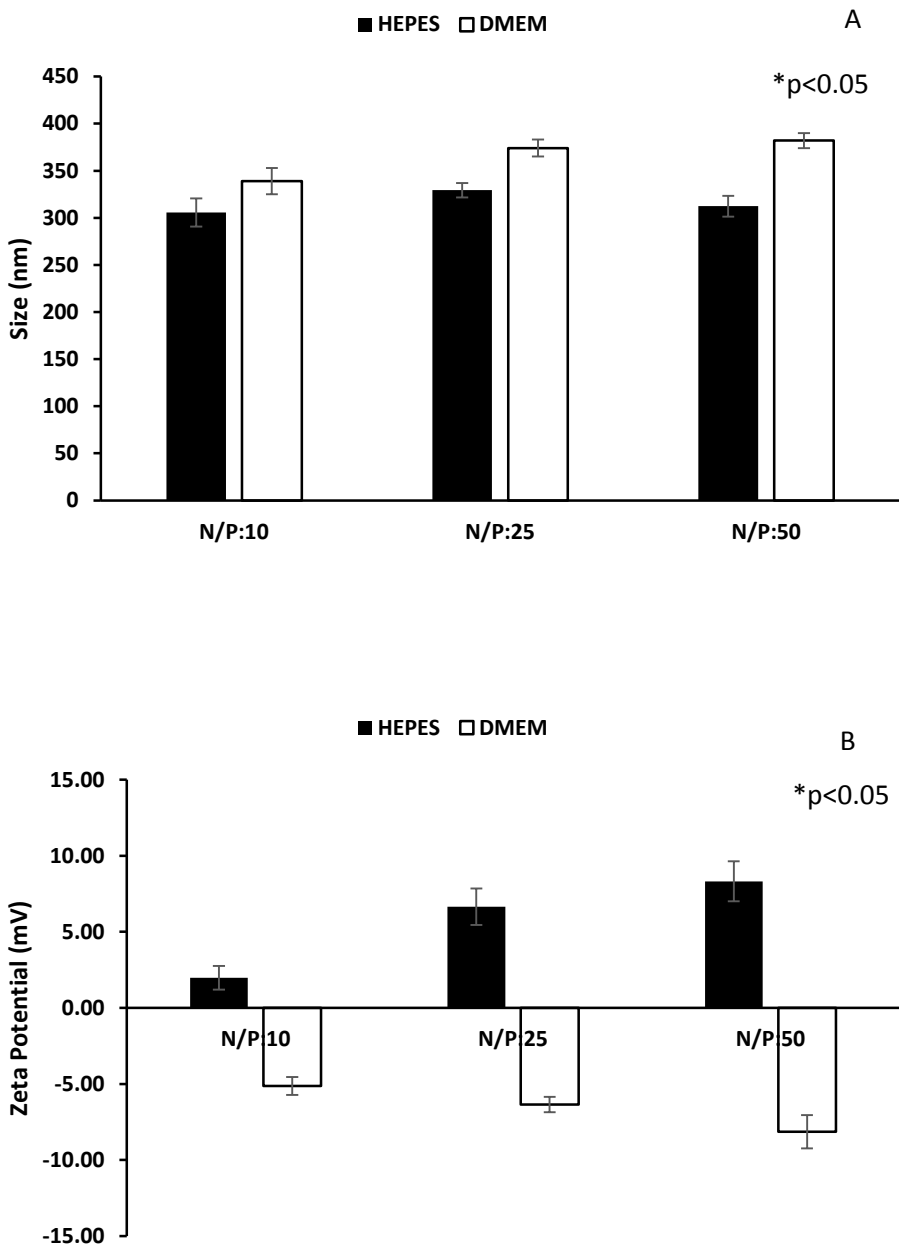

Figure 4.22. The change in the size (A) and zeta potential (B) values of siRNA/Polymer A polyplex systems (N/P ratio: 10, 25 and 50). Even after preparation in HEPES buffer (HEPES) and after 24h of incubation at 37 °C in serum containing DMEM growth medium (DMEM). * represents statistically significant difference ($p<0.05$).

4.2.2.2. Luciferase Activity and Toxicity of siRNA/Polymer Polyplexes

To evaluate the cellular transfection efficiency and toxicity of the siRNA/Polymer polyplexes, they were administered to the SKOV3 cells at different doses (N/P ratio: 10, 25, 50). Compared to the control cases, the polyplexes formed at N/P ratios of 25 and 50 were able to suppress almost all of the luciferase expression at the maximum applied siRNA dose, 400nM (Figure 4.23 and 4.24.). However, significant toxicity was observed at this dose (Figure 4.25. and 4.26.), leading to the conclusion that suppression of the luciferase expression was not as a result of siRNA activity but was due to the toxic effect of the polyplexes. The polyplexes induced the toxicity since the required amount of polymer to condense 400 nM of siRNA is severely high. Similarly gene silencing caused by the polymers alone (without siRNA) at the highest dose (control groups in Figure 4.23 and 4.24.) can be attributed to toxic effect of the polymers on the cells (Figure 4.25. and 4.26.). At lower doses, the polymers exhibited neither luciferase expression suppression nor toxicity. In general, toxicity and luciferase activity did not change in a dose dependent manner as N/P ratio increased. At the 50 nM dose, almost all of the polyplexes showed approximately a 50% decrease in luciferase expression without causing significant toxic effects. The siRNA/polymer polyplex systems present toxicity problem since the amount of siRNA required for sufficient gene silencing effect is usually high which brings about the use of high amount of polymer for a complete condensation of siRNA.

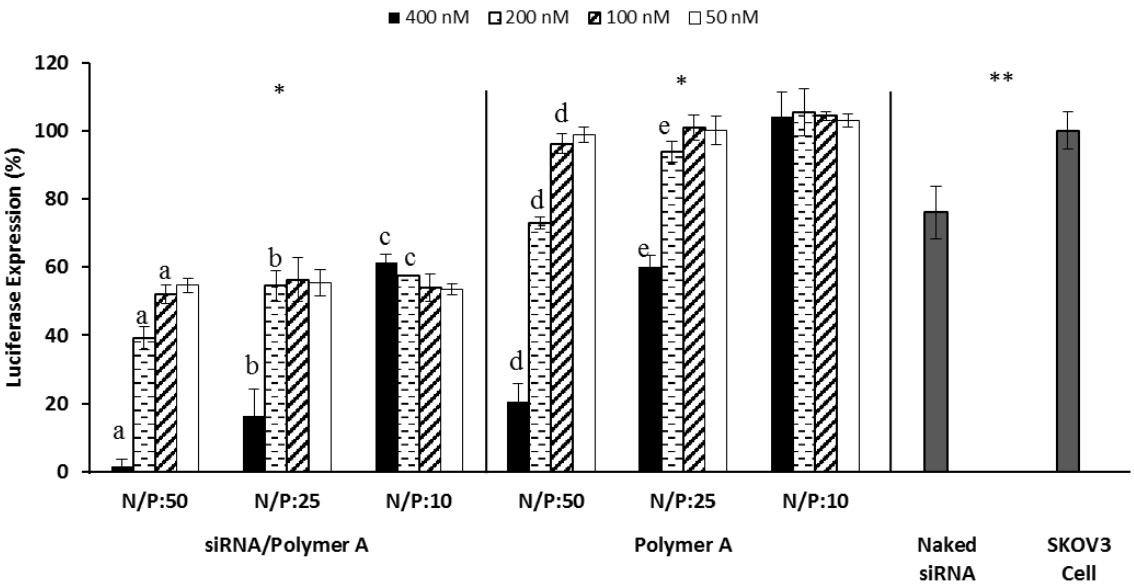

Figure 4.23. Luciferase expression suppression of prepared siRNA/Polymer A polyplexes. N/P: 50, 25, 10. Applied siRNA dose: 400, 200, 100, 50 nM. Initial SKOV3 cell density: $2x10^4$ cell/well. Controls: Amount of Polymer A required to form polyplexes possessing N/P ratio 50, 25, 10 (without siRNA), naked siRNA, SKOV3 control cell. Incubation time: 24h. For each N/P ratio, the same letters on the bars represent doses of siRNA/Polymer A polyplexes or Polymer A alone which caused significant difference in luciferase expression suppression ($p<0.05$). *Compared to siRNA/Polymer A polyplexes, Polymer A alone showed significantly lower luciferase expression suppression ($p<0.05$) at all N/P ratios and doses applied. ** The luciferase expression suppression values obtained with 400 nM naked siRNA or SKOV3 cells were also found significantly lower ($p<0.05$) than the suppression provided by 400 nM siRNA/Polymer A polyplex prepared at N/P ratio of 50.

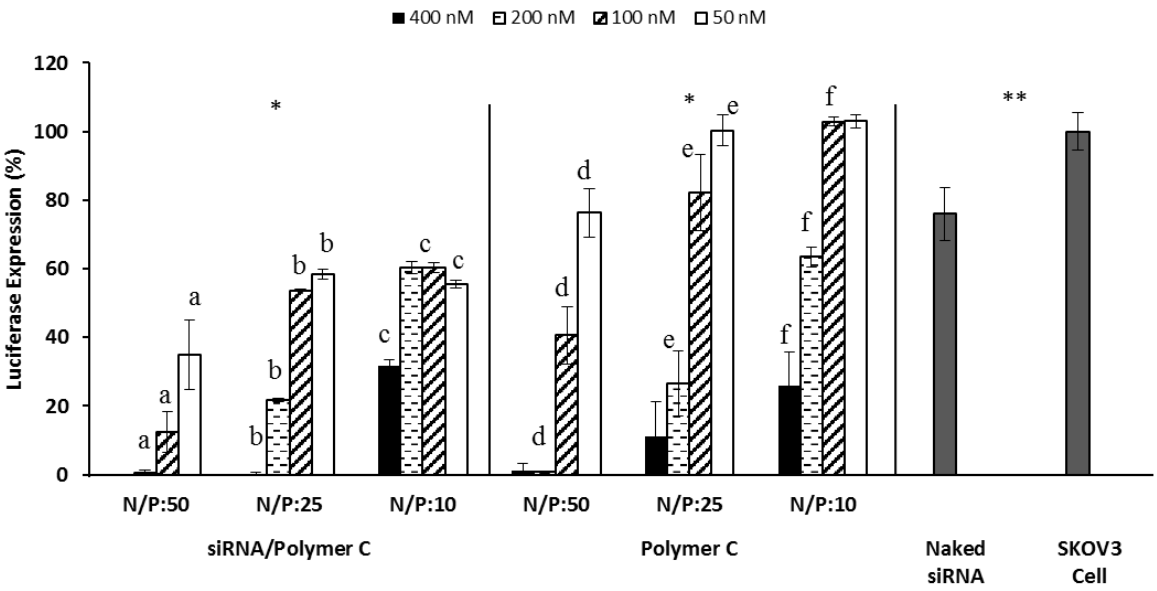

Figure 4.24. Luciferase suppression of prepared siRNA/Polymer C polyplexes. N/P: 50, 25, 10. Applied siRNA dose: 400, 200, 100, 50 nM. Initial SKOV3 cell density: $2x10^4$ cell/well. Controls: Amount of Polymer C required to form polyplexes possessing N/P ratio 50, 25, 10 (without siRNA), naked siRNA, SKOV3 control cell. Incubation time: 24h. For each N/P ratio, the same letters on the bars represent doses of siRNA/Polymer C polyplexes or Polymer C alone which caused significant difference in luciferase expression suppression ($p<0.05$). *Compared to siRNA/Polymer C polyplexes, Polymer C alone showed significantly lower luciferase expression suppression ($p<0.05$) at 100 and 50 nM doses for all N/P ratios. ** The luciferase expression suppression values obtained with 400 nM naked siRNA or SKOV3 cells were also found significantly lower ($p<0.05$) than the suppression provided by 400 nM siRNA/Polymer C polyplex prepared at N/P ratio of 50.

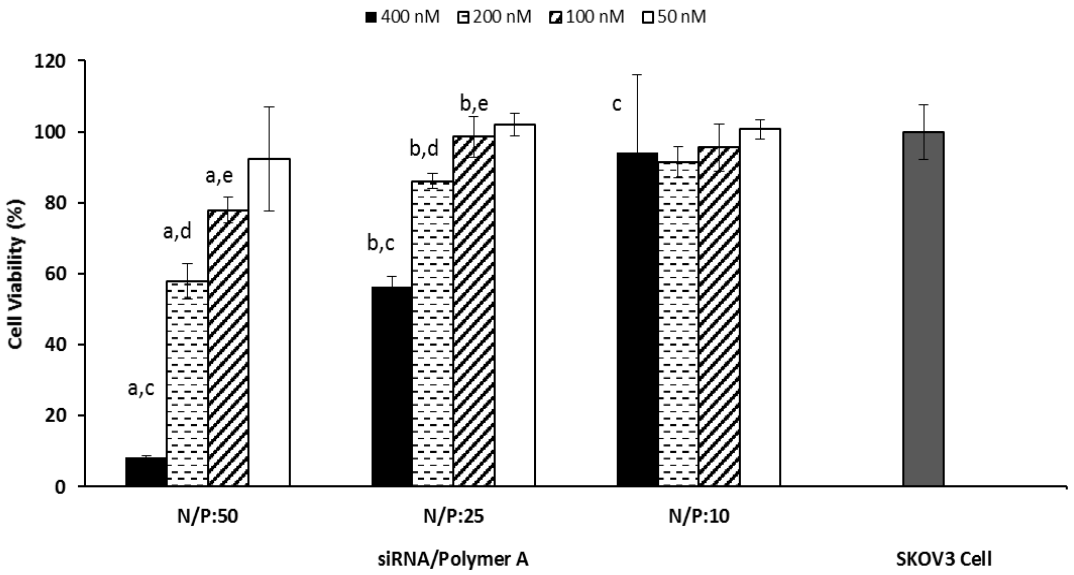

Figure 4.25. Cell viability of siRNA/Polymer A polyplexes administered to SKOV3 cells. N/P: 50, 25, 10. Applied siRNA dose: 400, 200, 100, 50 nM. Initial SKOV3 cell density: $2x10^4$ cell/well. Incubation time: 24h. a,b: represent doses of siRNA/Polymer A polyplexes which caused significant difference in cell viability ($p<0.05$) for N/P ratios of 50 and 25, respectively. c, d, e : represent the siRNA/Polymer A polyplexes prepared at different N/P ratios which showed significant difference ($p<0.05$) in cell viability at doses of 400, 200 and 100 nM, respectively.

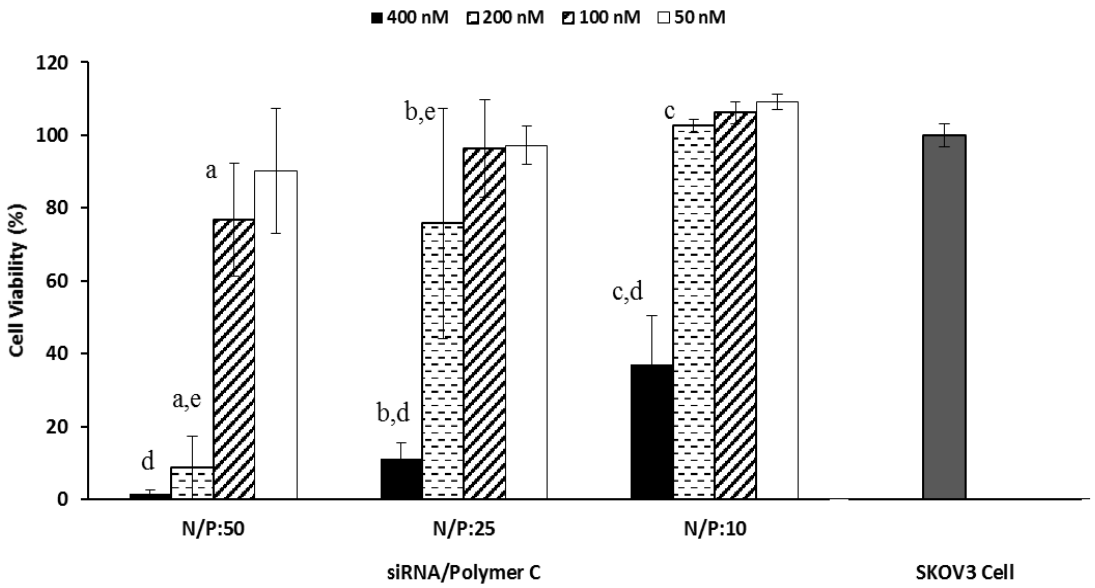

Figure 4.26. Cell viability of siRNA/Polymer C polyplex administered SKOV3 cells. N/P: 50, 25, 10. Applied siRNA dose: 400, 200, 100, 50 nM. Initial SKOV3 cell density: $2x10^4$ cell/well. Incubation time: 24h. a,b,c: represent doses of siRNA/Polymer C polyplexes which caused significant difference in cell viability ($p<0.05$) for all N/P ratios. d, e : represent the siRNA/Polymer C polyplexes prepared at different N/P ratios which showed significant difference ($p<0.05$) in cell viability at doses of 400 and 200 nM, respectively.

4.2.3. The AuNP and Pentablock Copolymer Based Multilayer siRNA Delivery System

4.2.3.1. Synthesis and Characterization of Multilayer siRNA Delivery System

In this section, we present a new multilayer siRNA delivery system based on AuNPs and pentablock copolymers (Figure 4.18 B). The first step in the synthesis was modification of the AuNPs with heterobifunctional PEG to increase stability and facilitate the attachment of subsequent layers through cleavable disulfide bonds. In addition to providing conjugation sites for further surface modifications, the PEG layer on AuNPs also acted as a buffer layer avoiding the possible reactions between the bare AuNP surface and disulfide bonds, through which the siRNA attached to the PEG layer, since such interactions have possibility to induce siRNA release (Lee et al. 2009). The PEG coating resulted in an increase in the cumulative size of the AuNPs from ~12.5 to ~18 nm as

shown by DLS data represented in Table 4.6. Despite the increase in size, there was not a significant increase in polydispersity index (PDI) values. The PEG layer coated on the AuNPs was also observed in TEM images (Figure 4.27.). The thickness of the PEG layer was evaluated as ~6 nm from both DLS data (Table 4.6.) and TEM images (Figure 4.27.). Another indication of successful PEG coating was the change in the zeta potential values. Upon PEG attachment, the negatively charged surface of the bare AuNPs (-33.3 mV) becomes positively charged (+20.2 mV) due to the presence of $–NH_2$ groups at the open end of the PEG (Table 4.6.). The change in the UV-vis spectra of the multilayer system can also give clues about the success of the surface modifications (Figure 4.28.). Maximum absorption in the spectra for the 13 nm sized bare AuNPs is observed at 520 nm and a red shift from 520 to 525 nm without severe broadening in the spectra indicated successful PEG coating.

Table 4.6. Size, zeta potential and polydispersity index (PDI) values of bare and modified AuNPs.

	Bare AuNP	**AuNP-PEG**	**AuNP-PEG-SPDP**	**AuNP-PEG-siRNA**	**AuNP-PEG-siRNA-Polymer**
Size (nm)	12.46 ±0.66	18.09 ±0.64	20.35 ±0.91	31.77 ±0.11	168.93 ±3.48
PDI	0.23	0.25	0.24	0.25	0.57
Zeta Potential (mV)	-33.30 ±0.98	20.23 ±1.18	3.88 ±1.49	-2.64 ±0.67	6.98 ±0.90

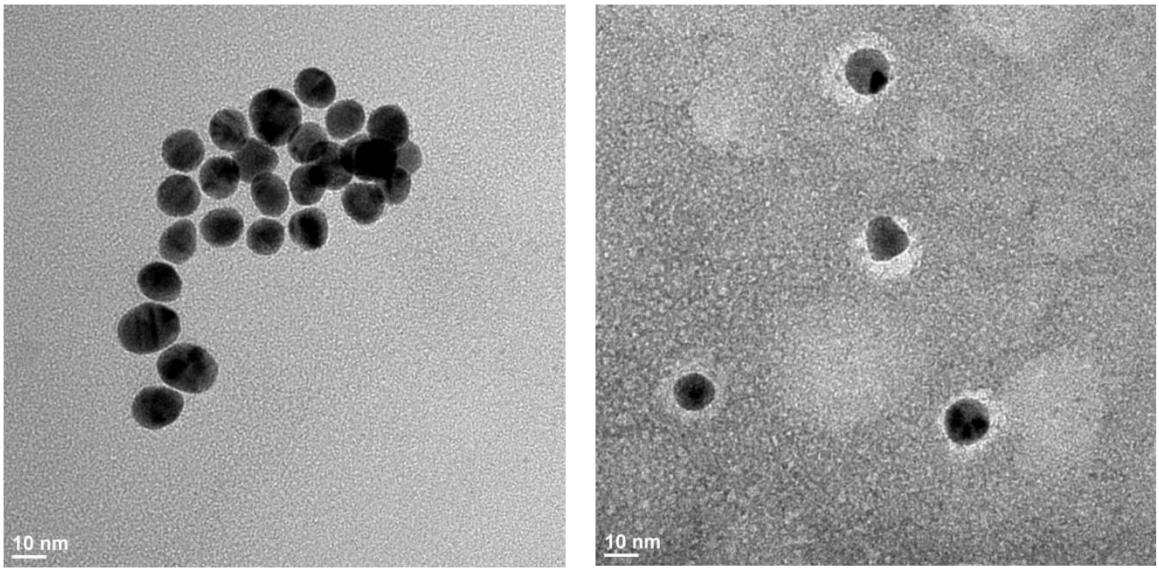

Figure 4.27. TEM images of bare and PEG modified AuNPs

In order to introduce disulfide bonds on the particles, the PEG modification was further followed by the SPDP attachment to the PEG coated AuNPs through the amide bond. The SPDP conjugation was verified by the red shift indicating a movement from 525 (AuNP-PEG) to 527 nm (AuNP-PEG-SPDP) on the absorption maximum in the UV-vis spectra (Figure 4.28.). Moreover, due to the successful SPDP attachment, there was a decrease in the surface charge from +20.2 to +3.88 mV (Table 4.6.), however, the cumulative size of PEG coated AuNPs did not increase significantly since the size of the SPDP cross linker is too small.

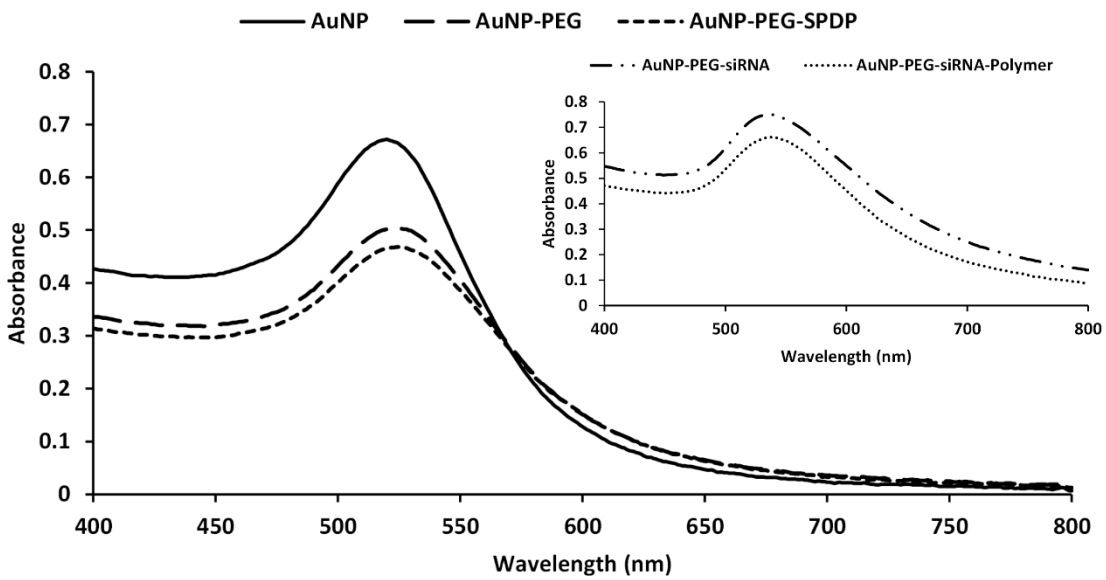

Figure 4.28. UV-vis spectra of AuNP, PEG modified AuNP, SPDP and siRNA modified AuNP-PEG multilayer system.

The deprotected thiol modified siRNA (SH-siRNA) was attached to the AuNP-PEG-SPDP multilayer system through the thiol-disulfide exchange reaction. The zeta potential of the multilayer system turned from positive (+3.88 mV) to slightly negative (-2.64 mV) and size increased from ~20 to ~32 nm upon attachment of the siRNA (Table 4.6.). In addition, the maximum absorbance wavelength shifted from 527 (AuNP-PEG-SPDP) to 534 nm with significant broadening in the spectra (Figure 4.28.). The siRNA loaded multilayer system along with naked siRNA were run in gel electrophoresis. As shown in Figure 4.29., the multilayer systems were retarded compared to the naked siRNA and these results provided another evidence of siRNA attachment to the AuNPs.

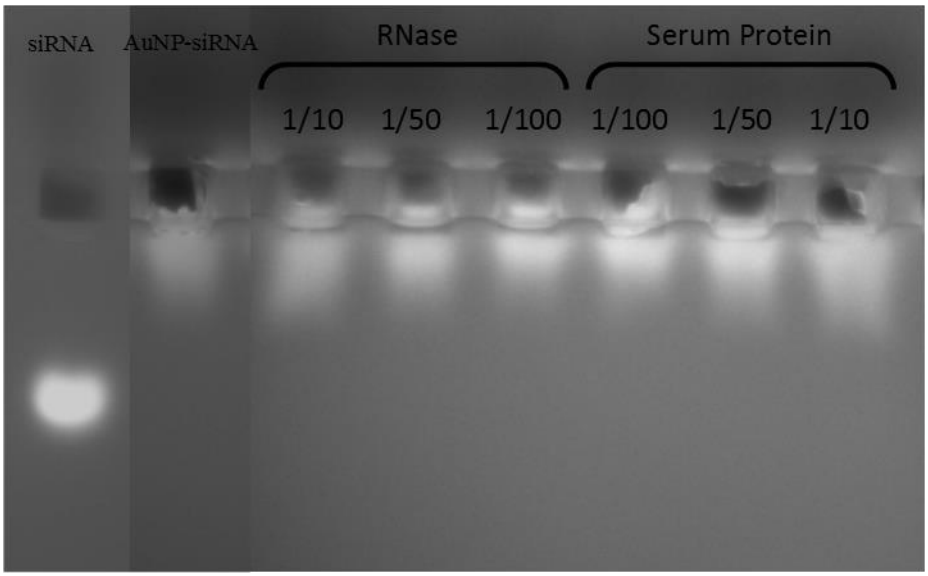

Figure 4.29. Agarose gel electrophoresis retardation of AuNP-siRNA multilayer system (without polymer) and naked siRNA. RNase and serum protein stabilities of the multilayer systems prepared with Polymer A at AuNP/Polymer ratios of 1/100, 1/50 and 1/10.

The amount of siRNA loaded onto the nanoparticles was determined to be 560 nM while the maximum theoretical loading to achieve a complete surface coverage was calculated as 880 nM (Appendix A.1.). The last step in the synthesis of multicomponent system was to coat siRNA loaded AuNPs with pentablock copolymers through electrostatic interactions between negatively charged siRNA and positively charged groups on the copolymer. Table 4.6. shows that the polymer coating resulted in an increase in zeta potential of the AuNP-PEG-siRNA from -2mV to +7mV. The change in the surface charge from negative to positive subsequent to polymer coating may be due to the excess cationic groups of the polymer. In addition, the size of the multilayer systems increased from ~31 to ~169 nm (Table 4.6.) and a significant shift in the maximum absorbance wavelength and broadening in the spectra (Figure 4.28.) were observed upon the assembly of polymer layer on the surface.

The RNase and serum protein stabilities of the multilayer systems were also tested through gel retardation. Figure 4.29. illustrated that the siRNA loaded multilayer systems with polymer coating on the outer surface showed a good siRNA protection against RNAse and serum proteins since the intensity of these multilayer systems were almost the same with the naked siRNA used as control. This result confirms that the multilayer systems did not show any dissociation in the presence of serum proteins or RNases by protecting loaded siRNA.

The stability of the multilayer systems was observed through the changes in the size and zeta potential values. The results indicated that the zeta potential of multilayer did not change significantly, while slight increase in size from ~160 to ~170 nm was observed for the multilayer system with AuNP/Polymer ratio of 1/100 at the end of 72 h incubation (Figure 4.30.). In the presence of serum containing DMEM medium, the multilayer systems showed a very slight increase in size (Figure 4.31 A). However, the surface of multilayer systems became completely negatively charged upon the serum incibation due to the deposition of negatively charged moieties (Figure 4.31 B).

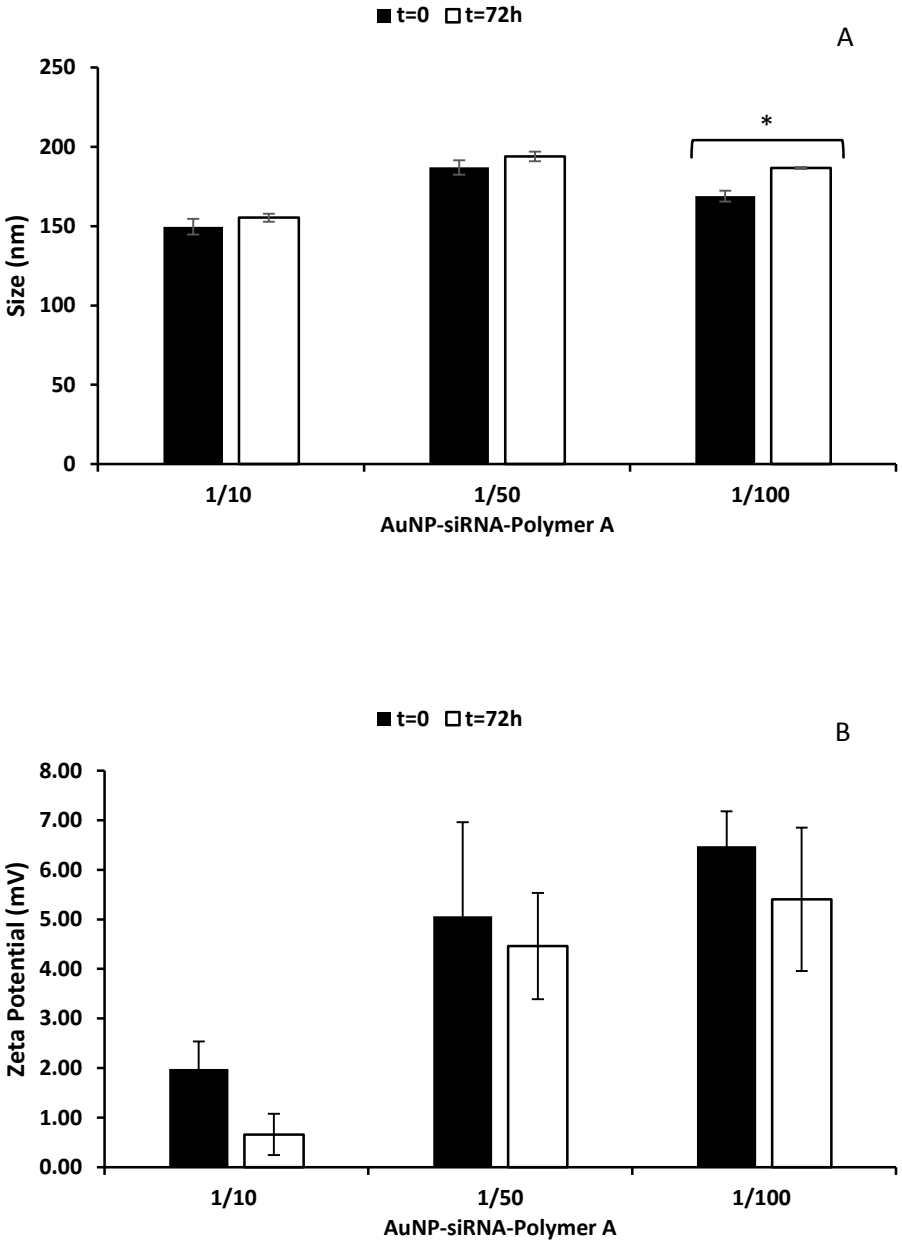

Figure 4.30. The change in the size (A) and zeta potential (B) values of AuNP-siRNA-PolymerA multilayer systems (AuNP/Polymer ratio: 1/10, 1/50 and 1/100). After preparation (t=0) and after 72h of incubation in HEPES buffer at pH 7.4 at +4°C (t=72h). * represents statistically significant difference ($p<0.05$).

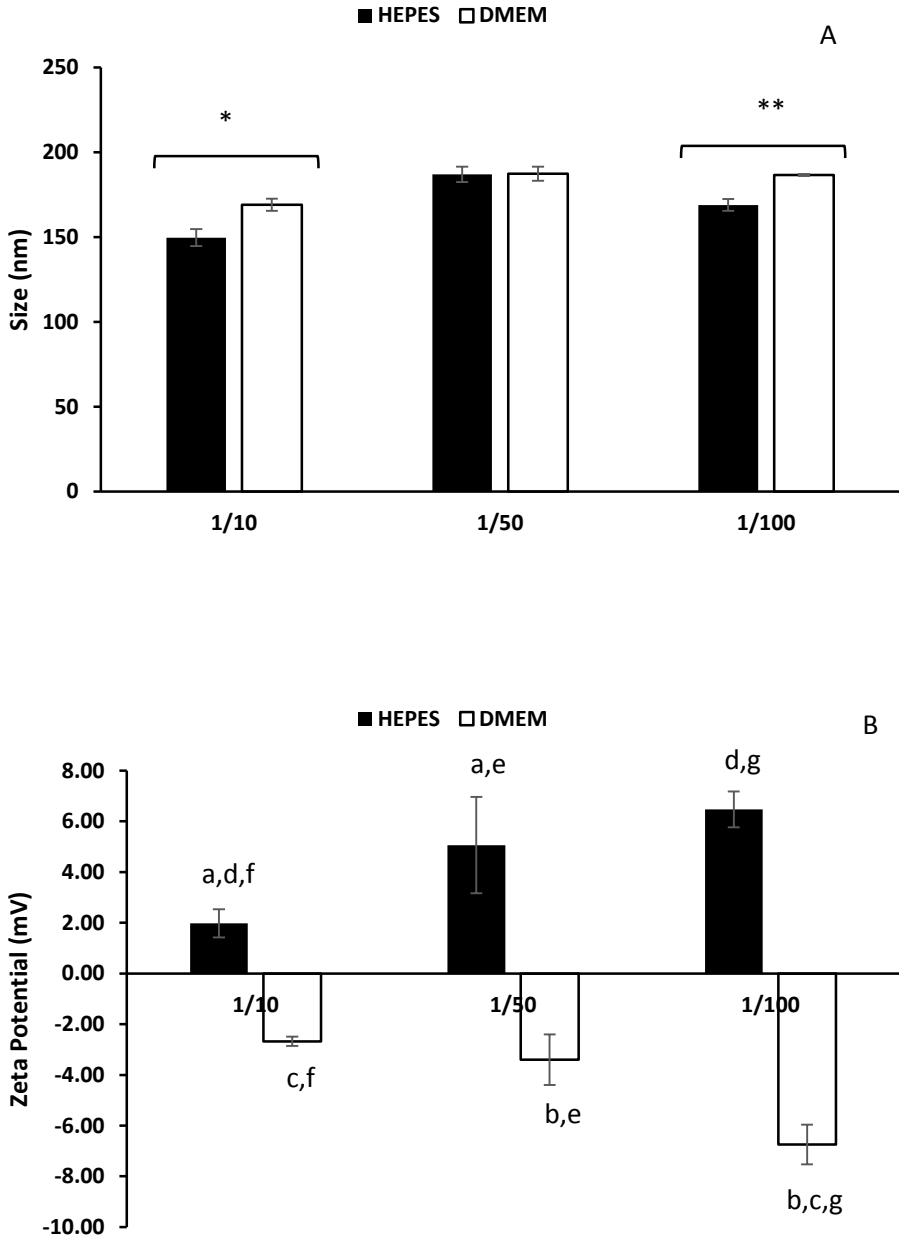

Figure 4.31. The change in the size (A) and zeta potential (B) values of AuNP-siRNA-Polymer A multilayer systems (AuNP/Polymer ratio: 1/10, 1/50 and 1/100). Even after preparation in HEPES buffer (HEPES) and after 24h of incubation at 37 °C in serum containing DMEM growth medium (DMEM). *, **, and letters represent statistically significant difference ($p<0.05$).

4.2.3.2. Luciferase Activity and Toxicity of AuNP-siRNA-Polymer Multilayer Systems

The cellular transfection efficiency and toxicity of AuNP-siRNA-Polymer multilayer systems on the SKOV3 cell line were also evaluated. In general, it was observed that the transfection efficiency of the multilayer systems including polymer A increased with the dose and did not change with the AuNP/Polymer ratio (Figure 4.32.). On the other hand, the multilayer systems without polymer (AuNP-siRNA) did not display any silencing effect at the same doses. This result clearly illustrates the benefit of the pentablock copolymer in providing siRNA protection and enhancing the silencing effect. Compared to the siRNA/Polymer polyplexes, the multilayer systems systems achieved better transfection efficiencies without showing severe toxicity although they possess lower siRNA loadings. For instance, the sRNA/Polymer A polyplex formed at N/P ratio of 50 with 100 nM siRNA loading managed to decrease luciferase expression by 50% while the multicomponent system prepared with 5 nM siRNA loading succeeded in providing ~65% luciferase expression suppression without causing any toxic effect. The main reason for better transfection efficiencies of the multilayer systems at lower doses is the presence of cleavable disulfide bonds in their structure which is broken by the glutathione existing in the cytoplasm facilitating the siRNA release, hence, increasing its luciferase activity within the cell. On the contrary, the strong electrostatic interactions between the polymer and siRNA in the polyplex systems prevents the efficient release of siRNA. To achieve similar gene silencing efficiency with the polyplex systems, larger amounts of siRNA and polymer are needed. However, this may potentially exacerbate the toxicity problem. We have previously shown that the cationic polyplexes are moderately toxic which probably originates from their high doses, excess cationic charge and strong interactions with the cell surface, leading to cell membrane disruption (Figures 4.25. and 4.26.). The AuNP-siRNA-Polymer A multilayer systems displayed no decrease in cell viability as shown in Figure 4.33.

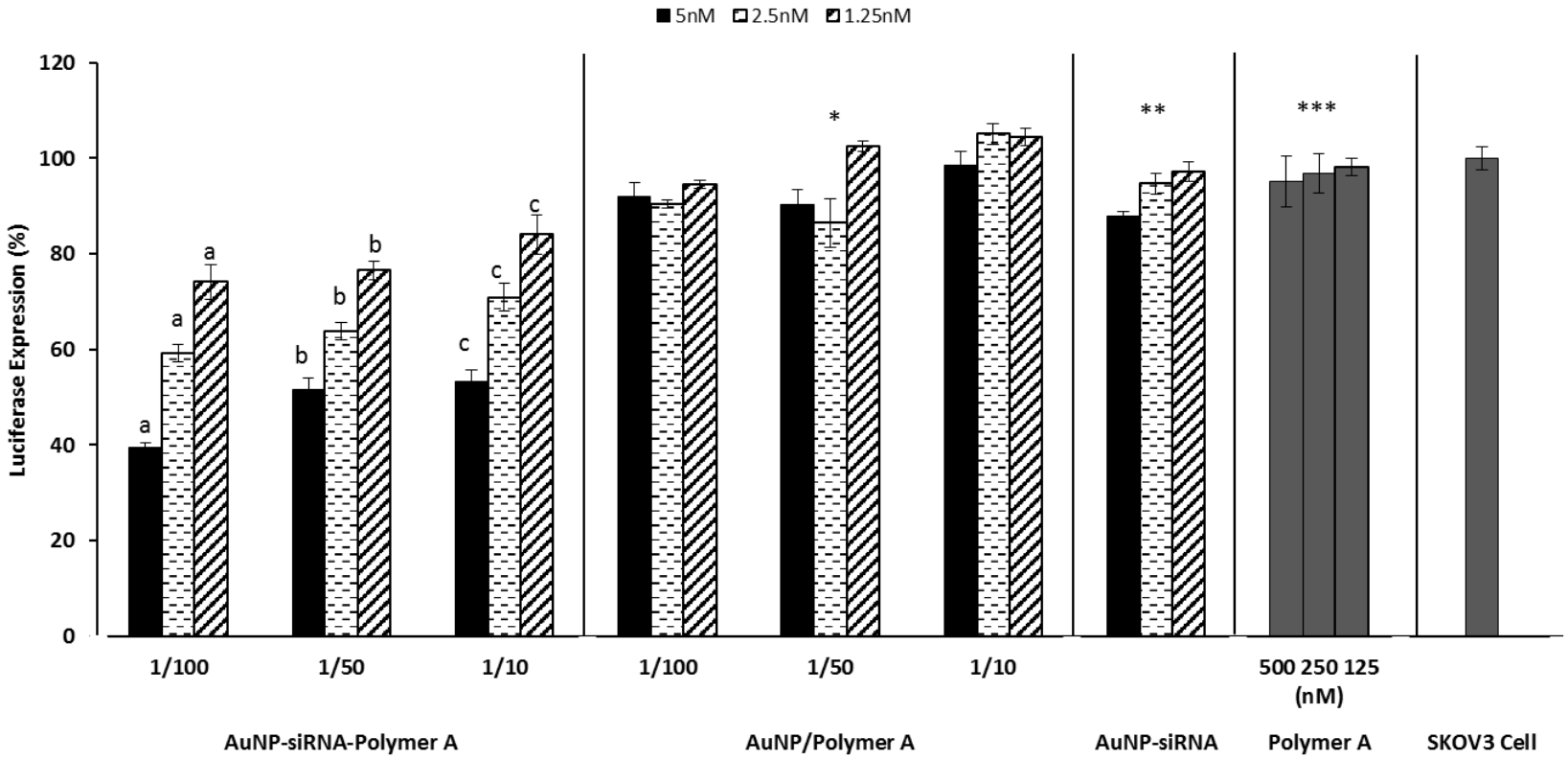

Figure 4.32. Luciferase suppression of prepared AuNP-siRNA-Polymer A multilayer systems. Applied multilayer systems dose (based on AuNP amount): 5, 2.5, 1.25 nM/well. Applied siRNA dose: 100, 50, 25 nM/well. Initial SKOV3 cell density: $1.5x10^4$ cell/well. Controls: AuNP-Polymer A (without siRNA), Polymer A alone, uncoated AuNP-siRNA multilayer systems (without Polymer A), naked siRNA SKOV3 cell. Incubation time: 24h. a,b,c: represent doses of AuNP-siRNA-Polymer A multilayer systems which caused significant difference in luciferase expression ($p<0.05$) for AuNP/Polymer ratios of 1/100, 1/50 and 1/10, respectively. *: Compared to AuNP-siRNA-Polymer A multilayer systems, AuNP/Polymer A multilayer systems showed significantly lower luciferase expression suppression ($p<0.05$) at all AuNP/Polymer ratios and doses applied. **: Uncoated AuNP/siRNA multilayer systems, at all doses applied showed significantly lower luciferase expression suppression than AuNP-siRNA-Polymer A multilayer systems.

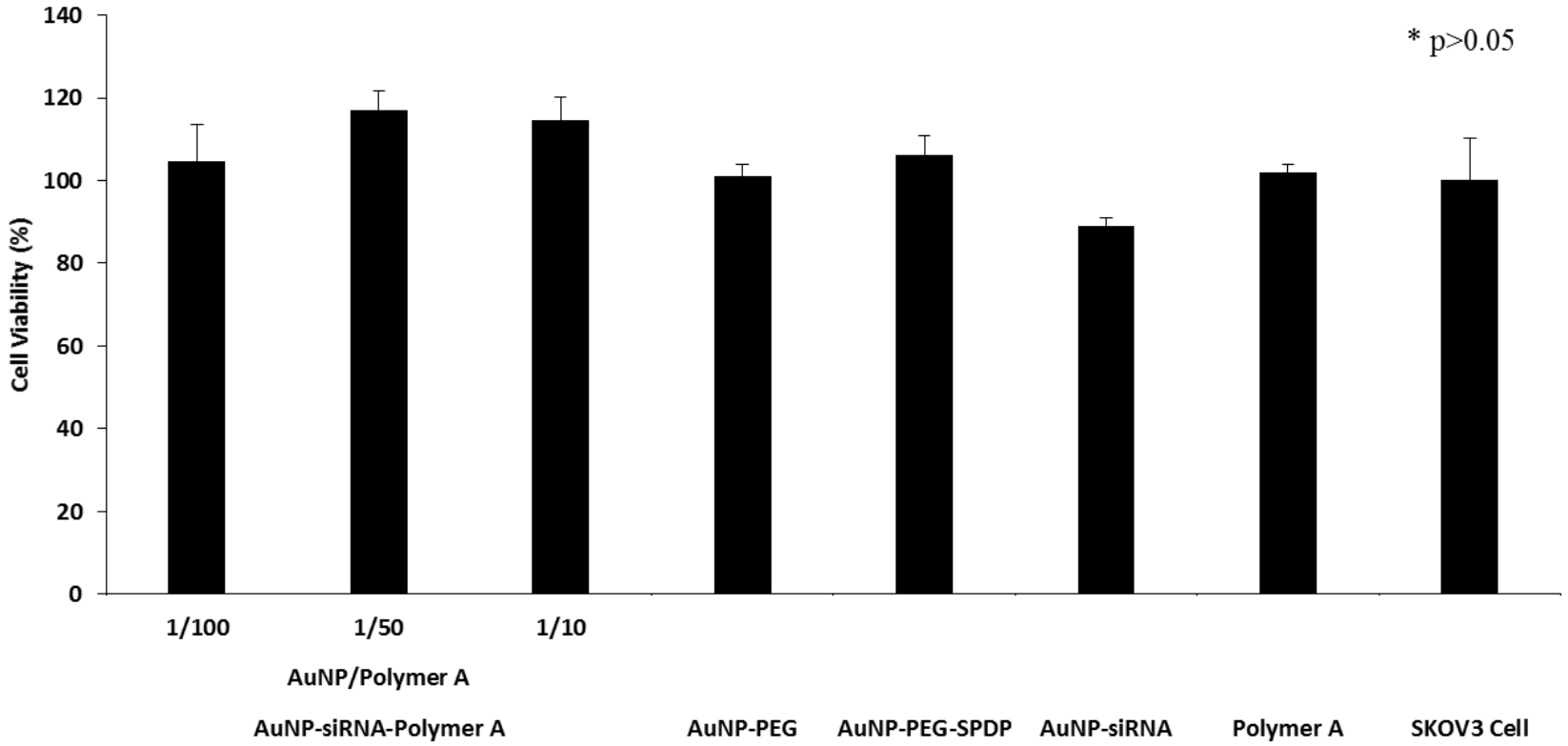

Figure 4.33. Cell viability of AuNP-siRNA-Polymer A multilayer systems treated SKOV3 cells. Applied multilayer systems dose (based on AuNP amount): 5 nM/well. Applied siRNA dose: 100 nM/well. Applied polymer dose: 500 nM/well. Initial SKOV3 cell density: $1.5x10^4$ cell/well. Controls: AuNP-Polymer A (without siRNA), Polymer A alone, uncoated AuNP-siRNA multilayer systems (without Polymer A), naked siRNA SKOV3 cell. Incubation time: 24h. AuNP-siRNA-Polymer A multilayer systems prepared with different polymer amounts, the layers of this multicomponent system (AuNP-PEG, AuNP-PEG-SPDP and AuNP-siRNA) and Polymer A alone did not cause significantly different cell viabilities compared with the SKOV3 cell alone ($p>0.05$).

The transfection efficiencies of the multilayer systems fabricated with polymer C were found to be similar to those of the AuNP-siRNA-polymer A multilayer systems (Figure 4.34.). On the other hand, when toxicity profile in Figure 4.35. is considered, it becomes clear that most of the decrease in the luciferase expression is not due to siRNA activity but because of the cell death resulting from the toxic effect of the multilayer systems. This toxic effect could be due to the massive cationic nature of Polymer C involving longer PDEAEM chains. The result clearly demonstrated that the length of the cationic blocks and the ratio between the cationic and non-cationic blocks in the pentablock copolymers has a significant influence on the toxicity of the multilayer systems as it determines the amount of positively charged groups, hence, the degree of interaction with the cell membrane. This allows us to easily tune the cytotoxicity of the pentablock copolymers by varying the lengths of the cationic blocks and the ratio between the cationic and non-ionic blocks.

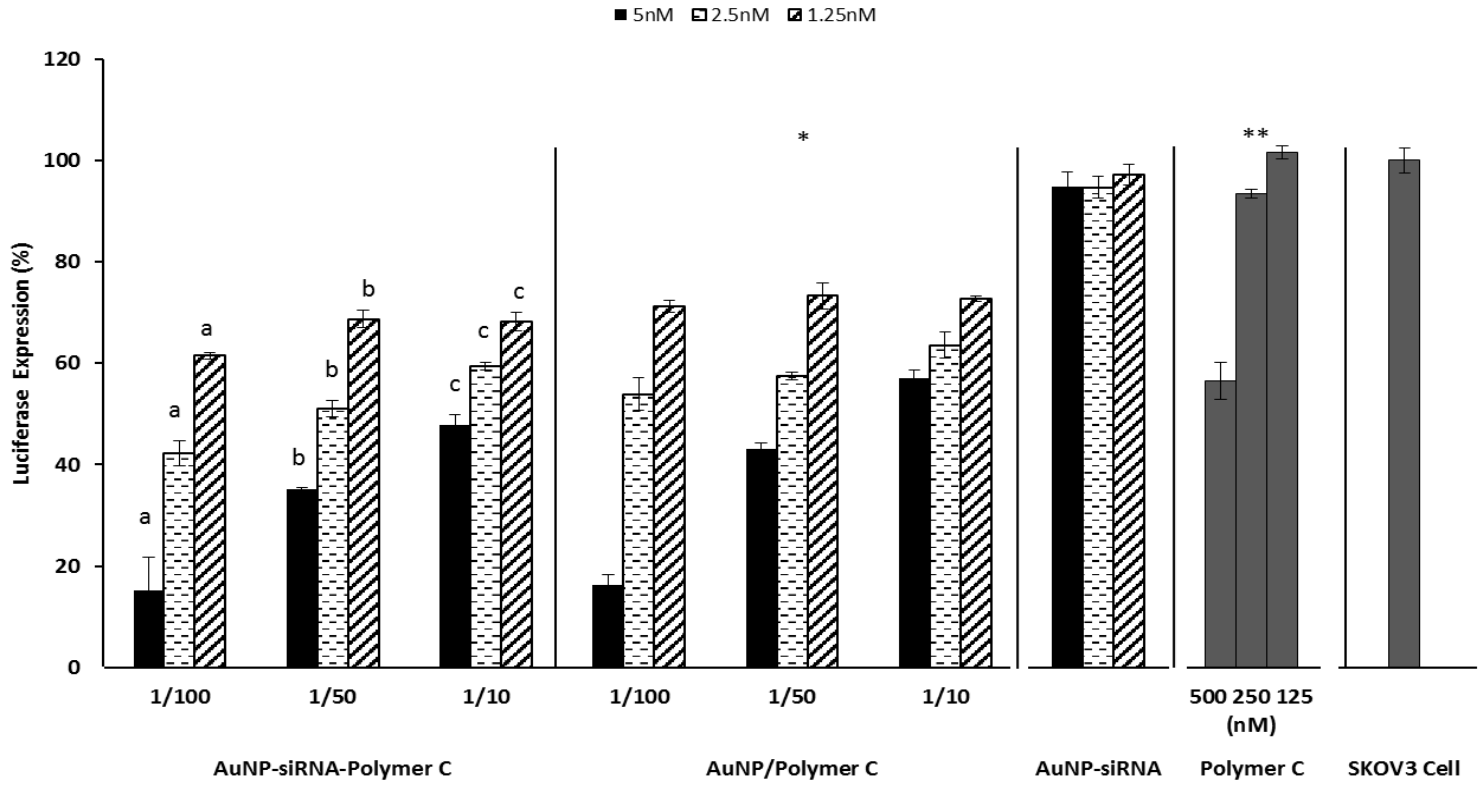

Figure 4.34. Luciferase suppression of prepared AuNP-siRNA-Polymer C multilayer systems. Applied multilayer systems dose (based on AuNP amount): 5, 2.5, 1.25 nM/well. Applied siRNA dose: 100, 50, 25 nM/well. Initial SKOV3 cell density: $1.5x10^4$ cell/well. Controls: AuNP-Polymer A (without siRNA), Polymer A alone, uncoated AuNP-siRNA multilayer systems (without Polymer A), naked siRNA SKOV3 cell. Incubation time: 24h. a,b,c: Represent doses of AuNP-siRNA-Polymer C multilayer systems which caused significant difference in luciferase expression ($p<0.05$) for AuNP/Polymer ratios of 1/100, 1/50 and 1/10, respectively. *: Compared to AuNP-siRNA-Polymer C multilayer systems, AuNP/Polymer C polyplexes showed significantly lower luciferase expression suppression ($p<0.05$) at all AuNP/Polymer ratios and doses applied. **: Polymer C alone applied at 250 and 125 nM doses showed significantly lower luciferase expression suppression than AuNP-siRNA-Polymer C multilayer systems prepared with AuNP/Polymer ratio of 1/100.

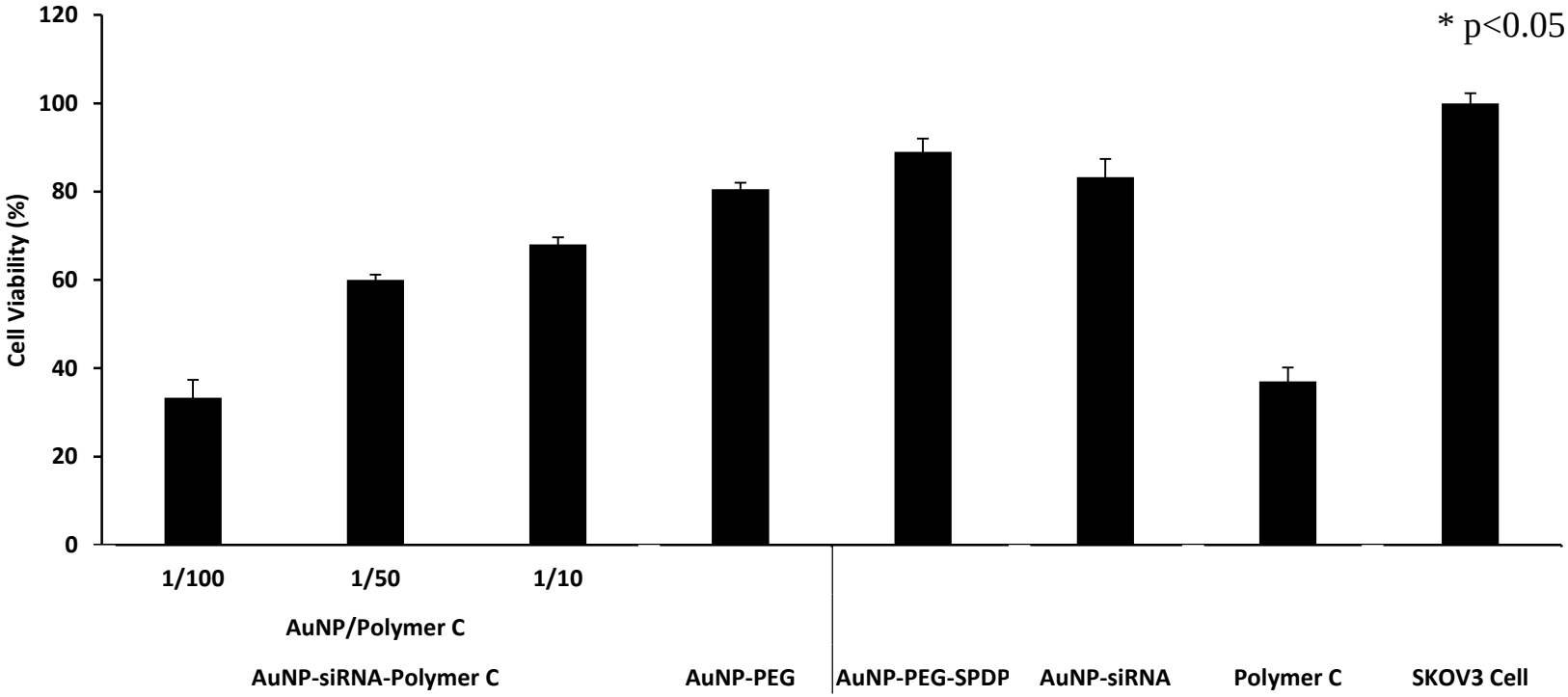

Figure 4.35. Cell viability of AuNP-siRNA-Polymer C multilayer systems treated SKOV3 cells. Applied multilayer systems dose (based on AuNP amount): 5 nM/well. Applied siRNA dose: 100 nM/well. Applied polymer dose: 500 nM/well. Initial SKOV3 cell density: $1.5x10^4$ cell/well. Controls: AuNP-Polymer C (without siRNA), Polymer C alone, uncoated AuNP-siRNA multilayer systems (without Polymer C), naked siRNA SKOV3 cell. Incubation time: 24h. * AuNP-siRNA-Polymer C comjugates prepared with different polymer amounts, the layers of this multicomponent system (AuNP-PEG, AuNP-PEG-SPDP and AuNP-siRNA) and Polymer C alone caused significantly different cell viabilities compared with the SKOV3 cell alone ($p<0.05$).

4.2.3.3. Cellular Uptake and Visualization of siRNA-Polymer Polyplexes and AuNP-siRNA-Polymer Multilayer Systems

The cellular uptake of the multilayer systems fabricated only by polymer A was evaluated due to its sufficient siRNA activity and slight toxic effect on the cells. Quantification of gold nanoparticle uptake by the cells was performed by ICP-MS which has a high specificity and low detection limit. Figure 4.36. shows that a significant increase in the cellular uptake was observed as the AuNP/Polymer ratio changed from 1/10 to 1/100. This could be due to micellization of Pluronic F127 blocks and enhanced interaction between the positively charged tertiary amine groups and negatively charged cell membrane as a consequence of increased polymer amount on the surface of the nanoparticles. Previous studies demonstrated the effect of temperature responsive Pluronic F127 block micellization on the cellular uptake of DNA and the effect of positively charged PDEAEM block inducing the cell membrane attachment (Brandenberger et al. 2010, Chen et al. 2011, Cho and Caruso 2005, Huhn et al. 2013, Marquis et al. 2011). Moreover, the time dependent cell uptake of multilayer system with AuNP/Polymer ration of 1/100 was investigated. Figure 4.37. indicates that the internalized amount of multilayer systems increased with time.

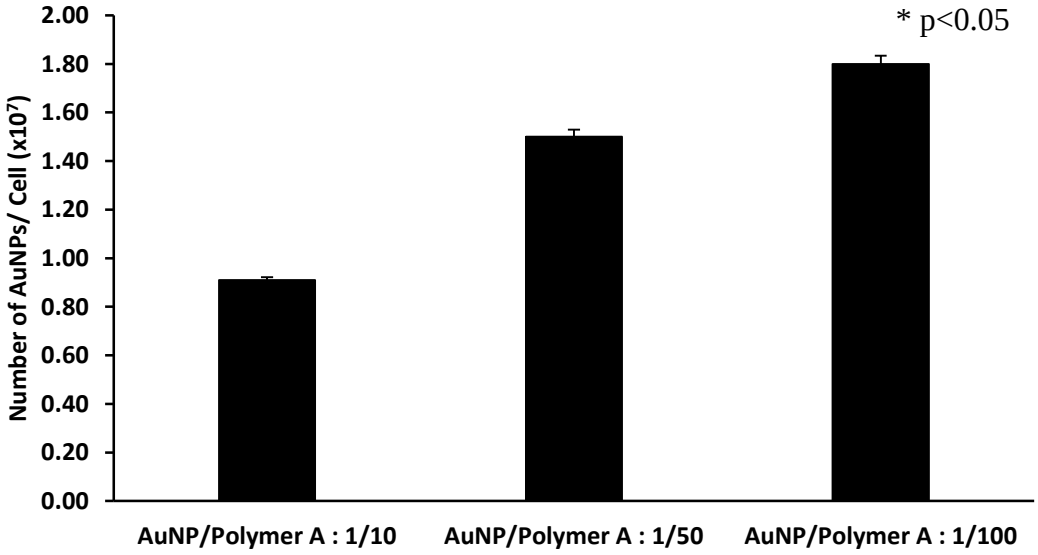

Figure 4.36. The number of AuNPs in SKOV3 cells measured by ICP-MS. The ratio of AuNP/Polymer A caused significant difference in number of AuNPs in the cell ($p<0.05$).

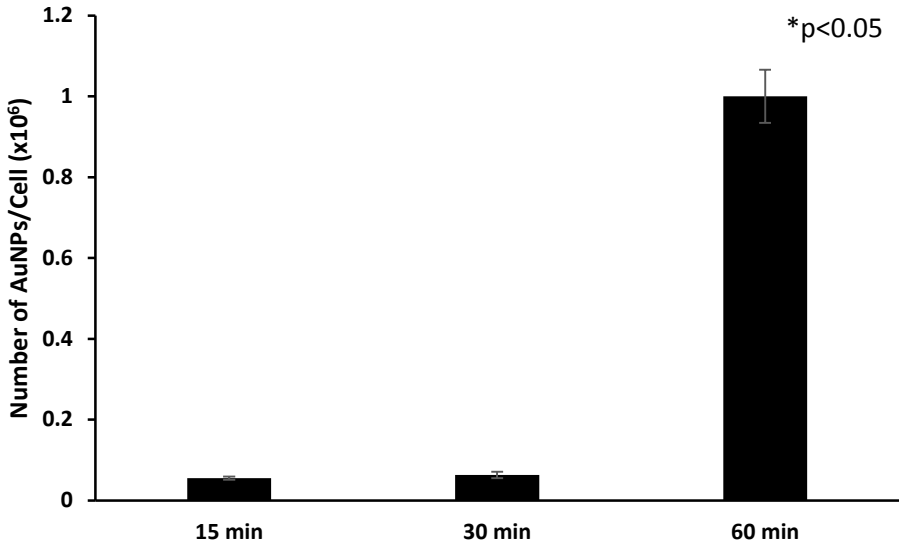

Figure 4.37. Time dependent cellular uptake of AuNP-siRNA-Polymer multilayer systems (AuNP/Polymer ratio: 1/100). Time: 15, 30 and 60 min. * represents statistical significant difference ($p<0.05$).

In addition to the multicomponent system, the cellular uptakes of the polyplexes prepared by fluorescence dye attached to Polymer A were also investigated through flow cytometry. The results indicated that the increase in N/P ratio induced the cellular uptake of the polyplexes (Figure 4.38.). The enhanced cellular uptake seems to provide higher luciferase suppression; however, it also resulted in severe toxicity (Figures 4.23. and 4.25.). Similar to the multilayer systems, the time dependent internalization of polyplexes was also investigated. The results in Figure 4.39. indicated that the internalization rate of polyplex, with N/P ratio of 50, increased with time.

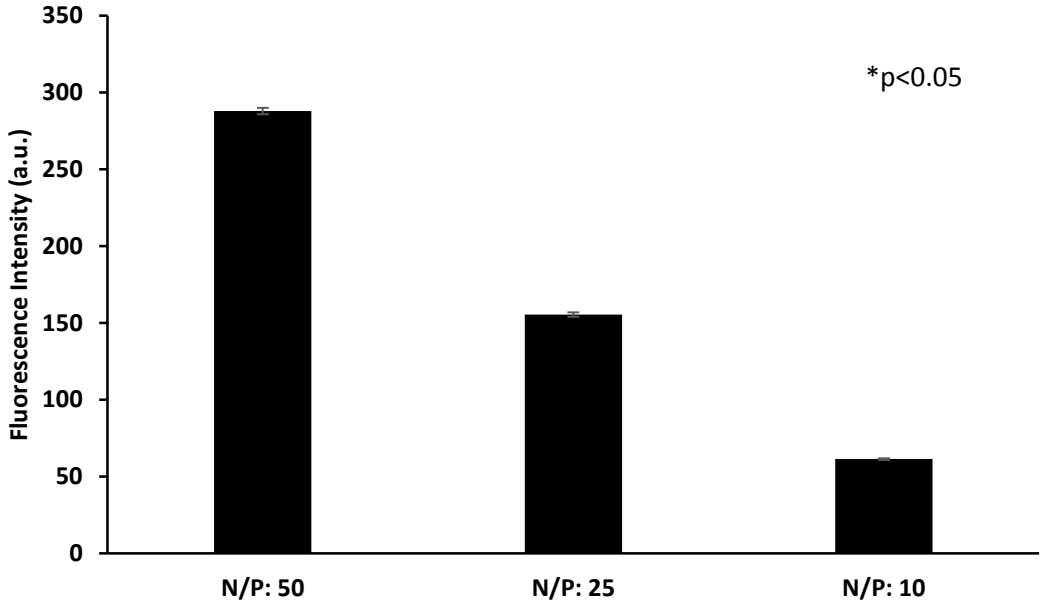

Figure 4.38. The cellular uptake of siRNA/Polymer A polyplexes at different N/P ratios. The ratio of N/P caused significant difference in cellular uptake ($p<0.05$).

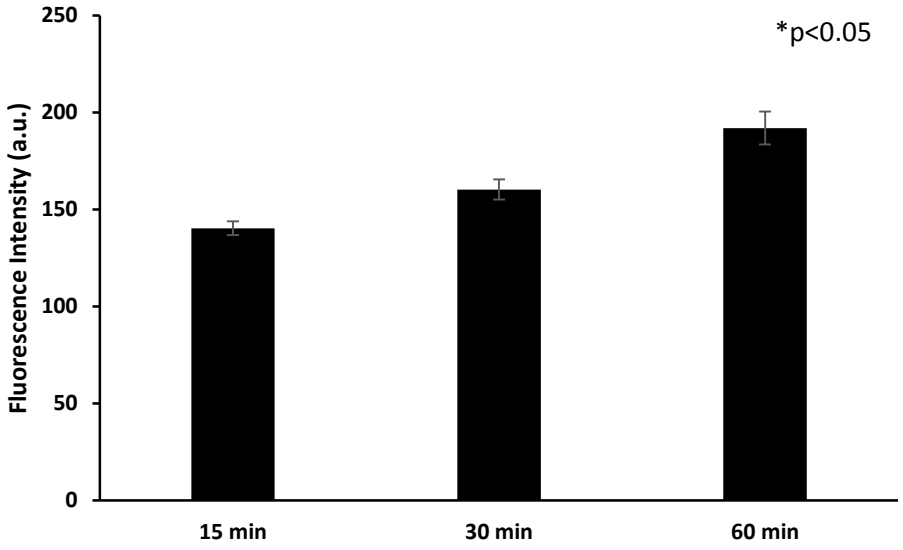

Figure 4.39. Time dependent cellular uptake of siRNA/Polymer A polyplexes (N/P ratio: 50). Time: 15, 30 and 60 min. * represents statistical significant difference ($p<0.05$).

It is known that after an efficient entry into the cells, the nanocarrier should escape from the endo-lysosomal pathway in order to prevent degradation of siRNA by many enzymes in the structure of the cell (Varkouhi et al. 2011). The intracellular distribution of the prepared multilayer systems and polyplex systems was investigated by confocal microscopy images. Figure 4.40. shows that most of the polyplexes were captured by

lysosomes preventing their accumulation in the cytoplasm. This could be attributed to insufficient amount of free positively charged tertiary amine groups in the polyplexes, which are capable of providing proton sponge effect by pH buffering and critical for endosomal escape. On the contrary, most multicomponent multilayer systems escaped from lysosomes and were distributed in the cytoplasm, which is necessary for an effective gene silencing effect (Figure 4.41.). Consequently, the improved endosomal escape ability of multicomponent systems may also be another reason for their high transfection efficiency compared to the polyplexes.

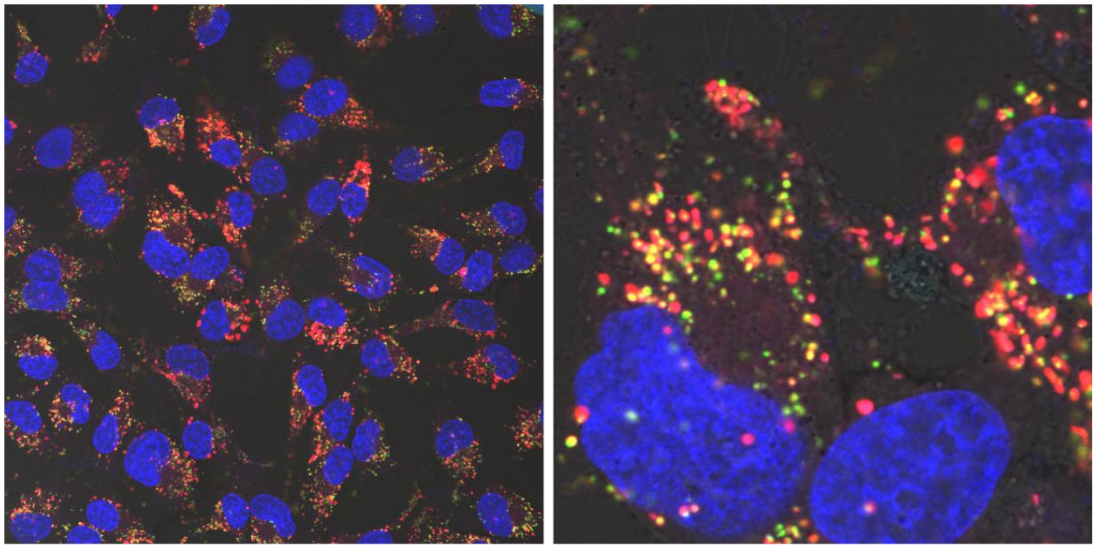

Figure 4.40. Confocal images of siRNA/Polymer A polyplexes prepared by N/P ratio of 50. Green: Polyplexes stained by Alexaflour488, Red: Lysosome stained by LysotrackerRed, Blue: Nucleus stained by Hoechst.

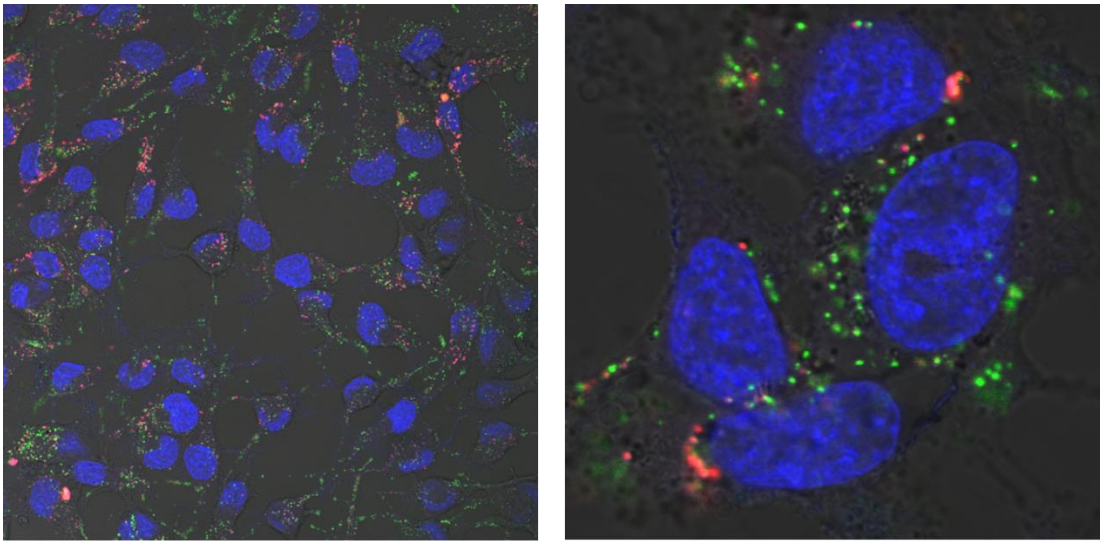

Figure 4.41. Confocal images of AuNP-siRNA-Polymer A multilayer system prepared by AuNP/Polymer ratio of 1/100. Green: Polyplexes stained by Alexaflour488, Red: Lysosome stained by LysotrackerRed, Blue: Nucleus stained by Hoechst.

4.3. Development of AuNP and Peptide Based siRNA Delivery Systems

In this section, AuNP and fusogenic peptide based multilayer siRNA delivery system was developed by using disulfide bonds and electrostatic interactions through layer by layer approach. In addition, a siRNA/peptide peptideplex system, obtained by direct electrostatic complexation of negatively charged siRNA and positively charged peptide, was used as control. The efficiencies of both systems were tested in terms of siRNA protection, cellular uptake, endosomal escape, siRNA activity and cytotoxicity against SKOV3 cell line.

4.3.1. Development of siRNA/Peptide Peptideplex System

4.3.1.1. Characterization of siRNA/Peptide Complexes

TAT-HA2 fusion peptide, with the amino acid sequence of, RRRQRRKKRGGDIMGEWGNEIFGAIAGFLG, was used for the development of peptide based siRNA delivery systems. The first 20 amino acids

(GDIMGEWGNEIFGAIAGFLG) belongs to influenza A virus hemagglutinin protein (HA2) connected to following 10 amino acid sequence (RRRQRRKKRG) which belongs to cell permeable HIV Trans-Activator of Transcription (TAT) protein transduction domain (PTD). TAT-HA2 as a combined peptide is capable of being used as a large macromolecule drug delivery peptide. The TAT PTD binds to the cell surface and penetrates the membrane via lipid raft-dependent macropinocytosis to provide cellular entry. On the other hand, the endosomal escape and transduction of the fusion peptide are enhanced by the HA2 domain, which has a pH-sensitive lipid membrane destabilizing sequence (Wadia, Stan, and Dowdy 2004). siRNA/Peptide complexes were obtained through the direct electrostatic interactions between the positively charged amine groups of the arginine amino acids present in the TAT domain of the peptide and negatively charged phosphate groups of siRNA. Due to the presence of positively charged amine groups of the arginine amino acids present of the TAT domain of the peptide and negatively charged phosphate groups of siRNA, electrostatically driven complexation can occur spontaneously between the peptide and the siRNA. To achieve complete condensation of siRNA, the ratio of nitrogen to phosphate was varied between 2.5 and 12.5. Gel electrophoresis data in Figure 4.42 A showed that the N/P ratio of 2.5 is not sufficient to provide complete condensation of siRNA. By keeping the amount of siRNA fixed and systematically increasing the amount of added peptide, which increases the N/P ratio, complete complexation was achieved between the siRNA and peptide. This was confirmed by the results shown in Figure 4.42 A that the siRNA in peptideplexes, formed at N/P ratios of above ~5 (i.e., at N/P=5, 7.5 and 10), did not migrate through the gel.

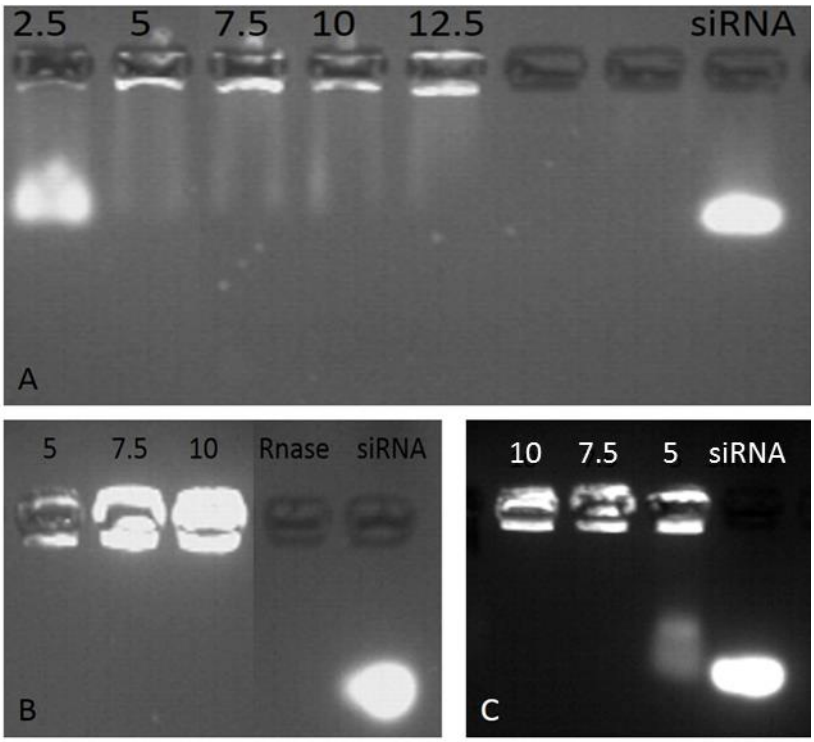

Figure 4.42. A) Gel electrophoresis of siRNA/Peptide complexes at various N/P ratios: 2.5, 5, 7.5, 10, 12.5. Control: Naked siRNA. B) RNase exposed siRNA/Peptide complexes at various N/P ratios: 5, 7.5, 10. Control: Naked siRNA and RNase exposed naked siRNA. RNase concentration: 0.25% (v/v). Incubation: 1h at 37°C. C) Serum protein stability of the siRNA/Peptide complexes at N/P ratios of 5, 7.5 and 10. Serum content: 50% (v/v). Incubation: 6h at 37°C.

The selected complexes were exposed to RNase enzymes and serum proteins in order to determine siRNA protection provided by the peptide complexation. The results in Figure 4.42 B showed that the naked siRNA completely degraded in the presence of RNase enzyme, while, the peptideplexes formed at N/P ratios of 7.5 and 10 provided and efficient siRNA protection against RNase enzyme. However, the poor siRNA intensity of the peptideplex with N/P ratio of 5 on the gel indicated that this complex did not managed to provide an efficient siRNA protection against RNase enzyme probably due to the weak complexation between siRNA and peptide. The serum stability results in Figure 4.42 C showed that peptideplexes with N/P ratios of 7.5 and 10 did not dissociate in the presence of serum proteins, whereas, the peptideplex with N/P ratio of 5 depicted a slight dissociation.

Besides, the stabilities of peptideplexes were also investigated in terms of size and zeta potential change. When the peptideplexes were incubated with serum containing medium their size did not changed significantly, whereas, their zetapotential values

became negative due to the protein attachment (Figure 4.43.). The stability in size indicates that particles maintained their complexation in the presence of serum proteins.

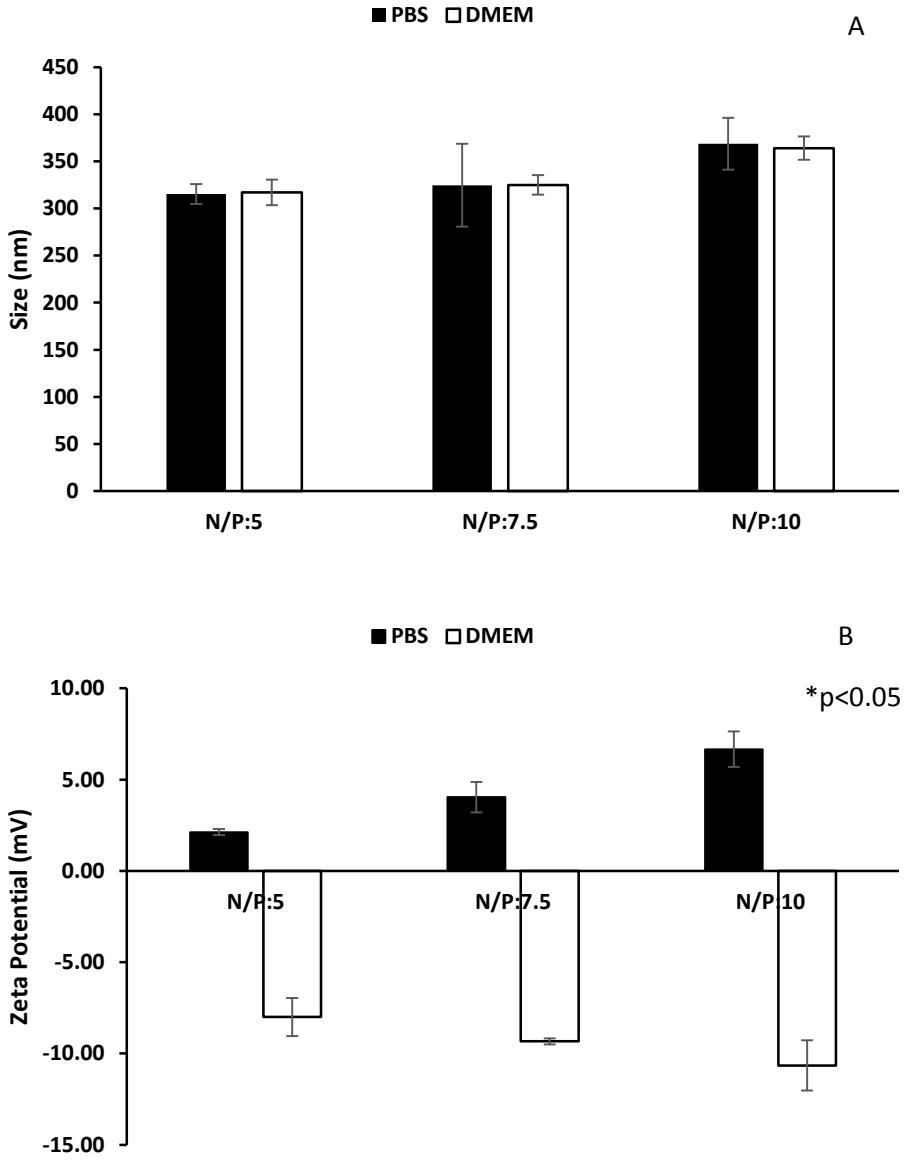

Figure 4.43. The change in the size (A) and zeta potential (B) values of siRNA/Peptide peptideplex systems (N/P ratio: 5, 7.5 and 10). Even after preparation in PBS buffer (PBS) and after 24h of incubation at 37 °C in serum containing DMEM growth medium (DMEM). * represents statistically significant difference ($p<0.05$).

4.3.1.2. Luciferase Activity and Toxicity of siRNA/Peptide Peptideplexes

The siRNA/Peptide complexes formed at different N/P ratios (5, 7.5 and 10) were administered to the SKOV3 cells at variable doses and the decrease in the luciferase expression was monitored (Figure 4.44.). All of the conjugates showed ~50% decrease in luciferase expression at their maximum doses (400 nM) compared to control. As the dose decreased to 100 nM, the suppression of the luciferase expression decreased to ~30% (Figure 4.44.). The complexes formed at different N/P ratios did not cause a significant change in luciferase expression suppression. Compared to previous studies published in the literature (Hoyer and Neundorf 2012a, Lee, Kim, and Park 2007, Mok and Park 2008, Oliveira et al. 2007), the biological activity of the siRNA/peptide complexes on luciferase expression was found to be moderate. This is mainly due to strong electrostatic forces resulting from the use of excess peptide which avoids the release of sufficient emount of siRNA. Another reason might be the reduced cellular uptake due to neutralization of cationic arginine amino acids during complexation (Nakase, Tanaka, and Futaki 2013). The arginine amino acids in the TAT domain of the peptide is responsible from the cell membrane attachment and penetration to the membrane via lipid raft-dependent macropinocytosis. None of the complexes tested showed any toxic effect at 100 nM dose, on the other hand, cell viabilities decreased to 80% when the dose was increased to 400 nM (Figure 4.45.). The toxic effect at the highest dose is a consequence of excess cationic groups inducing nonspecific electrostatic interactions.

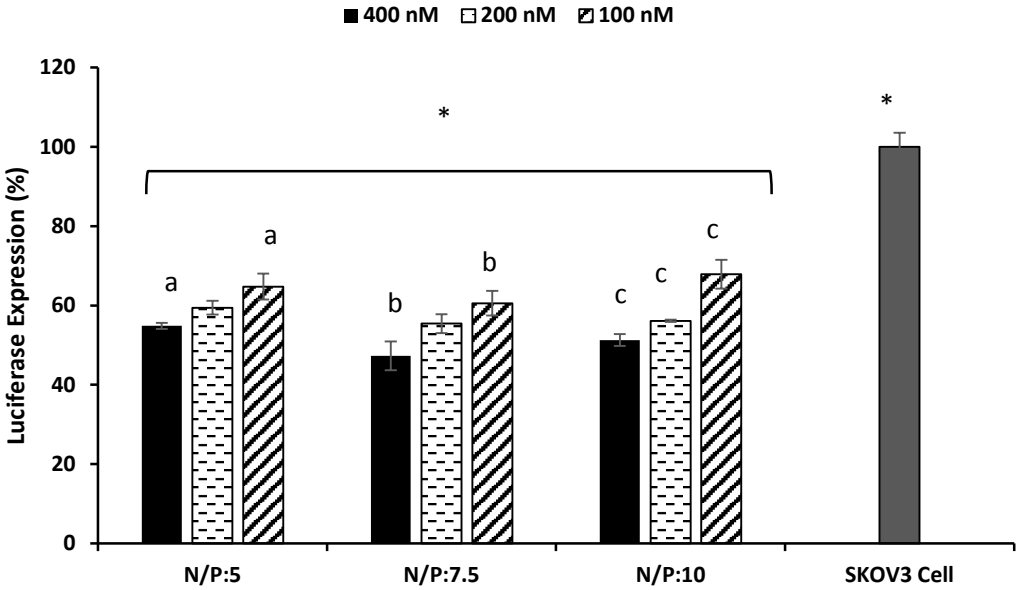

Figure 4.44. Luciferase expression suppression of prepared siRNA/Peptide complexes. N/P: 5, 7.5 and 10. Applied siRNA dose: 100, 200, 400 nM. Initial SKOV3 cell density: $1x10^4$ cell/well. Incubation time: 24h. a, b, c and * represent statistically significant difference ($p<0.05$).

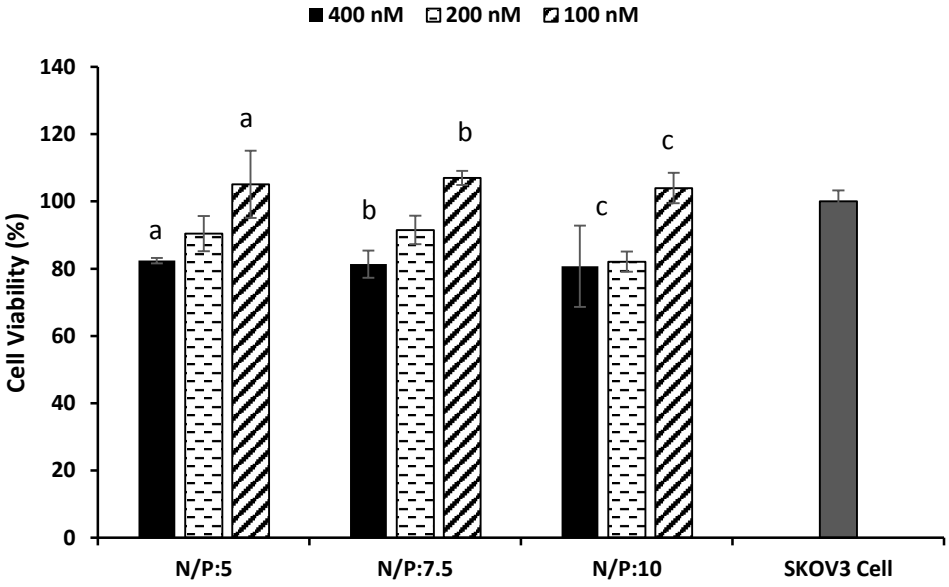

Figure 4.45. Cell viability of siRNA/Peptide complex administered SKOV3 cells. N/P: 5, 7.5 and 10. Applied siRNA dose: 100, 200, 400 nM. Initial SKOV3 cell density: $1x10^4$ cell/well. Incubation time: 24h. a, b, c represent statistically significant difference ($p<0.05$).

4.3.2. Development of AuNP and Peptide Based Multilayer siRNA Delivery Systems

4.3.2.1. Characterization of AuNP and Peptide Based Multilayer siRNA Delivery Systems

As an alternative to the siRNA/peptide complex systems, the AuNP-siRNA-Peptide multilayer system was developed in order to facilitate siRNA release and enhance its luciferase suppression activity. The system was constructed using the same protocol followed in the preparation of AuNP-siRNA-Polymer system except that the last layer of the assembly is formed from the TAT-HA2 peptide. The last layer has a critical role since it controls protection of siRNA from intra and extracellular effects, cell uptake, endosomal escape and siRNA delivery in the cytoplasm. The adsorption of peptides on AuNP-siRNA was demonstrated by the red shift from 520 to 530 nm as shown in Figure 4.46. A slight shift in the maximum wavelength is due to low molecular weight and small size of peptide.

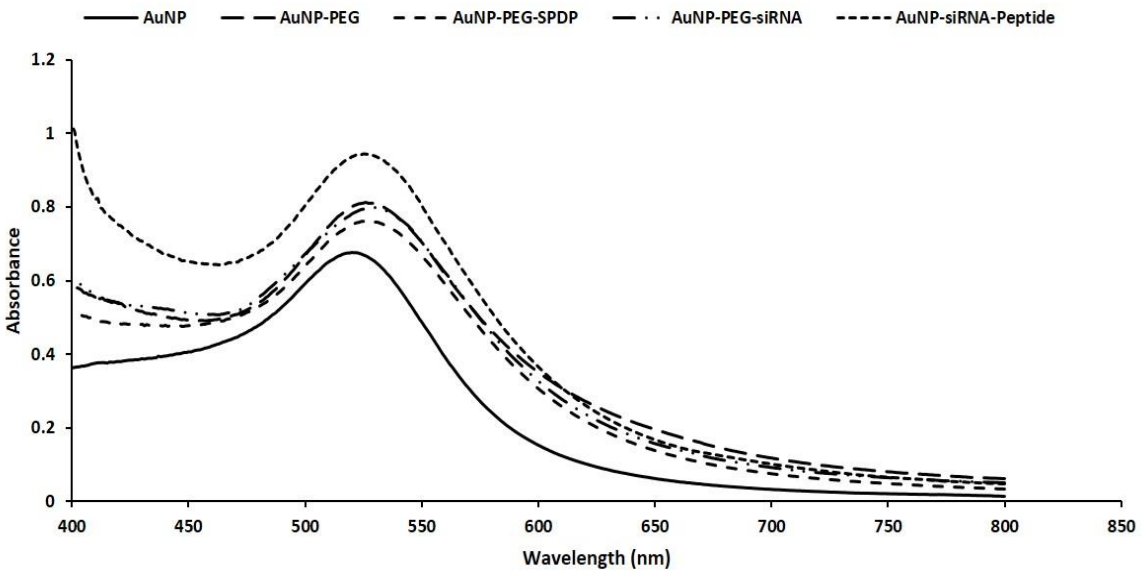

Figure 4.46. UV-vis spectra of AuNP, PEG modified AuNP, SPDP and siRNA modified AuNP-PEG and peptide coated AuNP-siRNA multilayer system.

The peptide coating resulted in an increase in the cumulative size of the assembly from ~13 nm to ~40 nm as shown by the DLS data (Figure 4.47.). The change in the ratio of AuNP/peptide from 1/125 to 1/500 did not cause a significant difference in the size of the AuNP-siRNA-Peptide multilayer assembly (Figure 4.47.). The zeta potential results also supported successful adsorption of peptide. Upon peptide attachment net negative charge of the siRNA attached surface (-2.64 mV) (Table 4.6.) become positive (Figure 4.47 B). The stabilities of the multilayer systems were tested in terms of size and zeta potential values in presence of serum containing DMEM medium. The results in Figure 4.47 A and B clearly indicated that the size and zeta potential of the peptide based multilayer systems changed significantly.

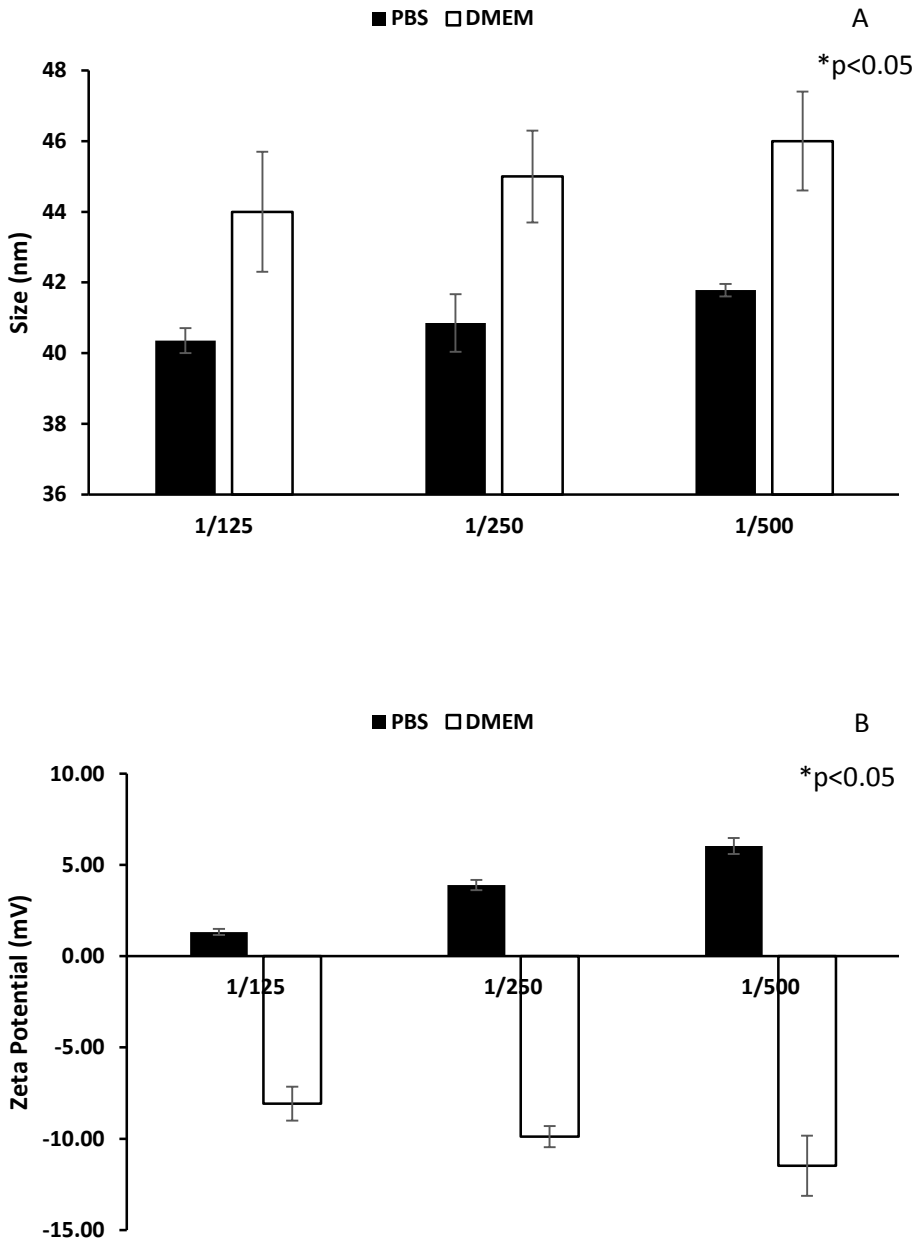

Figure 4.47. The change in the size (A) and zeta potential (B) values of AuNP-siRNA-Peptide multilayer systems (AuNP/Peptide ratio: 1/125, 1/250 and 1/500). Even after preparation in PBS buffer (PBS) and after 24h of incubation at 37 °C in serum containing DMEM growth medium (DMEM). * represents statistically significant difference ($p<0.05$).

The RNase and serum protein stabilities of the AuNP-siRNA-Peptide systems were assessed with the agarose gel electrophoresis. The results in Figure 4.48. clearly show that all of the multilayer peptide systems (AuNP/peptide ratio: 1/125, 1/250, 1/500) provide protection of siRNA against degradation by RNase or in the presence of serum proteins.

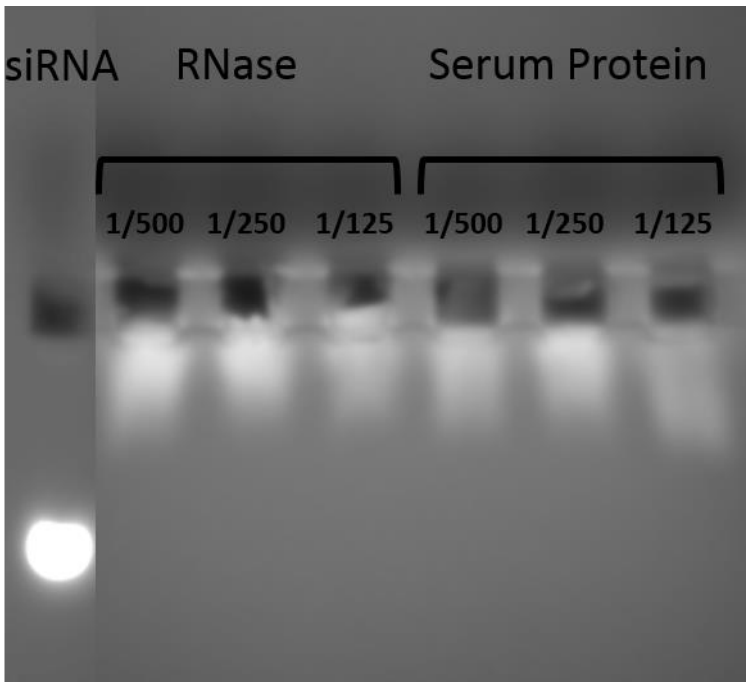

Figure 4.48. Agarose gel electrophoresis retardation of AuNP-siRNA-Peptide and naked siRNA. RNase and serum protein stabilities of the conjugates prepared with Peptide at AuNP/Peptide ratios of 1/500, 1/250 and 1/125.

4.3.2.2. Luciferase Activity and Toxicity of AuNP-siRNA-Peptide Multilayer Systems

Figure 4.49. shows the knockdown of the luciferase expression depending on the AuNP/peptide ratio and the dose of the siRNA. Increasing the peptide concentration did not improve the transfection efficiency in fact, all of multilayer systems prepared, showed similar suppression levels for luciferase expression (~30% at 1.25 nM dose and ~45% at 5 nM dose) at all doses applied. The AuNP based peptide systems have considerably higher siRNA activity at lower doses (~45% at 120 nM) than the siRNA/peptide complex system (~60% at 400 nM). The cleavable disulfide bonds in the AuNP-siRNA-Peptide multicomponent system apparently facilitates the siRNA release leading to better siRNA

activity in cytoplasm compared to siRNA/Peptide complex system in which siRNA binds to cationic peptide groups through strong electrostatic forces. In addition, in the multilayer only a small fraction of positively charged arginine amino acids is used for binding to the siRNA. Thus, free arginine moieties enhance the cellular uptake compared to the siRNA/Peptide complexes in which most of the arginine amino acids is neutralized by siRNA complexation. Small loadings of siRNA in the AuNP based systems require small amount of peptide for efficient siRNA condensation resulting in a non-toxic delivery system. Figure 4.50. shows that none of the AuNP-siRNA-Peptide multilayer systems at three different doses applied showed a significant toxic effect on the cells.

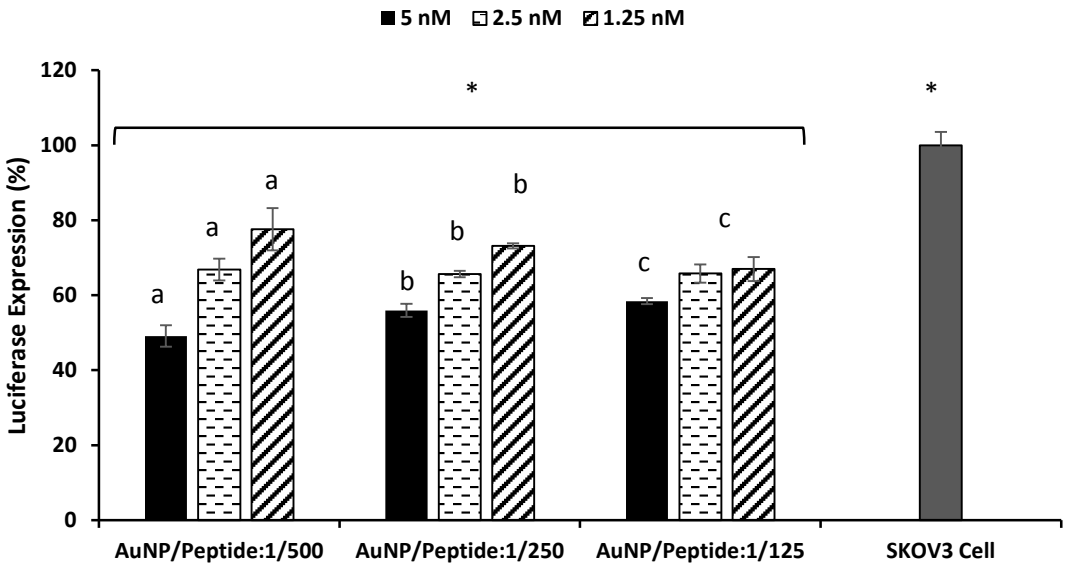

Figure 4.49. Luciferase suppression of prepared AuNP-siRNA-Peptide multilayer systems (AuNP/Peptide ratio: 1/500, 1/250, 1/125). Applied conjugate dose (based on AuNP amount): 5, 2.5, 1.25 nM/well. Applied siRNA dose: 100, 50, 25 nM/well. Initial SKOV3 cell density: $1.5x10^4$ cell/well. Incubation time: 24h. a, b, c and * represent statistically significant difference ($p<0.05$).

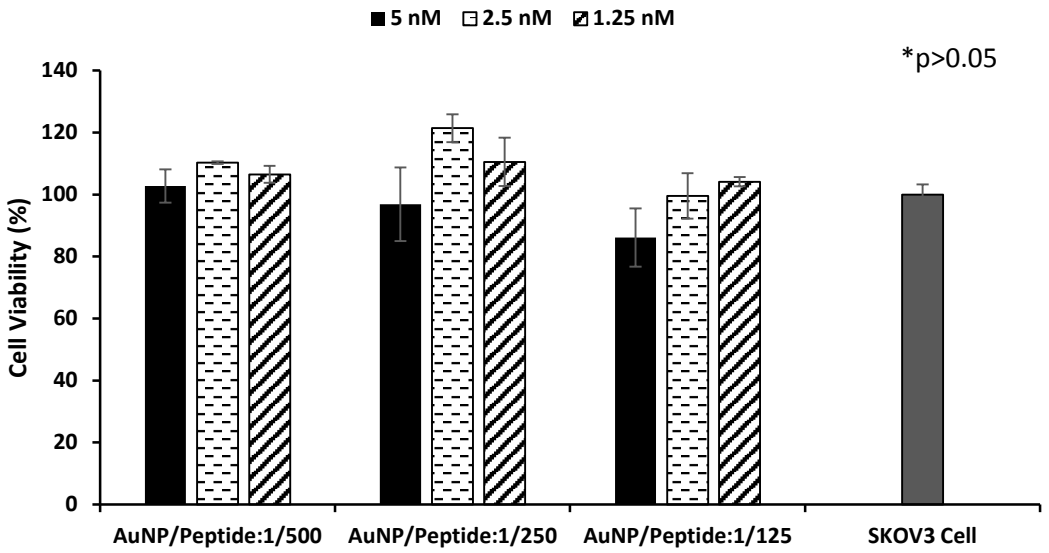

Figure 4.50. Cell viability of AuNP-siRNA-Peptide multilayer systems treated SKOV3 cells (AuNP/Peptide ratio: 1/500, 1/250, 1/125). Applied conjugate dose (based on AuNP amount): 5 nM/well. Applied siRNA dose: 100 nM/well. Initial SKOV3 cell density: $1.5x10^4$ cell/well. Incubation time: 24h. * represents statistically insignificant difference ($p>0.05$).

4.3.3. Cellular Uptake and Visualization of siRNA/Peptide Peptideplexes and AuNP-siRNA-Peptide Multilayer Systems

The cellular uptake of the AuNP-siRNA-Peptide multilayer system was evaluated through ICP-MS analysis. The results of ICP-MS analysis in Figure 4.51. represented that the increase in the amount of peptide covering the outer layer of the system enhanced the cellular uptake and particle accumulation at the end of 24 h. The increase in peptide concentration cannot be understood from the increase in size shown in Figure 4.47 A due to the small size of peptide molecules. However, the increased zeta potential values were indication of higher peptide amount deposition on the surface (Figure 4.47 B). The uptake mechanism of this peptide depends on the fact that the TAT protein transducing domain of the peptide facilitating the cell membrane attachment and enhance the cell membrane penetration through lipid raft-dependent macropinocytosis. Therefore, the increased peptide concentration on the surface of the multilayer system allows the presence of free arginine amino acids on the surface leading to enhanced cellular entry. Moreover, HA2 domain of the peptide, which possesses a pH-sensitive lipid membrane destabilizing sequence, is expected facilitate the endosomal escape (Wadia, Stan, and Dowdy 2004).

In addition to the effect of peptide concentration on the surface, the increase in the applied dose resulted in an increase in the cellular uptake (Figure 4.51.). Figure 4.52. shows that the cellular uptake of particles increased with respect to time.

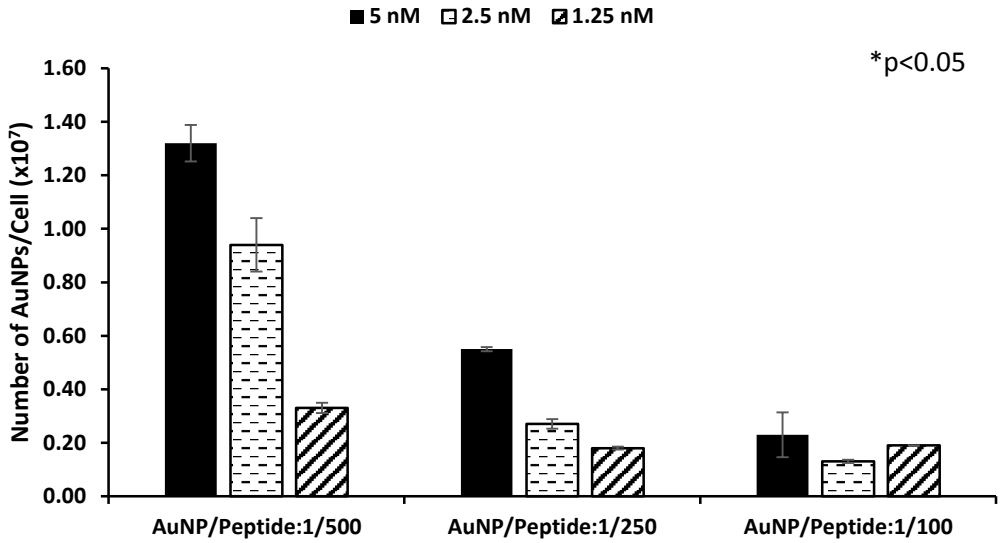

Figure 4.51. The number of AuNPs in SKOV3 cells measured by ICP-MS. Applied dose based on AuNP amount: 5, 2.5, 1.25 nM. Incubation time: 24h. The ratio of AuNP/Peptide caused significant difference in number of AuNPs in the cell ($p<0.05$).

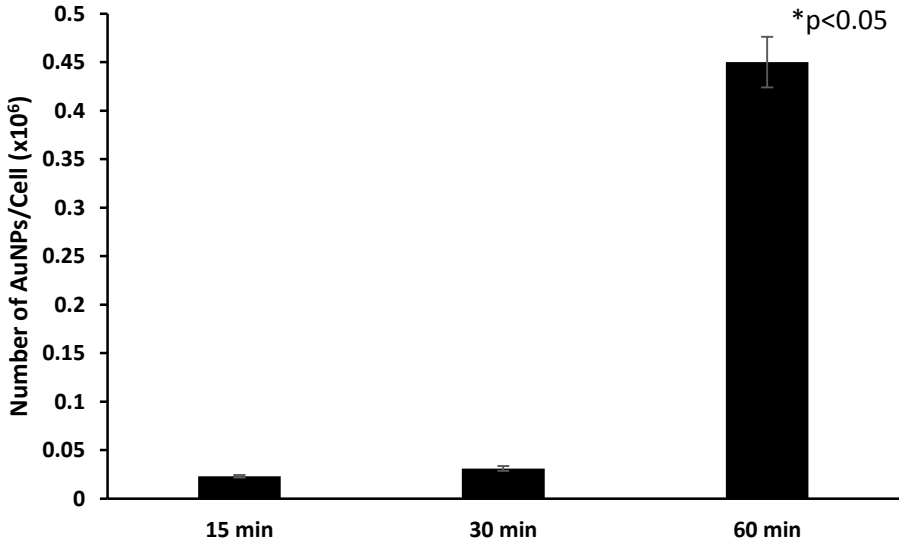

Figure 4.52. Time dependent cellular uptake of AuNP-siRNA-Peptide multilayer systems (AuNP/Peptide ratio: 1/500). Applied dose: 5 nM based on AuNP Time: 15, 30 and 60 min. * represents statistical significant difference ($p<0.05$).

Similarly the cell uptake of the siRNA/Peptide complexes were evaluated through the flow cytometry. The fluorescence dye was attached to the free -NH_2 groups in arginine amino acids present in TAT domain, which is responsible from cell membrane attachment and cell uptake, and siRNA/Peptide complexes were obtained by changing N/P ratio. The results in Figure 4.53. showed that the increase in N/P ratio led to an increase in the cellular uptake and complex accumulation in 24h. Although the change in N/P ratio significantly varied the cell uptake, these differences in cell uptake did not show a significant difference in luciferase expression suppression and toxicity represented in Figures 4.44. and 4.45., respectively. Several studies have revealed that in the case of TAT base gene delivery systems, the size of the peptide complexes play an essential role in the uptake mechanism by endosomes. Particle smaller than 300 nm do not enter the cell through the endosome pathway, in contrast to particles of 500–700 nm which are taken up by endocytosis (Varkouhi et al. 2011). It was also noticed that the size of the complexes are higher that 300nm, however, they did not significantly change with respect to N/P ratio (Figure 4.43 A). Therefore, considering the size of the complexes, we assume that the complexes enter the cell through the endosomal pathway. Figure 4.54. also showed that the cellular entry of the complexes increased with time.

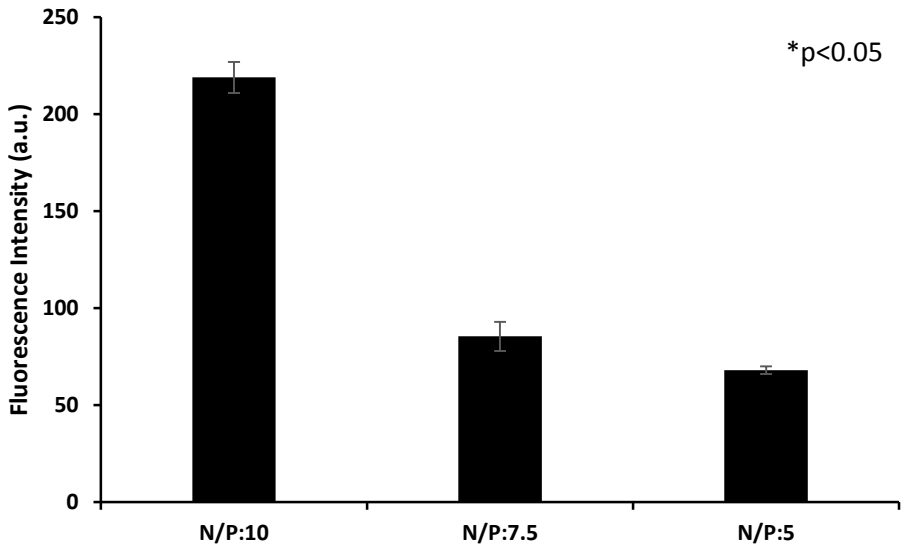

Figure 4.53. The cellular uptake of siRNA/Peptide complexes at different N/P ratios. Applied dose: 400 nM based on siRNA. Incubation: 24h. The ratio of N/P caused significant difference in cellular uptake ($p<0.05$).

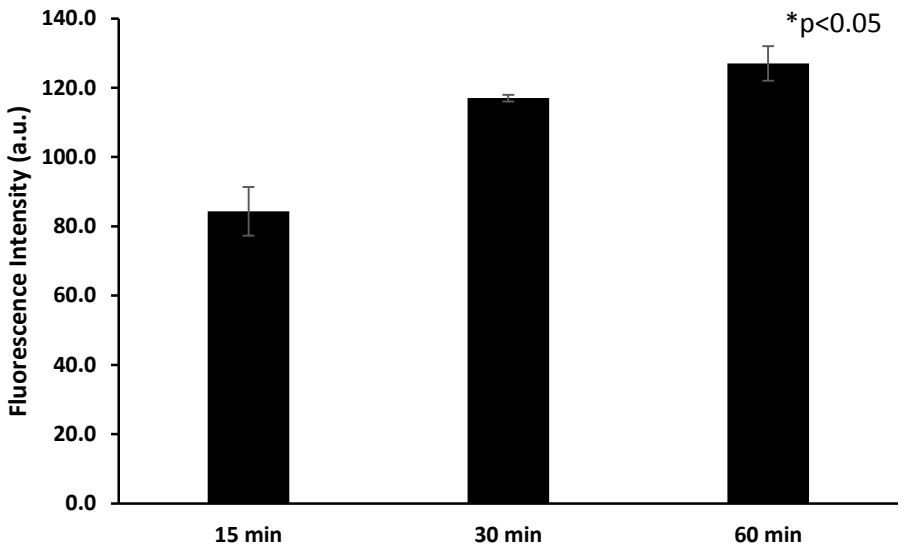

Figure 4.54. Time dependent cellular uptake of siRNA/Peptide peptideplexes (N/P ratio: 10). Applied dose: 400 nM based on siRNA. Time: 15, 30 and 60 min. * represents statistical significant difference ($p<0.05$).

The dye attached complexes were visualized by confocal microscopy in Figure 4.55. It was observed that the complexes managed to provide cellular entry and escape from the endososome.

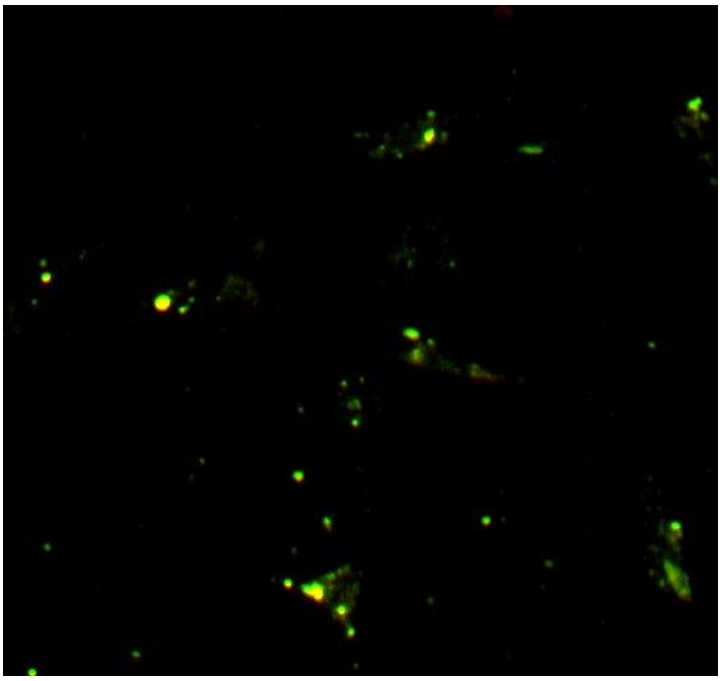

Figure 4.55. Confocal images of siRNA/Peptide complexes prepared by N/P ratio of 10. Green: Complexes stained by FITC, Red: Lysosome stained by LysotrackerRed.

4.3.4. Development of siRNA-Peptide Conjugates

4.3.4.1. Characterization of siRNA-Peptide Conjugates

Alternative siRNA delivery system based on the direct attachment of thiol modified siRNA to the peptides through the cleavable disulfide bonds was developed. The siRNA was attached through the multifunctional cross linker (SPDP). Following the attachment of amine reactive end of the SPDP to the peptide, thiol modified siRNA was linked to the sulfhydryl reactive portion of SPDP forming cleavable disulfide bonds which facilitates the siRNA release in cytoplasm and increase the luciferase activity.

The successful synthesis of siRNA-peptide conjugate was confirmed by agarose gel electrophoresis (Figure 4.56 A). The complete siRNA attachment was observed for the conjugates formed at N/P ratio of 7.5 and 10. At N/P ratio of 5, the unattached siRNA showed a mobility on the gel. Figures 4.56 B and C show that for the conjugation, N/P ratios of 5 and 7.5 are not sufficiently high to protect siRNA against degradation by RNase enzyme or dissociation by serum proteins. On the other hand, siRNA conjugated to peptide at the N/P ratios of 10 remained stable after incubation with RNase and serum proteins.

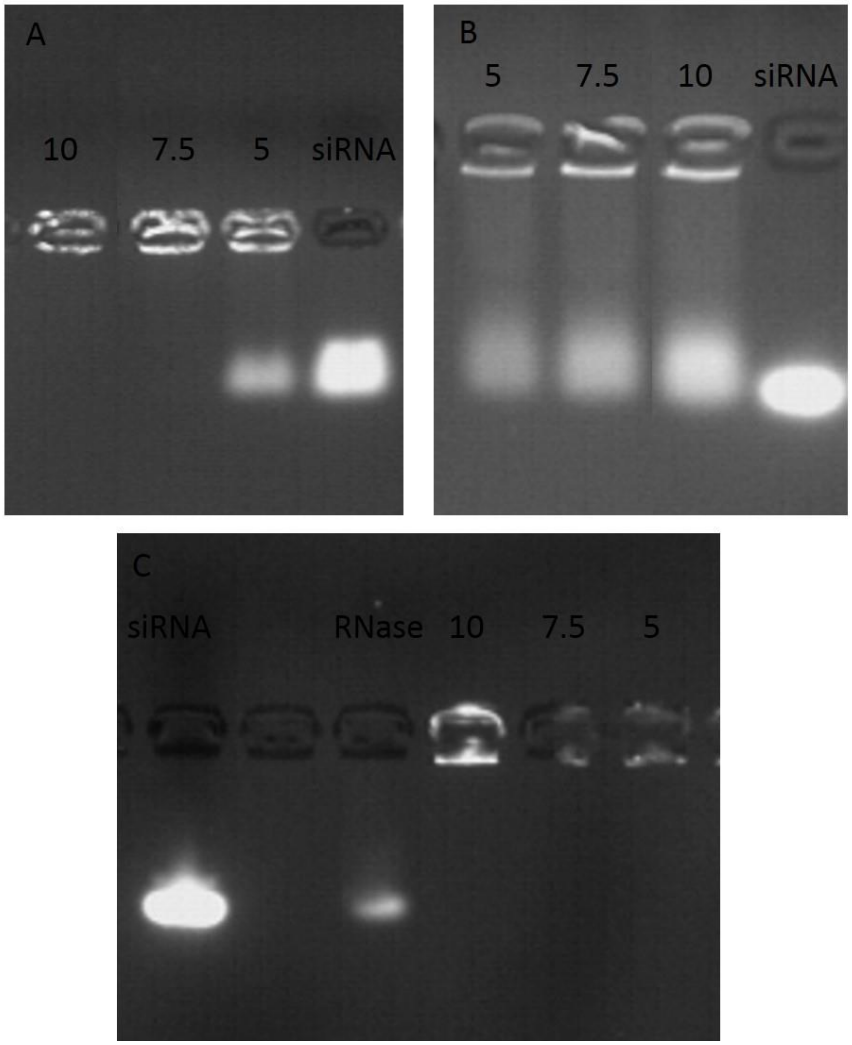

Figure 4.56. A) Gel electrophoresis of siRNA-Peptide conjugates at various N/P ratios: 10, 7.5, 5. Control: Naked siRNA. B) RNase exposed siRNA-Peptide conjugates at various N/P ratios: 10, 7.5, 5. Control: Naked siRNA and RNase exposed naked siRNA. RNase concentration: 0.25% (v/v). Incubation: 1h at 37°C. **C)** Serum protein stability of the siRNA-Peptide conjugates at N/P ratios of 10, 7.5 and 5. Serum content: 50% (v/v). Incubation: 6h at 37°C.

4.3.4.2. Luciferase Activity and Toxicity of siRNA-Peptide Conjugates

Figure 4.57 shows that all the conjugates formed at different N/P ratios reduced the luciferase expression down to ~65% at the maximum dose (200 nM) applied. The gene silencing efficiencies of the conjugates reduced significantly as the dose decreased to 50 nM. The conjugate formed at N/P ratio of 10 showed higher toxicity than the other conjugates prepared as shown in Figure 4.58. The relatively higher toxicity of this conjugate could be ascribed to presence of more positively charged groups on its surface.

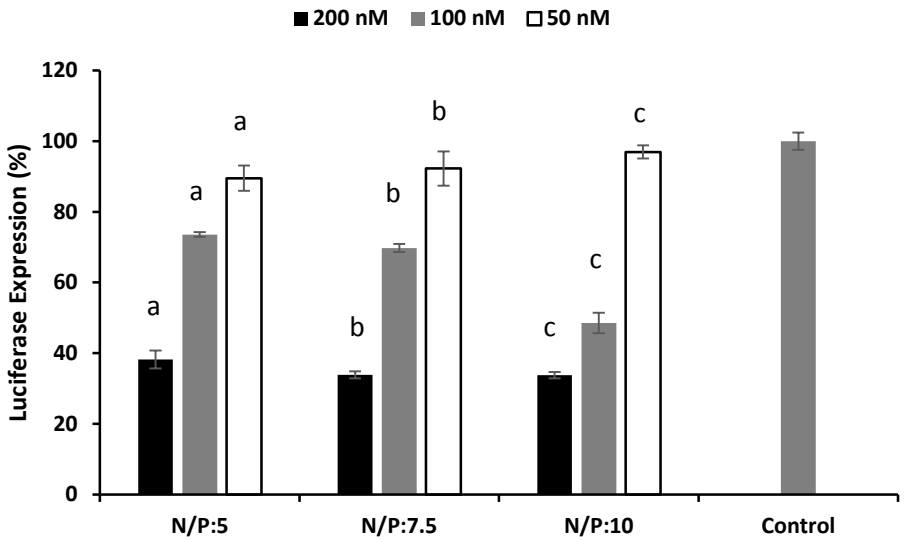

Figure 4.57. Luciferase expression suppression of prepared siRNA/Peptide conjugates. N/P: 10, 7.5 and 5. Applied siRNA dose: 200, 100, 50 nM. Initial SKOV3 cell density: $1x10^4$ cell/well. Incubation time: 24h.

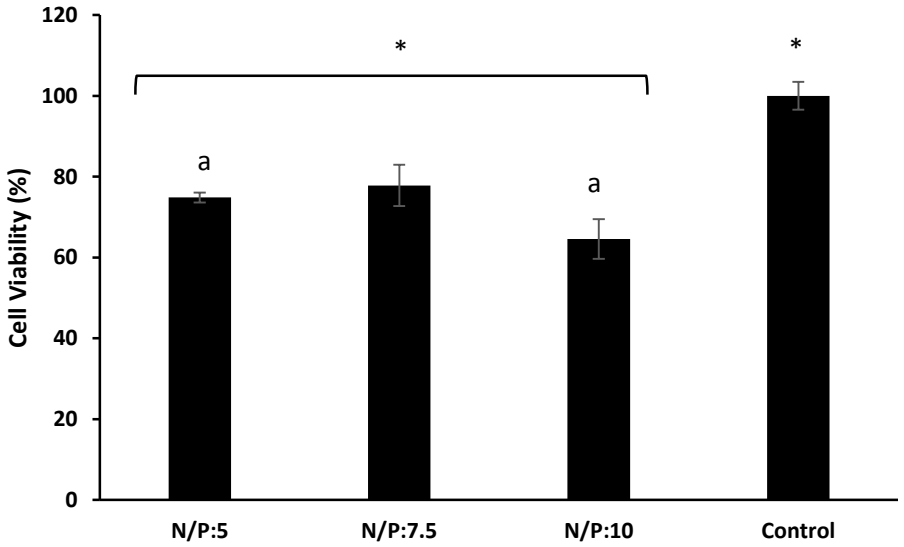

Figure 4.58. Cell viability of siRNA/Peptide conjugate administered SKOV3 cells. N/P: 10, 7.5 and 5. Applied siRNA dose: 200, 100, 50 nM. Initial SKOV3 cell density: $1x10^4$ cell/well. Incubation time: 24h. a and * represent statistically significant difference ($p<0.05$).

4.4. In vitro Release of siRNA from Hydrogels

The developed AuNP-siRNA-Polymer A multilayer system was embedded in a hydrogel system composed of Pluronic F127, which can go thermal micellization at 37 °C and control the release of cargo. Therefore sustained release of siRNA was aimed to achieve. With the thermal micellization of Pluronic F127, the AuNP-siRNA-Polymer A multilayer system released to the medium (PBS containing 5% of DTT) in a controlled manner and then, as a consequence of cleavage of disulfide bonds in the presence of DTT, siRNA was released to the medium. As it is shown in Figure 4.59, controlled release of siRNA was achieved during 3 days.

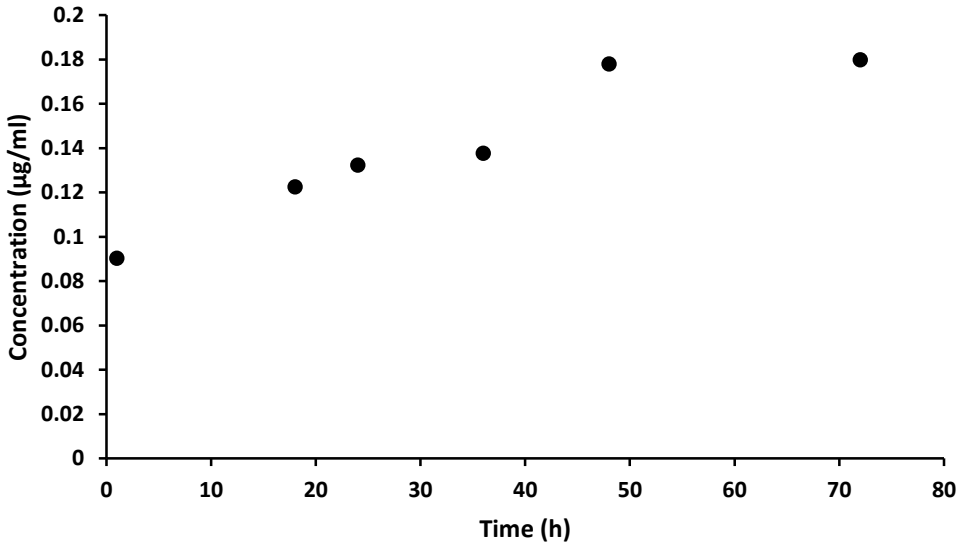

Figure 4.59. The controlled release of siRNA from hydrogels.

4.5. Comparison of the Developed siRNA Delivery Systems

Throughout this thesis, cationic pentablock copolymer and TAT-HA2 fusion peptide based siRNA delivery systems have been developed. The efficacies of these systems were evaluated in terms of the cell uptake, serum and RNase stability, cell viability, siRNA loading required to achieve sufficient gene silencing effect and luciferase expression suppression level (Table 4.7.).

Table 4.7. Comparison of the developed systems in terms of siRNA protection, cell uptake, toxicity and luciferase activity.

Type of Delivery System	**Luciferase Suppression (%)**	**Cell Viability (%)**	**siRNA Dose (nM)**	**Cell Uptake**	**Serum& RNase Stability**
siRNA/Polymer Complex (N/P:50)	45	80	100	275 intensity	good
siRNA/Peptide Complex (N/P:10)	50	80	400	200 intensity	good
AuNP-siRNA-Polymer (AuNP/Polymer A:1/100)	60	100	100	$1.8x10^7$ AuNP/cell	good
AuNP-siRNA-Peptide (AuNP/Peptide:1/500)	55	100	100	$1.3x10^7$ AuNP/cell	good
siRNA-Peptide Conjugate	60	70	200	-----	poor

It was observed that both of the complex systems prepared by polymer and peptide provided a good siRNA protection against RNase enzyme and serum proteins. This was achieved with complete condensation and complexation of siRNA molecules by cationic groups of peptide/polymers through strong electrostatic forces. The multilayer system based on AuNPs including polymer or peptide as the last layer of the assembly also protected siRNA from degradation in the presence of RNase and serum proteins although amount of polymer/peptide used is lower than the amount required for polyplex or peptideplex formation. Serum and RNase stabilities of the siRNA-Peptide conjugates were found relatively poor compared to the stabilities of multilayer or siRNA/polymer and siRNA/peptide complex systems. This could be due to the incomplete coverage of siRNA by peptide moieties which can leave siRNA strands open to external effects. This situation could be eliminated by coating the surface of the conjugate with a small amount of peptide or polymer to provide shielding effect. In this manner, besides the siRNA protection, an efficient cellular entry and endosomal escape can also be achieved.

In the case of polymer based delivery systems shown in Table 4.7., the Pluronic F127 block facilitates cellular entry through the temperature responsive micellization

while PDEAEM block enhances endosomal escape through the proton sponge effect of tertiary amine groups. Similarly, for the peptide based systems, the free arginine amino acids present in TAT domain facilitates the cell membrane attachment and penetration by lipid raft macropinocytosis, while HA2 domain provides endosomal escape by pH buffering effect. The cell uptake of both polymer based systems was found higher than the cell uptake of the peptide based ones. The sizes of the polyplexes and peptideplexes are similar (~300 nm) while the size of the AuNP-siRNA-Polymer (~150 nm) is considerably higher than the corresponding peptide based multilayer system (~40 nm). It should be noted that not only the size but also the surface charge of the nanoparticles influence the cell uptake. Previous studies have shown that the pentablock copolymer used in this thesis is uptaken into the cell by endocytosis (Zhang and Mallapragada 2011a, b), and TAT domain of the peptide penetrates the cell membrane through lipid raft dependent macropynositosis (Wadia, Stan, and Dowdy 2004). It can be concluded that the difference in internalization of polymer and peptide based delivery systems can be mainly ascribed to different uptake mechanism.

The complex and conjugate systems were found to be slightly toxic at the highest dose applied (400 nM) compared to AuNP based multilayer systems. The reason for the toxicity is the presence of excess cationic groups in order to condense 400 nM of siRNA and form stable polyplexes or peptideplexes. In the case of AuNP based multilayer systems, small amount of polymer or peptide is enough to cover the surface and protect siRNA leading to decrease in the toxicity.

The luciferase activity of siRNA/Peptide complex system is 5% higher than that of siRNA/Polymer complexes. The peptideplex systems allow high siRNA loadings (400 nM) without showing severe toxicity, on the other hand, the siRNA/polymer systems with 400 nM siRNA loadings caused serious toxic effect (Figure 4.25). The nontoxic siRNA/polymer complexes were obtained when the maximum siRNA loading was 100 nM (Figure 4.25). Consequently, the better luciferase expression suppression provided by peptideplexes is due to higher siRNA loadings compared to the loading levels in the polyplexes.

Both polymer and peptide based multilayer systems showed considerably better luciferase expression suppression (~15% more for polymers and 5% more for peptides) without showing toxic effect as compared to their complex counterparts, mainly due to the presence of disulfide bonds, which can easily be cleaved in the reduced cytosol environment and enhance siRNA release. In addition, compared to polyplexes and

peptideplexes, both multilayer systems managed to achieve higher gene silencing effect with lower siRNA loadings and lower amount of polymer or peptide coatings. The results in Table 4.7. indicate that polymer based multilayer system has 5% higher luciferase activity than the peptide based multilayer system. This could be due to higher cell uptake and endosomal escape properties of polymer based multilayer systems. Another reason could be higher rate of diffusion of small molecule glutathione through the polymer based multilayer systems which breaks the disulfide bonds and provide sufficient siRNA release.

CHAPTER 5

CONCLUSION

In the first section of this thesis, PEG coated AuNPs with different size and surface properties were developed for imaging and diagnostic purposes. The effects of bare AuNP size, and PEG concentration on the conformation and grafting density of PEG layer, consequently, on the cell uptake, toxicity and cell cycle phases against prostate PC3, CaCo2 and 3T3 cells were investigated. The PEGylated nanoparticles showed an enhanced cellular uptake compared to bare AuNPs for all cell types. Although adsorbed PEG molecules achieved brushed conformation on all nanoparticles, the PEG grafting densities on the 5-nm sized AuNPs were found higher than those on the 13 nm sized ones and the PEG densities increased with the increased PEG concentration of coating solution. The serum protein adsorption, cellular uptake and toxicity of the nanoparticles were strongly affected by the PEG grafting density. Increased PEG density decreased total serum protein adsorption, enhanced the cellular uptake and decreased the toxicity of the nanoparticles. The PEGylated nanoparticles disrupted the cell cycle phases for all cell types. The most significant alteration in cell cycle for three cell lines investigated was induced by the nanoparticle possessing the lowest PEG grafting density. The comet assay results combined with fluorescence images showed that most of the particles most of the particles accumulated around the nucleus, thus, caused DNA damage. The cell cycle disruption caused by the DNA damage did not exhibit apoptosis leading to the conclusion that nanoparticles acted through pathways other than the apoptosis to inhibit cell growth or they caused retarded cell proliferation without accompanied massive apoptosis.

In the second section of this thesis, the efficacy of multilayer systems based on gold nanoparticles, PDEAEM-PluronicF127-PDEAEM pentablock copolymers and TAT-HA2 fusogenic peptides were demonstrated for siRNA delivery. The siRNA/polymer polyplex and siRNA/peptide peptideplex controls were formed through the direct electrostatic interactions between negatively charged siRNA and positively charged pentablock copolymers or peptides. The multilayer systems were prepared by coating PEG modified AuNPs with the siRNA through the cleavable disulfide bonds and subsequently with the pentablock copolymers or fusogenic peptides by electrostatic

interactions. All of the delivery systems prepared protected siRNA from nuclease enzymes and serum proteins.

The polymer and peptide based complexes and multilayer systems provided an efficient cellular uptake and endosomal escape. We hypothesized that micellization of free Pluronic F127 blocks enhanced cellular uptake while free amine groups in the PDEAEM blocks enabled the proton sponge effect and subsequently endosomal escape. Similarly, in the case of peptide based systems, the free arginine amino acids present in TAT domain facilitates the cell membrane attachment and penetration by lipid raft macropinocytosis, while HA2 domain provides endosomal escape by pH buffering effect. Upon the cellular internalization and endosomal escape, the released siRNA showed an efficient luciferase suppression in SKOV3 cells. It was noted that the polymer or peptide based multilayer systems provided a better siRNA activity compared to the polyplexes and peptideplexes. The strong electrostatic interactions between siRNA and polymer/peptide in polyplexes and peptideplexes avoided the sufficient siRNA release. On the other hand, in the case of multilayer systems, the presence of cleavable disulfide bonds, which can break in the reductive environment of cytosol and enhance the siRNA release, provided a successful luciferase suppression. Moreover, to achieve the same level of luciferase expression suppression, the siRNA loading and polymer/peptide required in both multilayer systems is much lower than that in the polyplex or peptideplex system, thereby significantly reducing toxicity. The possibility of controlling the release rate of siRNA was tested. A hydrogel system was developed as depot for AuNP and pentablock copolymer based siRNA delivery system and provided a sustained release of siRNA during 3 days.

In conclusion, the use of block copolymers gives the opportunity to tune the ratio of blocks with different properties, therefore, the cell uptake, endosomal escape, toxicity and efficiency in therapeutic delivery can be adjusted. In addition, the properties of the peptides can also be manipulated through different variations of amino acid sequences. The addition or removal of some groups may also create available sites for chemical conjugations and modifications. Hence, the multilayer systems combining AuNPs with the pH and temperature responsive pentablock copolymer and cell penetrating fusogenic peptides are promising nonviral vectors to deliver siRNA, however, their potential use should be further evaluated with *in vivo* tests.

REFERENCES

Agarwal, A., and S. K. Mallapragada. 2008. "Synthetic sustained gene delivery systems." *Current Topics in Medicinal Chemistry* 8 (4):311-330.

Agarwal, A., R. C. Unfer, and S. K. Mallapragada. 2008. "Dual-role self-assembling nanoplexes for efficient gene transfection and sustained gene delivery." *Biomaterials* 29 (5):607-617.

Ambesajir, A., A. Kaushik, J. J. Kaushik, and S. T. Petros. 2012. "RNA interference: A futuristic tool and its therapeutic applications." *Saudi Journal of Biological Sciences* 19 (4):395-403.

Austin, L. A., B. Kang, C. W. Yen, and M. A. El-Sayed. 2011. "Nuclear Targeted Silver Nanospheres Perturb the Cancer Cell Cycle Differently than Those of Nanogold." *Bioconjugate Chemistry* 22 (11):2324-2331.

Ballarin-Gonzalez, B., and K. A. Howard. 2012. "Polycation-based nanoparticle delivery of RNAi therapeutics: Adverse effects and solutions." *Advanced Drug Delivery Reviews* 64 (15):1717-1729.

Beyerle, A., O. Merkel, T. Stoeger, and T. Kissel. 2010. "PEGylation affects cytotoxicity and cell-compatibility of poly(ethylene imine) for lung application: Structure-function relationships." *Toxicology and Applied Pharmacology* 242 (2):146-154.

Bhattacharya, R., and P. Mukherjee. 2008. "Biological properties of "naked" metal nanoparticles." *Advanced Drug Delivery Reviews* 60 (11):1289-1306.

Bora, R. S., D. Gupta, T. K. S. Mukkur, and K. S. Saini. 2012. "RNA interference therapeutics for cancer: Challenges and opportunities (Review)." *Molecular Medicine Reports* 6 (1):9-15.

Brandenberger, C., B. Rothen-Rutishauser, C. Muhlfeld, O. Schmid, G. A. Ferron, K. L. Maier, P. Gehr, and A. G. Lenz. 2010. "Effects and uptake of gold nanoparticles deposited at the air-liquid interface of a human epithelial airway model." *Toxicology and Applied Pharmacology* 242 (1):56-65.

Breunig, M., C. Hozsa, U. Lungwitz, K. Watanabe, I. Umeda, H. Kato, and A. Goepferich. 2008. "Mechanistic investigation of poly(ethylene imine)-based siRNA delivery: Disulfide bonds boost intracellular release of the cargo." *Journal of Controlled Release* 130 (1):57-63.

Butterworth, K. T., J. A. Coulter, S. Jain, J. Forker, S. J. McMahon, G. Schettino, K. M. Prise, F. J. Currell, and D. G. Hirst. 2010. "Evaluation of cytotoxicity and radiation enhancement using 1.9 nm gold particles: potential application for cancer therapy." *Nanotechnology* 21 (29):9.

Buyens, K., M. Meyer, E. Wagner, J. Demeester, S. C. De Smedt, and N. N. Sanders. 2010. "Monitoring the disassembly of siRNA polyplexes in serum is crucial for predicting their biological efficacy." *Journal of Controlled Release* 141 (1):38-41.

Cai, Q. Y., S. H. Kim, K. S. Choi, S. Y. Kim, S. J. Byun, K. W. Kim, S. H. Park, S. K. Juhng, and K. H. Yoon. 2007. "Colloidal gold nanoparticles as a blood-pool contrast agent for x-ray computed tomography in mice." *Investigative Radiology* 42 (12):797-806.

Cantini, L., C. C. Attaway, B. Butler, L. M. Andino, M. L. Sokolosky, and A. Jakymiw. 2013. "Fusogenic-Oligoarginine Peptide-Mediated Delivery of siRNAs Targeting the CIP2A Oncogene into Oral Cancer Cells." *Plos One* 8 (9).

Chen, L. A., J. M. McCrate, J. C. M. Lee, and H. Li. 2011. "The role of surface charge on the uptake and biocompatibility of hydroxyapatite nanoparticles with osteoblast cells." *Nanotechnology* 22 (10):10.

Cheng, R., F. Feng, F. H. Meng, C. Deng, J. Feijen, and Z. Y. Zhong. 2011. "Glutathione-responsive nano-vehicles as a promising platform for targeted intracellular drug and gene delivery." *Journal of Controlled Release* 152 (1):2-12.

Chithrani, B. D., A. A. Ghazani, and W. C. W. Chan. 2006. "Determining the size and shape dependence of gold nanoparticle uptake into mammalian cells." *Nano Letters* 6 (4):662-668.

Chithrani, B. D., J. Stewart, C. Allen, and D. A. Jaffray. 2009. "Intracellular uptake, transport, and processing of nanostructures in cancer cells." *Nanomedicine-Nanotechnology Biology and Medicine* 5 (2):118-127.

Cho, J., and F. Caruso. 2005. "Investigation of the interactions between ligand-stabilized gold nanoparticles and polyelectrolyte multilayer films." *Chemistry of Materials* 17 (17):4547-4553.

Cho, W. S., M. Cho, J. Jeong, M. Choi, B. S. Han, H. S. Shin, J. Hong, B. H. Chung, J. Jeong, and M. H. Cho. 2010. "Size-dependent tissue kinetics of PEG-coated gold nanoparticles." *Toxicology and Applied Pharmacology* 245 (1):116-123.

Choi, S. W., S. H. Lee, H. Mok, and T. G. Park. 2010. "Multifunctional siRNA Delivery System: Polyelectrolyte Complex Micelles of Six-arm PEG Conjugate of siRNA and Cell Penetrating Peptide with Crosslinked Fusogenic Peptide." *Biotechnology Progress* 26 (1):57-63.

Choi, S. Y., S. Jeong, S. H. Jang, J. Park, J. H. Park, K. S. Ock, S. Y. Lee, and S. W. Joo. 2012. "In vitro toxicity of serum protein-adsorbed citrate-reduced gold nanoparticles in human lung adenocarcinoma cells." *Toxicology in Vitro* 26 (2):229-237.

Christie, R. J., K. Miyata, Y. Matsumoto, T. Nomoto, D. Menasco, T. C. Lai, M. Pennisi, K. Osada, S. Fukushima, N. Nishiyama, Y. Yamasaki, and K. Kataoka. 2011. "Effect of Polymer Structure on Micelles Formed between siRNA and Cationic Block Copolymer Comprising Thiols and Amidines." *Biomacromolecules* 12 (9):3174-3185.

Chuang, Show-Mei, Yi-Hui Lee, Ruei-Yue Liang, Gwo-Dong Roam, Zih-Ming Zeng, Hsin-Fang Tu, Shi-Kwun Wang, and Pin Ju Chueh. 2013. "Extensive evaluations of the cytotoxic effects of gold nanoparticles." *Biochimica et Biophysica Acta (BBA) - General Subjects* 1830 (10):4960-4973.

Conde, J., A. Ambrosone, V. Sanz, Y. Hernandez, V. Marchesano, F. R. Tian, H. Child, C. C. Berry, M. R. Ibarra, P. V. Baptista, C. Tortiglione, and J. M. de la Fuente. 2012. "Design of Multifunctional Gold Nanoparticles for In Vitro and In Vivo Gene Silencing." *Acs Nano* 6 (9):8316-8324.

Conner, S. D., and S. L. Schmid. 2003. "Regulated portals of entry into the cell." *Nature* 422 (6927):37-44.

Connor, E. E., J. Mwamuka, A. Gole, C. J. Murphy, and M. D. Wyatt. 2005. "Gold nanoparticles are taken up by human cells but do not cause acute cytotoxicity." *Small* 1 (3):325-327.

Convertine, A. J., D. S. W. Benoit, C. L. Duvall, A. S. Hoffman, and P. S. Stayton. 2009. "Development of a novel endosomolytic diblock copolymer for siRNA delivery." *Journal of Controlled Release* 133 (3):221-229.

Convertine, A. J., C. Diab, M. Prieve, A. Paschal, A. S. Hoffman, P. H. Johnson, and P. S. Stayton. 2010. "pH-Responsive Polymeric Micelle Carriers for siRNA Drugs." *Biomacromolecules* 11 (11):2904-2911.

Damodaran, V. B., C. J. Fee, T. Ruckh, and K. C. Popat. 2010. "Conformational Studies of Covalently Grafted Poly(ethylene glycol) on Modified Solid Matrices Using X-ray Photoelectron Spectroscopy." *Langmuir* 26 (10):7299-7306.

David, S., B. Pitard, J. P. Benoit, and C. Passirani. 2010. "Non-viral nanosystems for systemic siRNA delivery." *Pharmacological Research* 62 (2):100-114.

Deshayes, S., M. Morris, F. Heitz, and G. Divita. 2008. "Delivery of proteins and nucleic acids using a non-covalent peptide-based strategy." *Advanced Drug Delivery Reviews* 60 (4-5):537-547.

Determan, M. D., J. P. Cox, S. Seifert, P. Thiyagarajan, and S. K. Mallapragada. 2005. "Synthesis and characterization of temperature and pH-responsive pentablock copolymers." *Polymer* 46 (18):6933-6946.

Devi, G. R. 2006. "siRNA-based approaches in cancer therapy." *Cancer Gene Therapy* 13 (9):819-829.

Dong, W. J., Y. J. Zhou, and W. Liang. 2012. "Lipid-based siRNA Delivery Systems." *Progress in Biochemistry and Biophysics* 39 (5):396-401.

Dykman, L. A., and N. G. Khlebtsov. 2014. "Uptake of Engineered Gold Nanoparticles into Mammalian Cells." *Chemical Reviews* 114 (2):1258-1288.

Elbakry, A., E. C. Wurster, A. Zaky, R. Liebl, E. Schindler, P. Bauer-Kreisel, T. Blunk, R. Rachel, A. Goepferich, and M. Breunig. 2012. "Layer-by-Layer Coated Gold Nanoparticles: Size-Dependent Delivery of DNA into Cells." *Small* 8 (24):3847-3856.

Elbakry, A., A. Zaky, R. Liebkl, R. Rachel, A. Goepferich, and M. Breunig. 2009. "Layer-by-Layer Assembled Gold Nanoparticles for siRNA Delivery." *Nano Letters* 9 (5):2059-2064.

Fischer, D., Y. X. Li, B. Ahlemeyer, J. Krieglstein, and T. Kissel. 2003. "In vitro cytotoxicity testing of polycations: influence of polymer structure on cell viability and hemolysis." *Biomaterials* 24 (7):1121-1131.

Gao, K., and L. Huang. 2009. "Nonviral Methods for siRNA Delivery." *Molecular Pharmaceutics* 6 (3):651-658.

Ghosh, P., G. Han, M. De, C. K. Kim, and V. M. Rotello. 2008. "Gold nanoparticles in delivery applications." *Advanced Drug Delivery Reviews* 60 (11):1307-1315.

Giljohann, D. A., D. S. Seferos, A. E. Prigodich, P. C. Patel, and C. A. Mirkin. 2009. "Gene Regulation with Polyvalent siRNA-Nanoparticle Conjugates." *Journal of the American Chemical Society* 131 (6):2072.

Gomes-da-Silva, L. C., S. Simoes, and J. N. Moreira. 2014. "Challenging the future of siRNA therapeutics against cancer: the crucial role of nanotechnology." *Cellular and Molecular Life Sciences* 71 (8):1417-1438.

Gu, J. J., X. Y. Chen, H. L. Xin, X. L. Fang, and X. Y. Sha. 2014. "Serum-resistant complex nanoparticles functionalized with imidazole-rich polypeptide for gene delivery to pulmonary metastatic melanoma." *International Journal of Pharmaceutics* 461 (1-2):559-569.

Gu, Y. J., J. P. Cheng, C. C. Lin, Y. W. Lam, S. H. Cheng, and W. T. Wong. 2009. "Nuclear penetration of surface functionalized gold nanoparticles." *Toxicology and Applied Pharmacology* 237 (2):196-204.

Gunasekaran, K., T. H. Nguyen, H. D. Maynard, T. P. Davis, and V. Bulmus. 2011. "Conjugation of siRNA with Comb-Type PEG Enhances Serum Stability and Gene Silencing Efficiency." *Macromolecular Rapid Communications* 32 (8):654-659.

Guo, J. F., L. Bourre, D. M. Soden, G. C. O'Sullivan, and C. O'Driscoll. 2011. "Can non-viral technologies knockdown the barriers to siRNA delivery and achieve the next generation of cancer therapeutics?" *Biotechnology Advances* 29 (4):402-417.

Guo, S. T., Y. Y. Huang, Q. A. Jiang, Y. Sun, L. D. Deng, Z. C. Liang, Q. A. Du, J. F. Xing, Y. L. Zhao, P. C. Wang, A. J. Dong, and X. J. Liang. 2010. "Enhanced Gene Delivery and siRNA Silencing by Gold Nanoparticles Coated with Charge-Reversal Polyelectrolyte." *Acs Nano* 4 (9):5505-5511.

Guo, S. T., Y. Y. Huang, T. Wei, W. D. Zhang, W. W. Wang, D. Lin, X. Zhang, A. Kumar, Q. A. Du, J. F. Xing, L. D. Deng, Z. C. Liang, P. C. Wang, A. J. Dong, and X. J. Liang. 2011. "Amphiphilic and biodegradable methoxy polyethylene glycol-block-(polycaprolactone-graft-poly(2-(dimethylamino)ethyl methacrylate)) as an effective gene carrier." *Biomaterials* 32 (3):879-889.

Hakkinen, H. 2012. "The gold-sulfur interface at the nanoscale." *Nature Chemistry* 4 (6):443-455.

Han, L., J. Zhao, X. Zhang, W. P. Cao, X. X. Hu, G. Z. Zou, X. L. Duan, and X. J. Liang. 2012. "Enhanced siRNA Delivery and Silencing Gold-Chitosan Nanosystem with Surface Charge-Reversal Polymer Assembly and Good Biocompatibility." *Acs Nano* 6 (8):7340-7351.

Hatakeyama, H., E. Ito, H. Akita, M. Oishi, Y. Nagasaki, S. Futaki, and H. Harashima. 2009. "A pH-sensitive fusogenic peptide facilitates endosomal escape and greatly enhances the gene silencing of siRNA-containing nanoparticles in vitro and in vivo." *Journal of Controlled Release* 139 (2):127-132.

Hillaireau, H., and P. Couvreur. 2009. "Nanocarriers' entry into the cell: relevance to drug delivery." *Cellular and Molecular Life Sciences* 66 (17):2873-2896.

Hinton, T. M., C. Guerrero-Sanchez, J. E. Graham, T. Le, B. W. Muir, S. N. Shi, M. L. V. Tizard, P. A. Gunatillake, K. M. McLean, and S. H. Thang. 2012. "The effect of RAFT-derived cationic block copolymer structure on gene silencing efficiency." *Biomaterials* 33 (30):7631-7642.

Hoyer, J., and I. Neundorf. 2012a. "Knockdown of a G protein-coupled receptor through efficient peptide-mediated siRNA delivery." *Journal of Controlled Release* 161 (3):826-834.

Hoyer, J., and I. Neundorf. 2012b. "Peptide Vectors for the Nonviral Delivery of Nucleic Acids." *Accounts of Chemical Research* 45 (7):1048-1056.

Huhn, D., K. Kantner, C. Geidel, S. Brandholt, I. De Cock, S. J. H. Soenen, P. R. Gil, J. M. Montenegro, K. Braeckmans, K. Mullen, G. U. Nienhaus, M. Klapper, and W. J. Parak. 2013. "Polymer-Coated Nanoparticles Interacting with Proteins and Cells: Focusing on the Sign of the Net Charge." *Acs Nano* 7 (4):3253-3263.

Jang, J. H., and L. D. Shea. 2006. "Intramuscular delivery of DNA releasing microspheres: Microsphere properties and transgene expression." *Journal of Controlled Release* 112 (1):120-128.

Jeon, O., H. W. Lim, M. Lee, S. J. Song, and B. S. Kim. 2007. "Poly(L-lactide-co-glycolide) nanospheres conjugated with a nuclear localization signal for delivery of plasmid DNA." *Journal of Drug Targeting* 15 (3):190-198.

Jones, S. W., P. M. de Souza, and M. A. Lindsay. 2004. "siRNA for gene silencing: a route to drug target discovery." *Current Opinion in Pharmacology* 4 (5):522-527.

Kang, B., M. A. Mackey, and M. A. El-Sayed. 2010. "Nuclear Targeting of Gold Nanoparticles in Cancer Cells Induces DNA Damage, Causing Cytokinesis Arrest and Apoptosis." *Journal of the American Chemical Society* 132 (5):1517.

Kastan, M. B., and J. Bartek. 2004. "Cell-cycle checkpoints and cancer." *Nature* 432 (7015):316-23.

Kesharwani, P., V. Gajbhiye, and N. K. Jain. 2012. "A review of nanocarriers for the delivery of small interfering RNA." *Biomaterials* 33 (29):7138-7150.

Kettler, K., K. Veltman, D. van de Meent, A. van Wezel, and A. J. Hendriks. 2014. "Cellular uptake of nanoparticles as determined by particle properties, experimental conditions, and cell type." *Environmental Toxicology and Chemistry* 33 (3):481-492.

Khalil, I. A., K. Kogure, H. Akita, and H. Harashima. 2006. "Uptake pathways and subsequent intracellular trafficking in nonviral gene delivery." *Pharmacological Reviews* 58 (1):32-45.

Kim, D., S. Park, J. H. Lee, Y. Y. Jeong, and S. Jon. 2007. "Antibiofouling polymer-coated gold nanoparticles as a contrast agent for in vivo x-ray computed tomography imaging." *Journal of the American Chemical Society* 129 (24):7661-7665.

Kim, J. A., C. Aberg, A. Salvati, and K. A. Dawson. 2012. "Role of cell cycle on the cellular uptake and dilution of nanoparticles in a cell population." *Nature Nanotechnology* 7 (1):62-68.

Kirkland-York, S., Y. L. Zhang, A. E. Smith, A. W. York, F. Q. Huang, and C. L. McCormick. 2010. "Tailored Design of Au Nanoparticle-siRNA Carriers Utilizing Reversible Addition - Fragmentation Chain Transfer Polymers." *Biomacromolecules* 11 (4):1052-1059.

Kong, W. H., K. H. Bae, S. D. Jo, J. S. Kim, and T. G. Park. 2012. "Cationic Lipid-Coated Gold Nanoparticles as Efficient and Non-Cytotoxic Intracellular siRNA Delivery Vehicles." *Pharmaceutical Research* 29 (2):362-374.

Krebs, M. D., O. Jeon, and E. Alsberg. 2009. "Localized and Sustained Delivery of Silencing RNA from Macroscopic Biopolymer Hydrogels." *Journal of the American Chemical Society* 131 (26):9204.

Lee, C. C., Y. Liu, and T. M. Reineke. 2008. "General structure-activity relationship for poly(glycoamidoamine)s: The effect of amine density on cytotoxicity and DNA delivery efficiency." *Bioconjugate Chemistry* 19 (2):428-440.

Lee, J. M., T. J. Yoon, and Y. S. Cho. 2013. "Recent Developments in Nanoparticle-Based siRNA Delivery for Cancer Therapy." *Biomed Research International*:10.

Lee, J. S., J. J. Green, K. T. Love, J. Sunshine, R. Langer, and D. G. Anderson. 2009. "Gold, Poly(beta-amino ester) Nanoparticles for Small Interfering RNA Delivery." *Nano Letters* 9 (6):2402-2406.

Lee, M. Y., S. J. Park, K. Park, K. S. Kim, H. Lee, and S. K. Hahn. 2011. "Target-Specific Gene Silencing of Layer-by-Layer Assembled Gold-Cysteamine/siRNA/PEI/HA Nanocomplex." *Acs Nano* 5 (8):6138-6147.

Lee, S. H., K. H. Bae, S. H. Kim, K. R. Lee, and T. G. Park. 2008. "Amine-functionalized gold nanoparticles as non-cytotoxic and efficient intracellular siRNA delivery carriers." *International Journal of Pharmaceutics* 364 (1):94-101.

Lee, S. H., S. H. Kim, and T. G. Park. 2007. "Intracellular siRNA delivery system using polyelectrolyte complex micelles prepared from VEGF siRNA-PEG conjugate and cationic fusogenic peptide." *Biochemical and Biophysical Research Communications* 357 (2):511-516.

Lee, Y. J., G. Johnson, and J. P. Pellois. 2010. "Modeling of the Endosomolytic Activity of HA2-TAT Peptides with Red Blood Cells and Ghosts." *Biochemistry* 49 (36):7854-7866.

Lee, Y. J., G. Johnson, G. C. Peltier, and J. P. Pellois. 2011. "A HA2-Fusion tag limits the endosomal release of its protein cargo despite causing endosomal lysis." *Biochimica Et Biophysica Acta-General Subjects* 1810 (8):752-758.

Lee, Y., S. H. Lee, J. S. Kim, A. Maruyama, X. S. Chen, and T. G. Park. 2011. "Controlled synthesis of PEI-coated gold nanoparticles using reductive catechol chemistry for siRNA delivery." *Journal of Controlled Release* 155 (1):3-10.

Lehto, T., K. Kurrikoff, and U. Langel. 2012. "Cell-penetrating peptides for the delivery of nucleic acids." *Expert Opinion on Drug Delivery* 9 (7):823-836.

Li, J. J., S. L. Lo, C. T. Ng, R. L. Gurung, D. Hartono, M. P. Hande, C. N. Ong, B. H. Bay, and L. Y. L. Yung. 2011. "Genomic instability of gold nanoparticle treated human lung fibroblast cells." *Biomaterials* 32 (23):5515-5523.

Li, J. L., L. Wang, X. Y. Liu, Z. P. Zhang, H. C. Guo, W. M. Liu, and S. H. Tang. 2009. "In vitro cancer cell imaging and therapy using transferrin-conjugated gold nanoparticles." *Cancer Letters* 274 (2):319-326.

Li, J., Y. Wang, Y. Zhu, and D. Oupicky. 2013. "Recent advances in delivery of drug-nucleic acid combinations for cancer treatment." *Journal of Controlled Release* 172 (2):589-600.

Li, X., Y. J. Chen, M. Q. Wang, Y. J. Ma, W. L. Xia, and H. C. Gu. 2013. "A mesoporous silica nanoparticle - PEI - Fusogenic peptide system for siRNA delivery in cancer therapy." *Biomaterials* 34 (4):1391-1401.

Lin, Y. L., G. H. Jiang, L. K. Birrell, and M. E. H. El-Sayed. 2010. "Degradable, pH-sensitive, membrane-destabilizing, comb-like polymers for intracellular delivery of nucleic acids." *Biomaterials* 31 (27):7150-7166.

Liou, J. S., B. R. Liu, A. L. Martin, Y. W. Huang, H. J. Chiang, and H. J. Lee. 2012. "Protein transduction in human cells is enhanced by cell-penetrating peptides fused with an endosomolytic HA2 sequence." *Peptides* 37 (2):273-284.

Liu, P. F., H. Yu, Y. Sun, M. J. Zhu, and Y. R. Duan. 2012. "A mPEG-PLGA-b-PLL copolymer carrier for adriamycin and siRNA delivery." *Biomaterials* 33 (17):4403-4412.

Liu, X. Q., C. Y. Sun, X. Z. Yang, and J. Wang. 2013. "Polymeric-Micelle-Based Nanomedicine for siRNA Delivery." *Particle & Particle Systems Characterization* 30 (3):211-228.

Lundy, B. B., A. Convertine, M. Miteva, and P. S. Stayton. 2013. "Neutral Polymeric Micelles for RNA Delivery." *Bioconjugate Chemistry* 24 (3):398-407.

Lytton-Jean, A. K. R., R. Langer, and D. G. Anderson. 2011. "Five Years of siRNA Delivery: Spotlight on Gold Nanoparticles." *Small* 7 (14):1932-1937.

Malmsten, M. 2013. "Inorganic nanomaterials as delivery systems for proteins, peptides, DNA, and siRNA." *Current Opinion in Colloid & Interface Science* 18 (5):468-480.

Malumbres, M., and M. Barbacid. 2009. "Cell cycle, CDKs and cancer: a changing paradigm." *Nat Rev Cancer* 9 (3):153-66.

Mao, C. Q., J. Z. Du, T. M. Sun, Y. D. Yao, P. Z. Zhang, E. W. Song, and J. Wang. 2011. "A biodegradable amphiphilic and cationic triblock copolymer for the delivery of siRNA targeting the acid ceramidase gene for cancer therapy." *Biomaterials* 32 (11):3124-3133.

Marquis, B. J., Z. Liu, K. L. Braun, and C. L. Haynes. 2011. "Investigation of noble metal nanoparticle zeta-potential effects on single-cell exocytosis function in vitro with carbon-fiber microelectrode amperometry." *Analyst* 136 (17):3478-3486.

Matsumoto, S., R. J. Christie, N. Nishiyama, K. Miyata, A. Ishii, M. Oba, H. Koyama, Y. Yamasaki, and K. Kataoka. 2009. "Environment-Responsive Block Copolymer Micelles with a Disulfide Cross-Linked Core for Enhanced siRNA Delivery." *Biomacromolecules* 10 (1):119-127.

Merkel, O. M., D. Librizzi, A. Pfestroff, T. Schurrat, K. Buyens, N. N. Sanders, S. C. De Smedt, M. Behe, and T. Kissel. 2009. "Stability of siRNA polyplexes from poly(ethylenimine) and poly(ethylenimine)-g-poly(ethylene glycol) under in vivo conditions: Effects on pharmacokinetics and biodistribution measured by Fluorescence Fluctuation Spectroscopy and Single Photon Emission Computed Tomography (SPECT) imaging." *Journal of Controlled Release* 138 (2):148-159.

Miele, E., G. P. Spinelli, E. Miele, E. Di Fabrizio, E. Ferretti, S. Tomao, and A. Gulino. 2012. "Nanoparticle-based delivery of small interfering RNA: challenges for cancer therapy." *International Journal of Nanomedicine* 7:3637-3657.

Mok, H., and T. G. Park. 2008. "Self-crosslinked and reducible fusogenic peptides for intracellular delivery of siRNA." *Biopolymers* 89 (10):881-888.

Mok, H., O. Veiseh, C. Fang, F. M. Kievit, F. Y. Wang, J. O. Park, and M. Q. Zhang. 2010. "pH-Sensitive siRNA Nanovector for Targeted Gene Silencing and Cytotoxic Effect in Cancer Cells." *Molecular Pharmaceutics* 7 (6):1930-1939.

Morris, M. C., S. Deshayes, F. Heitz, and G. Divita. 2008. "Cell-penetrating peptides: from molecular mechanisms to therapeutics." *Biology of the Cell* 100 (4):201-217.

Nakase, I., G. Tanaka, and S. Futaki. 2013. "Cell-penetrating peptides (CPPs) as a vector for the delivery of siRNAs into cells." *Molecular Biosystems* 9 (5):855-861.

Nelson, C. E., J. R. Kintzing, A. Hanna, J. M. Shannon, M. K. Gupta, and C. L. Duvall. 2013. "Balancing Cationic and Hydrophobic Content of PEGylated siRNA Polyplexes Enhances Endosome Escape, Stability, Blood Circulation Time, and Bioactivity in Vivo." *Acs Nano* 7 (10):8870-8880.

Nguyen, K., P. N. Dang, and E. Alsberg. 2013. "Functionalized, biodegradable hydrogels for control over sustained and localized siRNA delivery to incorporated and surrounding cells." *Acta Biomaterialia* 9 (1):4487-4495.

Nuhn, L., M. Hirsch, B. Krieg, K. Koynov, K. Fischer, M. Schmidt, M. Helm, and R. Zentel. 2012. "Cationic Nanohydrogel Particles as Potential siRNA Carriers for Cellular Delivery." *Acs Nano* 6 (3):2198-2214.

Oh, Y. K., and T. G. Park. 2009. "siRNA delivery systems for cancer treatment." *Advanced Drug Delivery Reviews* 61 (10):850-862.

Oishi, M., J. Nakaogami, T. Ishii, and Y. Nagasaki. 2006. "Smart PEGylated gold nanoparticles for the cytoplasmic delivery of siRNA to induce enhanced gene silencing." *Chemistry Letters* 35 (9):1046-1047.

Olive, P. L., and J. P. Banath. 2006. "The comet assay: a method to measure DNA damage in individual cells." *Nature Protocols* 1 (1):23-29.

Oliveira, S., I. van Rooy, O. Kranenburg, G. Storm, and R. M. Schiffelers. 2007. "Fusogenic peptides enhance endosomal escape improving siRNA-induced silencing of oncogenes." *International Journal of Pharmaceutics* 331 (2):211-214.

Pan, Y., S. Neuss, A. Leifert, M. Fischler, F. Wen, U. Simon, G. Schmid, W. Brandau, and W. Jahnen-Dechent. 2007. "Size-dependent cytotoxicity of gold nanoparticles." *Small* 3 (11):1941-1949.

Patil, M. L., M. Zhang, and T. Minko. 2011. "Multifunctional Triblock Nanocarrier (PAMAM-PEG-PLL) for the Efficient Intracellular siRNA Delivery and Gene Silencing." *Acs Nano* 5 (3):1877-1887.

Patil, Y., and J. Panyam. 2009. "Polymeric nanoparticles for siRNA delivery and gene silencing." *International Journal of Pharmaceutics* 367 (1-2):195-203.

Pietenpol, J. A., and Z. A. Stewart. 2002. "Cell cycle checkpoint signaling: Cell cycle arrest versus apoptosis." *Toxicology* 181:475-481.

Pissuwan, D., T. Niidome, and M. B. Cortie. 2011. "The forthcoming applications of gold nanoparticles in drug and gene delivery systems." *Journal of Controlled Release* 149 (1):65-71.

Pittella, F., M. Z. Zhang, Y. Lee, H. J. Kim, T. Tockary, K. Osada, T. Ishii, K. Miyata, N. Nishiyama, and K. Kataoka. 2011. "Enhanced endosomal escape of siRNA-incorporating hybrid nanoparticles from calcium phosphate and PEG-block charge-conversional polymer for efficient gene knockdown with negligible cytotoxicity." *Biomaterials* 32 (11):3106-3114.

Prevost, S., S. Riemer, W. Fischer, R. Haag, C. Bottcher, J. Gummel, I. Grillo, M. S. Appavou, and M. Gradzielski. 2011. "Colloidal Structure and Stability of DNA/Polycations Polyplexes Investigated by Small Angle Scattering." *Biomacromolecules* 12 (12):4272-4282.

Rahme, K., L. Chen, R. G. Hobbs, M. A. Morris, C. O'Driscoll, and J. D. Holmes. 2013. "PEGylated gold nanoparticles: polymer quantification as a function of PEG lengths and nanoparticle dimensions." *Rsc Advances* 3 (17):6085-6094.

Resnier, P., T. Montier, V. Mathieu, J. P. Benoit, and C. Passirani. 2013. "A review of the current status of siRNA nanomedicines in the treatment of cancer." *Biomaterials* 34 (27):6429-6443.

Sakurai, Y., H. Hatakeyama, Y. Sato, H. Akita, K. Takayama, S. Kobayashi, S. Futaki, and H. Harashima. 2011. "Endosomal escape and the knockdown efficiency of liposomal-siRNA by the fusogenic peptide shGALA." *Biomaterials* 32 (24):5733-5742.

Scholz, C., and E. Wagner. 2012. "Therapeutic plasmid DNA versus siRNA delivery: Common and different tasks for synthetic carriers." *Journal of Controlled Release* 161 (2):554-565.

Segura, T., and J. A. Hubbell. 2007. "Synthesis and in vitro characterization of an ABC triblock copolymer for siRNA delivery." *Bioconjugate Chemistry* 18 (3):736-745.

Shenoy, D., W. Fu, J. Li, C. Crasto, G. Jones, C. DiMarzio, S. Sridhar, and M. Amiji. 2006. "Surface functionalization of gold nanoparticles using hetero-bifunctional poly(ethylene glycol) spacer for intracellular tracking and delivery." *International Journal of Nanomedicine* 1 (1):51-57.

Shrey, K., A. Suchit, M. Nishant, and R. Vibha. 2009. "RNA interference: Emerging diagnostics and therapeutics tool." *Biochemical and Biophysical Research Communications* 386 (2):273-277.

Shukla, R., V. Bansal, M. Chaudhary, A. Basu, R. R. Bhonde, and M. Sastry. 2005. "Biocompatibility of gold nanoparticles and their endocytotic fate inside the cellular compartment: A microscopic overview." *Langmuir* 21 (23):10644-10654.

Shukla, S., A. Priscilla, M. Banerjee, R. R. Bhonde, J. Ghatak, P. V. Satyam, and M. Sastry. 2005. "Porous gold nanospheres by controlled transmetalation reaction: A novel material for application in cell imaging." *Chemistry of Materials* 17 (20):5000-5005.

Simpson, C. A., A. C. Agrawal, A. Balinski, K. M. Harkness, and D. E. Cliffel. 2011. "Short-Chain PEG Mixed Monolayer Protected Gold Clusters Increase Clearance and Red Blood Cell Counts." *Acs Nano* 5 (5):3577-3584.

Simpson, C. A., B. J. Huffman, A. E. Gerdon, and D. E. Cliffel. 2010. "Unexpected Toxicity of Mono layer Protected Gold Clusters Eliminated by PEG-Thiol Place Exchange Reactions." *Chemical Research in Toxicology* 23 (10):1608-1616.

Simpson, C. A., K. J. Salleng, D. E. Cliffel, and D. L. Feldheim. 2013. "In vivo toxicity, biodistribution, and clearance of glutathione-coated gold nanoparticles." *Nanomedicine-Nanotechnology Biology and Medicine* 9 (2):257-263.

Singh, S. K., and P. B. Hajeri. 2009. "siRNAs: their potential as therapeutic agents - Part II. Methods of delivery." *Drug Discovery Today* 14 (17-18):859-865.

Smith, D., A. C. Holley, and C. L. McCormick. 2011. "RAFT-synthesized copolymers and conjugates designed for therapeutic delivery of iRNA." *Polymer Chemistry* 2 (7):1428-1441.

Smith, M. H., and L. A. Lyon. 2012. "Multifunctional Nanogels for siRNA Delivery." *Accounts of Chemical Research* 45 (7):985-993.

Steele, T. W. J., X. B. Zhao, P. Tarcha, and T. Kissel. 2012. "Factors influencing polycation/siRNA colloidal stability toward aerosol lung delivery." *European Journal of Pharmaceutics and Biopharmaceutics* 80 (1):14-24.

Sun, T. M., J. Z. Du, L. F. Yan, H. Q. Mao, and J. Wang. 2008. "Self-assembled biodegradable micellar nanoparticles of amphiphilic and cationic block copolymer for siRNA delivery." *Biomaterials* 29 (32):4348-4355.

Tahara, K., H. Yamamoto, H. Takeuchi, and Y. Kawashima. 2007. "Development of gene delivery system using PLGA nanospheres." *Yakugaku Zasshi-Journal of the Pharmaceutical Society of Japan* 127 (10):1541-1548.

Takemoto, H., A. Ishii, K. Miyata, M. Nakanishi, M. Oba, T. Ishii, Y. Yamasaki, N. Nishiyama, and K. Kataoka. 2010. "Polyion complex stability and gene silencing efficiency with a siRNA-grafted polymer delivery system." *Biomaterials* 31 (31):8097-8105.

Tortorella, S., and T. C. Karagiannis. 2014. "Transferrin Receptor-Mediated Endocytosis: A Useful Target for Cancer Therapy." *Journal of Membrane Biology* 247 (4):291-307.

Troiber, C., D. Edinger, P. Kos, L. Schreiner, R. Klager, A. Herrmann, and E. Wagner. 2013. "Stabilizing effect of tyrosine trimers on pDNA and siRNA polyplexes." *Biomaterials* 34 (5):1624-1633.

Tsoli, M., H. Kuhn, W. Brandau, H. Esche, and G. Schmid. 2005. "Cellular uptake and toxicity of AU(55) clusters." *Small* 1 (8-9):841-844.

Turkevich, J., P. C. Stevenson, and J. Hillier. 1951. "A study of the nucleation and growth processes in the synthesis of colloidal gold." *Discussions of the Faraday Society* (11):55.

Vandenbroucke, R. E., S. C. De Smedt, J. Demeester, and N. N. Sanders. 2007. "Cellular entry pathway and gene transfer capacity of TAT-modified lipoplexes." *Biochimica Et Biophysica Acta-Biomembranes* 1768 (3):571-579.

Varkouhi, A. K., G. Mountrichas, R. M. Schiffelers, T. Lammers, G. Storm, S. Pispas, and W. E. Hennink. 2012. "Polyplexes based on cationic polymers with strong nucleic acid binding properties." *European Journal of Pharmaceutical Sciences* 45 (4):459-466.

Varkouhi, A. K., M. Scholte, G. Storm, and H. J. Haisma. 2011. "Endosomal escape pathways for delivery of biologicals." *Journal of Controlled Release* 151 (3):220-228.

Varkouhi, A. K., R. J. Verheul, R. M. Schiffelers, T. Lammers, G. Storm, and W. E. Hennink. 2010. "Gene Silencing Activity of siRNA Polyplexes Based on Thiolated N,N,N-Trimethylated Chitosan." *Bioconjugate Chemistry* 21 (12):2339-2346.

Verma, A., and F. Stellacci. 2010. "Effect of Surface Properties on Nanoparticle-Cell Interactions." *Small* 6 (1):12-21.

Vicentini, Ftmd, L. N. Borgheti-Cardoso, L. V. Depieri, D. D. Mano, T. F. Abelha, R. Petrilli, and Mvlb Bentley. 2013. "Delivery Systems and Local Administration Routes for Therapeutic siRNA." *Pharmaceutical Research* 30 (4):915-931.

Wadia, J. S., R. V. Stan, and S. F. Dowdy. 2004. "Transducible TAT-HA fusogenic peptide enhances escape of TAT-fusion proteins after lipid raft macropinocytosis." *Nature Medicine* 10 (3):310-315.

Walkey, C. D., J. B. Olsen, H. B. Guo, A. Emili, and W. C. W. Chan. 2012. "Nanoparticle Size and Surface Chemistry Determine Serum Protein Adsorption and Macrophage Uptake." *Journal of the American Chemical Society* 134 (4):2139-2147.

Wan, R., Y. Mo, L. Feng, S. Chien, D. J. Tollerud, and Q. Zhang. 2012. "DNA damage caused by metal nanoparticles: involvement of oxidative stress and activation of ATM." *Chem Res Toxicol* 25 (7):1402-11.

Wang, D. Q., D. R. Robinson, G. S. Kwon, and J. Samuel. 1999. "Encapsulation of plasmid DNA in biodegradable poly(D,L-lactic-co-glycolic acid) microspheres as a novel approach for immunogene delivery." *Journal of Controlled Release* 57 (1):9-18.

Wang, F. H., Y. Wang, X. Zhang, W. J. Zhang, S. R. Guo, and F. Jin. 2014. "Recent progress of cell-penetrating peptides as new carriers for intracellular cargo delivery." *Journal of Controlled Release* 174:126-136.

Wang, L. M., Y. Liu, W. Li, X. M. Jiang, Y. L. Ji, X. C. Wu, L. G. Xu, Y. Qiu, K. Zhao, T. T. Wei, Y. F. Li, Y. L. Zhao, and C. Y. Chen. 2011. "Selective Targeting of Gold Nanorods at the Mitochondria of Cancer Cells: Implications for Cancer Therapy." *Nano Letters* 11 (2):772-780.

Wong, S. Y., J. M. Pelet, and D. Putnam. 2007. "Polymer systems for gene delivery-past, present, and future." *Progress in Polymer Science* 32 (8-9):799-837.

Wu, Z. W., C. T. Chien, C. Y. Liu, J. Y. Yan, and S. Y. Lin. 2012. "Recent progress in copolymer-mediated siRNA delivery." *Journal of Drug Targeting* 20 (7):551-560.

Yang, J., Jim Yang Lee, Heng-Phon Too, Gan-Moog Chow, and Leong M. Gan. 2006. "Single stranded DNA stabilization and assembly of Au nanoparticles of different sizes." *Chemical Physics* 323 (2–3):304-312.

Ye, S. F., M. M. Tian, T. X. Wang, L. Ren, D. Wang, L. H. Shen, and T. Shang. 2012. "Synergistic effects of cell-penetrating peptide Tat and fusogenic peptide HA2-enhanced cellular internalization and gene transduction of organosilica nanoparticles." *Nanomedicine-Nanotechnology Biology and Medicine* 8 (6):833-841.

York, A. W., F. Q. Huang, and C. L. McCormick. 2010. "Rational Design of Targeted Cancer Therapeutics through the Multiconjugation of Folate and Cleavable siRNA to RAFT-Synthesized (HPMA-s-APMA) Copolymers." *Biomacromolecules* 11 (2):505-514.

Yu, H. J., Y. L. Zou, Y. G. Wang, X. N. Huang, G. Huang, B. D. Sumer, D. A. Boothman, and J. M. Gao. 2011. "Overcoming Endosomal Barrier by Amphotericin B-Loaded Dual pH-Responsive PDMA-b-PDPA Micelleplexes for siRNA Delivery." *Acs Nano* 5 (11):9246-9255.

Zhang, B. Q., F. Jia, M. Q. Fleming, and S. K. Mallapragada. 2012. "Injectable self-assembled block copolymers for sustained gene and drug co-delivery: An in vitro study." *International Journal of Pharmaceutics* 427 (1):88-96.

Zhang, B. Q., M. Kanapathipillai, P. Bisso, and S. Mallapragada. 2009. "Novel Pentablock Copolymers for Selective Gene Delivery to Cancer Cells." *Pharmaceutical Research* 26 (3):700-713.

Zhang, B. Q., and S. Mallapragada. 2011a. "The mechanism of selective transfection mediated by pentablock copolymers; Part I: Investigation of cellular uptake." *Acta Biomaterialia* 7 (4):1570-1579.

Zhang, B. Q., and S. Mallapragada. 2011b. "The mechanism of selective transfection mediated by pentablock copolymers; Part II: Nuclear entry and endosomal escape." *Acta Biomaterialia* 7 (4):1580-1587.

Zhang, S. B., Y. A. Zhao, D. F. Zhi, and S. F. Zhang. 2012. "Non-viral vectors for the mediation of RNAi." *Bioorganic Chemistry* 40:10-18.

Zhang, X. D., D. Wu, X. Shen, J. Chen, Y. M. Sun, P. X. Liu, and X. J. Liang. 2012. "Size-dependent radiosensitization of PEG-coated gold nanoparticles for cancer radiation therapy." *Biomaterials* 33 (27):6408-6419.

Zhang, X. D., D. Wu, X. Shen, P. X. Liu, N. Yang, B. Zhao, H. Zhang, Y. M. Sun, L. A. Zhang, and F. Y. Fan. 2011. "Size-dependent in vivo toxicity of PEG-coated gold nanoparticles." *International Journal of Nanomedicine* 6:2071-2081.

Zhao, E. Y., Z. X. Zhao, J. C. Wang, C. H. Yang, C. J. Chen, L. Y. Gao, Q. Feng, W. J. Hou, M. Y. Gao, and Q. Zhang. 2012. "Surface engineering of gold nanoparticles for in vitro siRNA delivery." *Nanoscale* 4 (16):5102-5109.

Zhao, Z. X., S. Y. Gao, J. C. Wang, C. J. Chen, E. Y. Zhao, W. J. Hou, Q. Feng, L. Y. Gao, X. Y. Liu, L. R. Zhang, and Q. Zhang. 2012. "Self-assembly nanomicelles based on cationic mPEG-PLA-b-Polyarginine(R-15) triblock copolymer for siRNA delivery." *Biomaterials* 33 (28):6793-6807.

Zheng, M. Y., D. Librizzi, A. Kilic, Y. Liu, H. Renz, O. M. Merkel, and T. Kissel. 2012. "Enhancing in vivo circulation and siRNA delivery with biodegradable polyethylenimine-graft-polycaprolactone-block-poly(ethylene glycol) copolymers." *Biomaterials* 33 (27):6551-6558.

Zhou, L., Z. F. Chen, F. F. Wang, X. Q. Yang, and B. L. Zhang. 2013. "Multifunctional triblock co-polymer mP3/4HB-b-PEG-b-lPEI for efficient intracellular siRNA delivery and gene silencing." *Acta Biomaterialia* 9 (4):6019-6031.

Zorko, M., and U. Langel. 2005. "Cell-penetrating peptides: mechanism and kinetics of cargo delivery." *Advanced Drug Delivery Reviews* 57 (4):529-545.

APPENDIX A

CALIBRATION CURVES AND CALCULATIONS

A.1. Theoretical siRNA Loading on AuNPs

AuNP Concentration: 20 nM
siRNA Molecular Weight: 13600 g/mole
Reaction volume: 500 µl
AuNP diameter: ~13 nm
siRNA diameter: ~2 nm
siRNA length: ~7.5 nm
NA: $6.02x10^{23}$

$$\frac{20\text{nmole}}{10^6\ \mu\text{l}} \text{ x } 500\mu\text{l x } \frac{6.02 \text{ x } 10^{23}\#\text{of AuNP}}{1 \text{ mole}} \text{ x } \frac{1 \text{ mole}}{10^9 \text{ nmole}} = 6x10^{12} \text{ \# of AuNP}$$

$$\text{Surface Area of 1 AuNP} = 4 \text{ x } 3.14 \text{ x } (6.5)^2 = 530 \text{ nm}^2$$

$$\text{Total Surface Area of AuNPs} = 530 \frac{\text{nm}^2}{1 \text{ AuNP}} \text{ x } 6x10^{12}\# \text{ ofAuNP} = 318x10^{13} \text{ nm}^2$$

$$\text{Area of 1 siRNA Molecule} = 4 \text{ x } 3.14 \text{ x } (1)^2 = 12 \text{ nm}^2$$

$$\frac{530 \text{ nm}^2}{12 \text{ nm}^2} = 44 \text{ \# of siRNA required to fully coat the surface of 1 AuNP}$$

$$\frac{318x10^{13} \text{ nm}^2}{12 \text{ nm}^2} = 26x10^{13} \text{ total \# of siRNA}$$

$$26x10^{13} \text{ \# of siRNA x } \frac{1 \text{ mole}}{6.02 \text{ x } 10^{23}\#\text{of siRNA}} = 4.4 \text{ x } 10^{-10} \text{ mole siRNA in total}$$

$$\frac{4.4 \text{ x } 10^{-10} \text{ mole}}{500 \text{ µl}} \text{ x } \frac{10^{6}\text{µl}}{1 \text{ L}} = 0.88\text{x}10^{-6} \text{ M} = 880 \text{ nM}$$

Experimental siRNA Loading on 20nM AuNP Solution

Measured average siRNA fluorescence value : 851
Dilution factor: 20
Slope of the calibration curve: 2236

$$\text{siRNA Concentration} = \frac{851}{2236} = 0.38 \text{ x } 20 \text{ (dilution factor)} = 7.62 \frac{\text{µg}}{\text{ml}}$$

$$\frac{7.62 \text{ µg}}{1000 \text{ µl}} \text{ x } \frac{1 \text{ mole}}{13600 \text{ g}} \text{ x } \frac{1\text{g}}{10^{6}\text{µg}} \text{ x } \frac{10^{6}\text{µl}}{1\text{L}} = 0.056\text{x}10^{-5} \text{ M} = 560 \text{ nM}$$

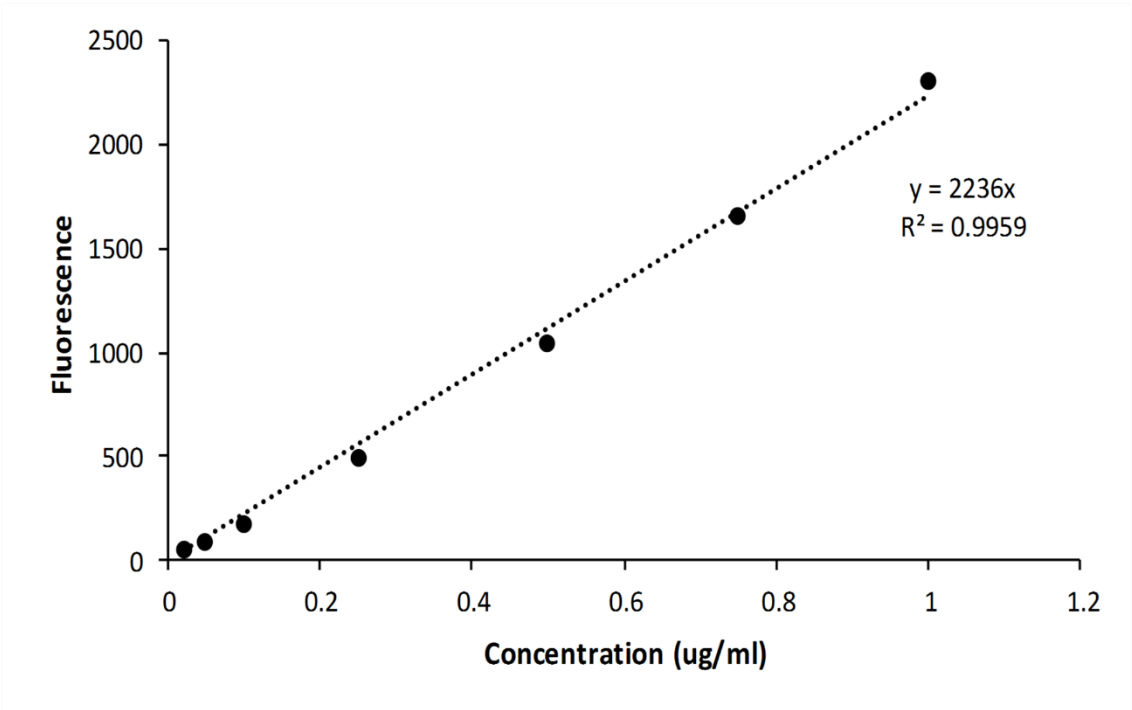

Figure A.1. Calibration curve for the determination of siRNA quantity.

A.2. Calculation of Number of AuNPs per Cell by ICP-MS Analysis

Measured Au Concentration by ICP-MS : 0.323 mg/L

Number of Au atoms in measured sample:

$$\text{Number of Au atoms} = 0.323\,\frac{\text{mg}}{\text{L}}\text{x}\frac{1\text{ mol}}{197\text{ g}}\text{x}\frac{1\text{ g}}{1000\text{ mg}}\text{x}\frac{6.02\text{x}10^{23}}{1\text{ mol}}\text{x}\frac{1\text{ L}}{1000\text{ ml}}\text{x}20\text{ml}$$

$$\text{Number of Au atoms} = 1.97\text{x}10^{17}$$

Number of Au atoms to form one AuNP:

$$\text{N} = \left(\frac{\text{Radius of AuNP}}{\text{Radius of Au atom}}\right)^3 = \left(\frac{6.5}{0.137}\right)^3 = 106801\text{ Number of Au atoms}$$

Number of AuNPs in measured sample:

$$\text{Number of AuNPs} = \frac{1.97\text{x}10^{17}}{106801} = 1.85\text{x}10^{12}$$

Number of AuNPs in cell:

Number of cells : $1\text{x}10^5$ cell

$$\text{Number of AuNP per cell} = \frac{1.85\text{x}10^{12}}{1\text{x}10^5} = 1.85\text{x}10^7$$

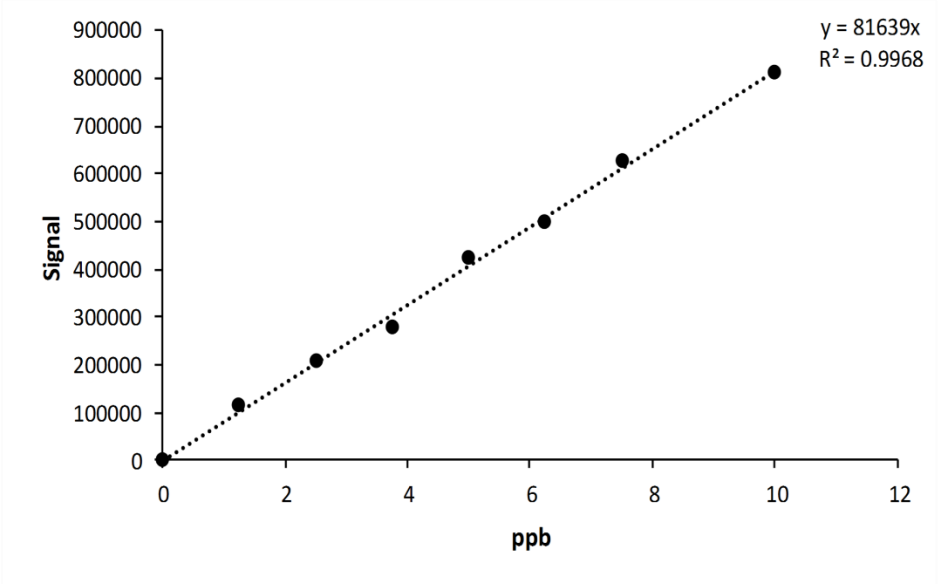

Figure A.2. Calibration curve for the determination of Au atoms by ICP-MS.

A.3. Calculation of SPDP Modification

ΔA343 = (Average A343 after DTT) – (Average A343 before DTT)

8080 reflects the extinction coefficient for pyridine-2-thione at 343 nm: 8.08 x 10^3 M^{-1} cm^1.

$$\frac{\Delta A}{8080} \text{x} \frac{\text{MW of Peptide}}{\frac{\text{mg}}{\text{ml}} \text{of Peptide}} = \text{moles of SPDP per moles of Peptide}$$

$$\frac{0.653 - 0.004}{8080} x \frac{3433}{0.4} = 0.69$$

A.4. Calculation of NHS-Fluorescein Labelling Degree of Peptides

$\varepsilon_{peptide}$ = peptide molar extinction coefficient (5690 M^{-1} cm^{-1})

$\varepsilon_{fluorescein}$ = 70,000 (NHS-Fluorescein molar extinction coefficient)

CF: correction factor: 0.3

$$\text{Protein Concentration (M)} = \frac{A_{280} - (A_{max} \text{xCF})}{\varepsilon_{protein}} \text{ x dilution factor}$$

$$\text{Moles fluorescein per mole peptid} = \frac{A_{max} \text{ of the labelled peptide}}{\varepsilon_{fluorescein} \text{xprotein concentration (M)}} \text{x dilution factor}$$

$$\frac{1.246 - (0.654x0.3)}{5690} x0.4 = 8.1x10^{-5}$$

$$\frac{0.654 \; x \; 20}{70000 \; x \; 8.1x10^{-5}} = 2.3$$

APPENDIX B

HISTOGRAMS OF CELL CYCLE ANALYSIS

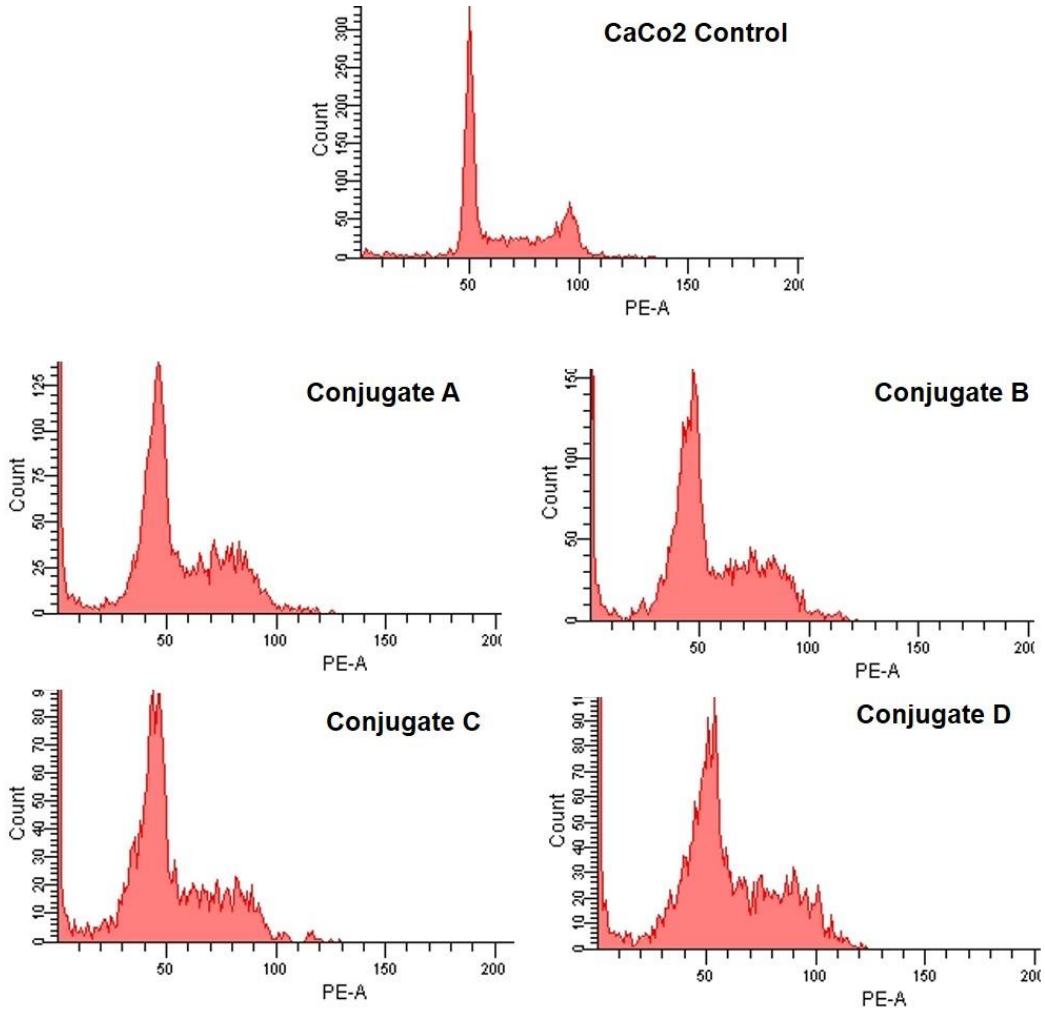

Figure B.1. Histograms of complete cell cycle for CaCo2 cells

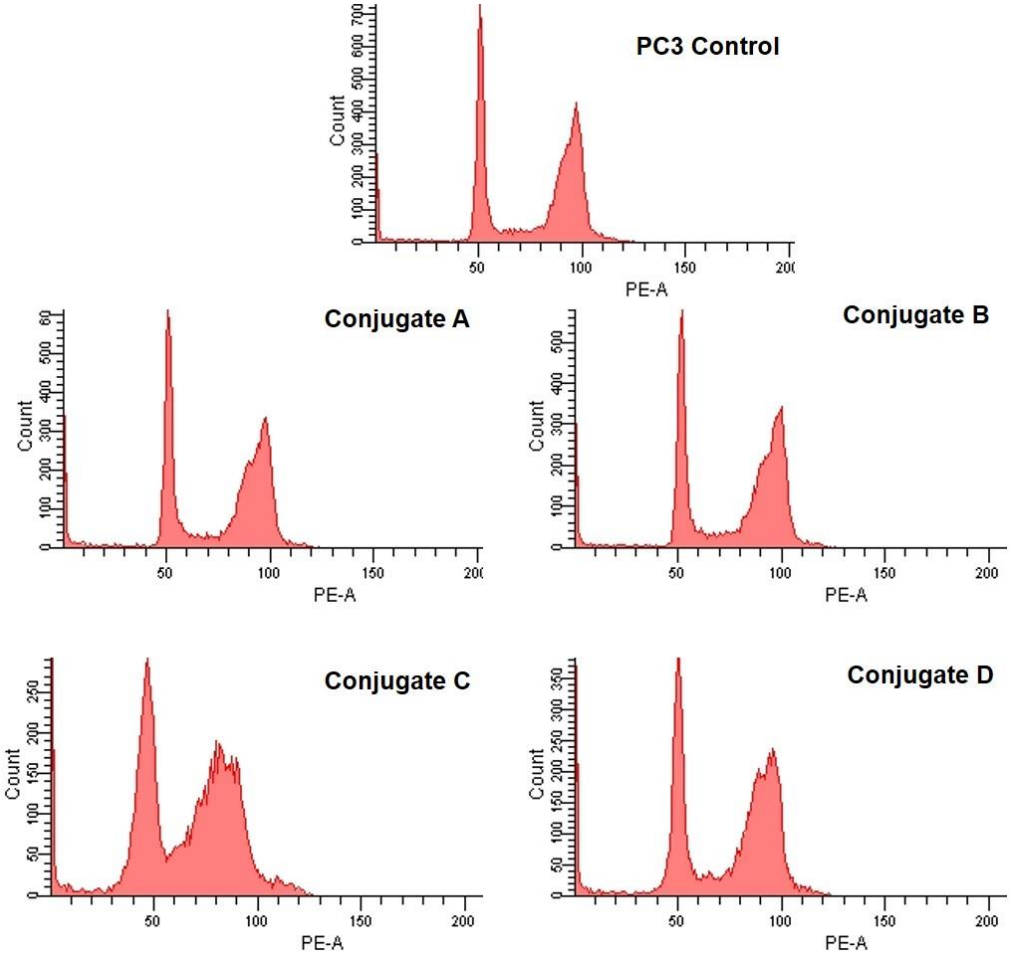

Figure B.2. Histograms of complete cell cycle for PC3 cells

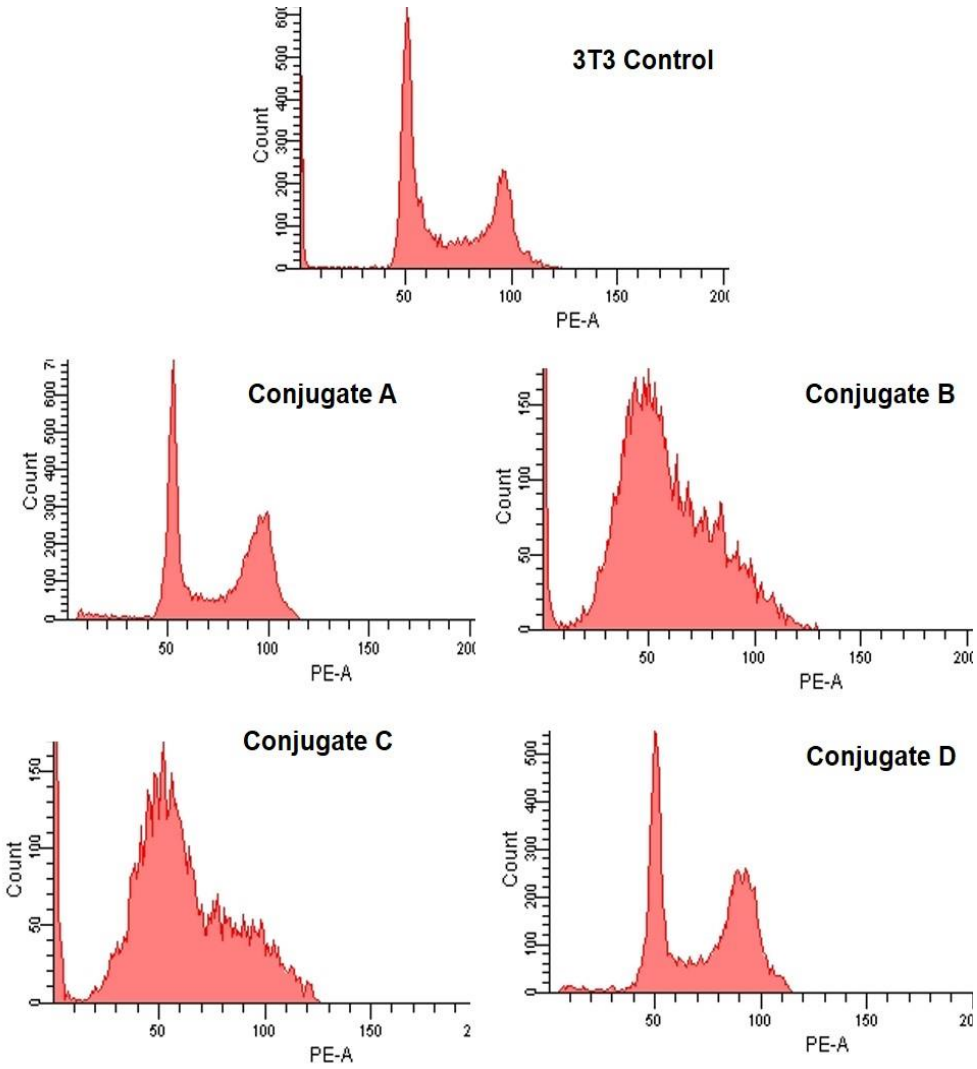

Figure B.3. Histograms of complete cell cycle for 3T3 cells.

APPENDIX C

XPS ANALYSIS RESULTS

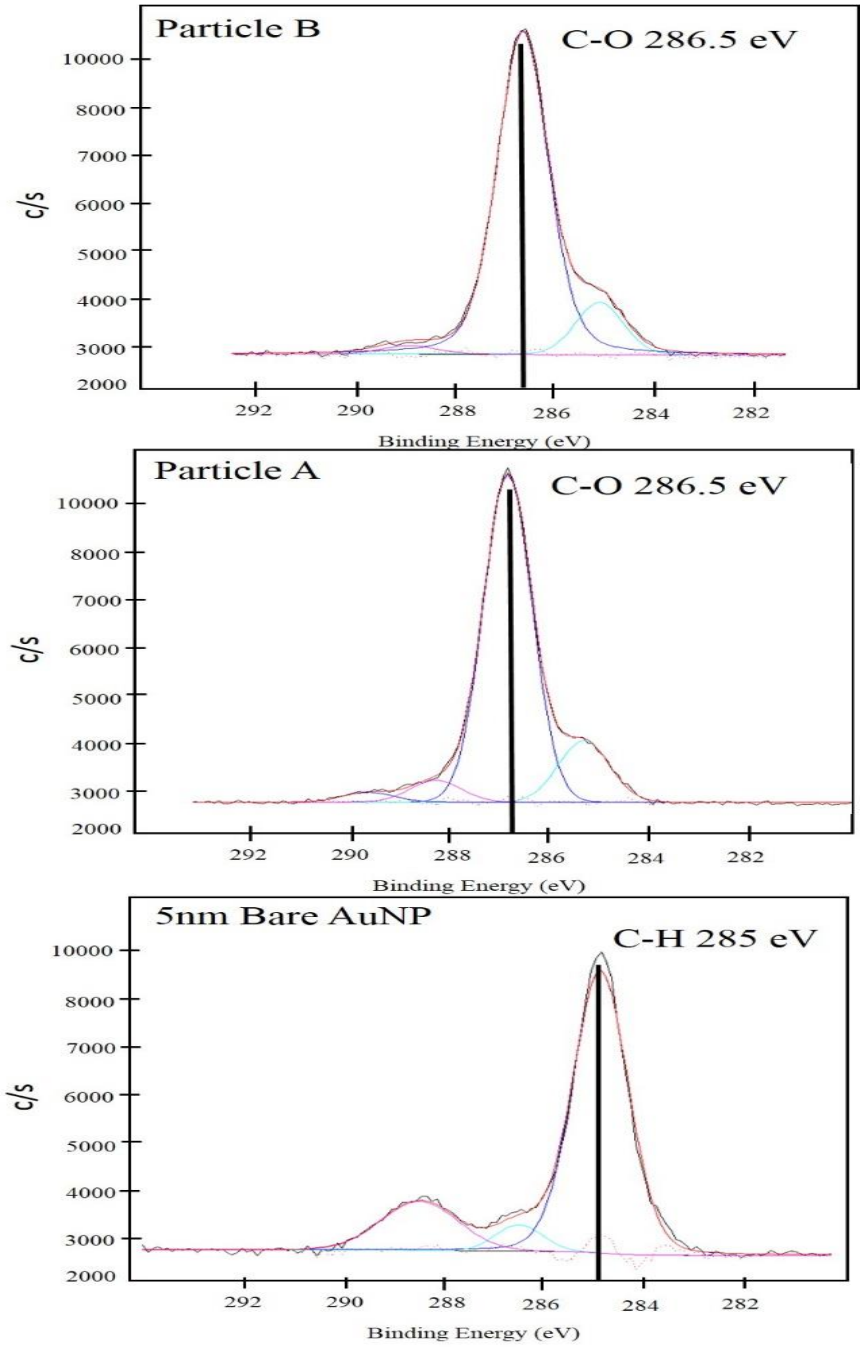

Figure C.1. XPS high-resolution C 1s scans of Particles A and B.

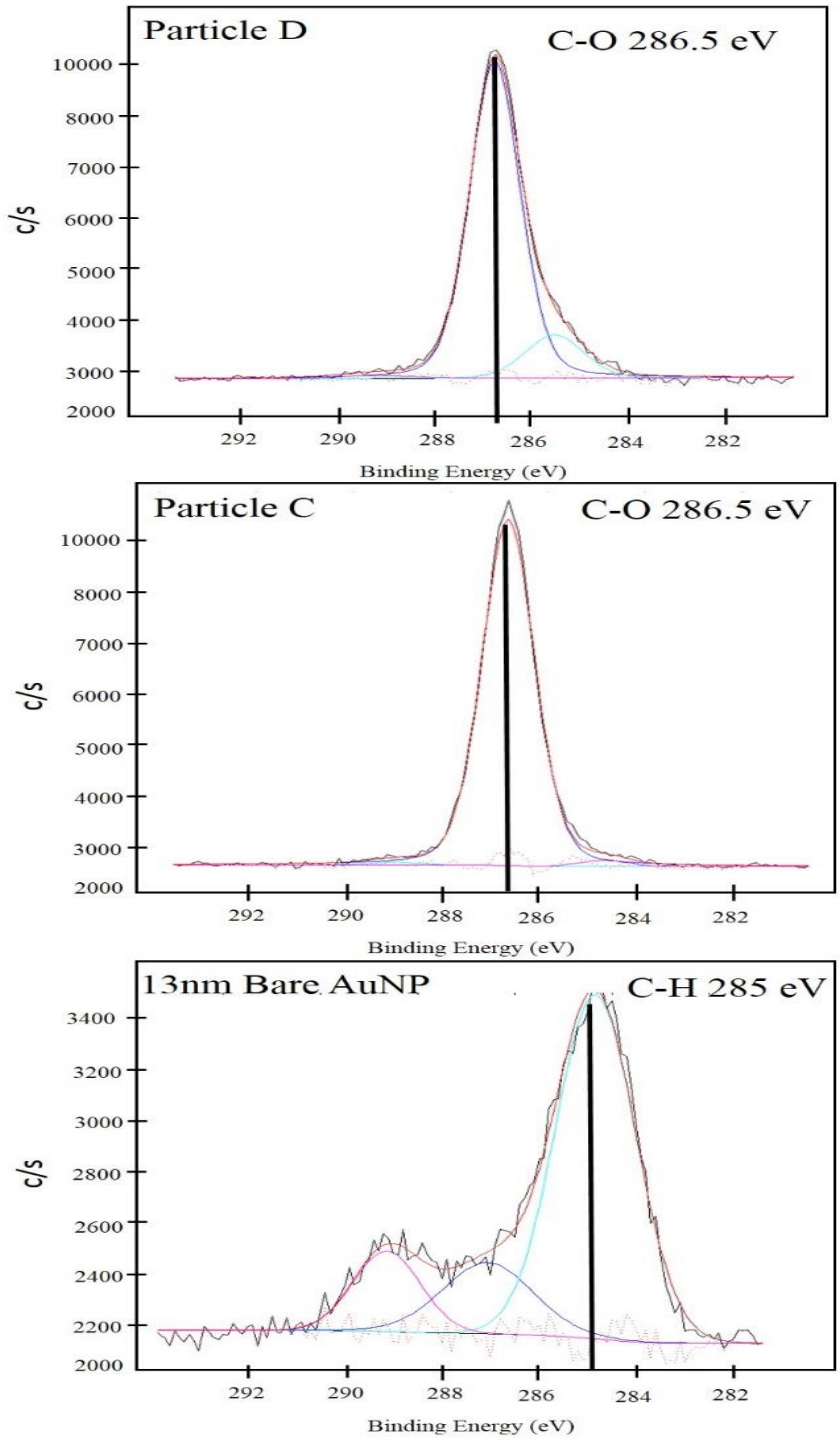

Figure C.2. XPS high-resolution C 1s scans of Particles C and D.

CURRICULUM VITAE

Education

Ph.D.	Chemical Engineering Department of Chemical Engineering Izmir Institute of Technology, Izmir, Turkey	August 2009 – July 2014
M.Sc.	Biotechnology Biotechnology and Bioengineering Izmir Institute of Technology, Izmir, Turkey	July 2009
B.S.	Chemical Engineering Department of Chemical Engineering Izmir Institute of Technology, Izmir, Turkey	June 2007

Projects

Project Title: Development of the Next Generation Membrane Bioreactor System (BioNexGen). Supported by European Union Commission, the 7th Framework Programme. Grant Agreement No: 246039.

Project Title: Development of Multifunctional Gene Delivery Systems. Supported by Scientific and Technological Research Council of Turkey (TÜBİTAK)

Project Title: Development of Nanocomposite Food Packaging Membranes with Controlled Release Properties. Supported by Scientific and Technological Research Council of Turkey (TÜBİTAK) Grant Agreement No: 110M440

Peer Reviewed Publications

Metin Uz, Sacide Alsoy Altınkaya; **Development of mono and multilayer antimicrobial food packaging materials for controlled release of potassium sorbate***;* *Lwt - Food Science and Technology*, 44. 2302-2309, (2011).

Conference Proceedings and Presentations

1. **Uz M.,** Tuncer M., Seker E., S.A. Altinkaya, **"Preparation and Characterization of Ag/ZnO/SiO_2 Incorporated Polysulfone Membranes for Water Treatment".** International Conference on Application of Nanotechnology in Membranes for Water Treatment (Nanomemwater), Izmir, Turkey. October 2013.

2. **Uz M.,** V. Bulmus, S. A. Altinkaya. **"Intracellular Trafficking of PEG Coated Gold Nanoparticles".** 7th Chemical Engineering Conference for Collaborative Research in Eastern Mediterranean Countries- EMCC7, Corfu, Greece. April 2012.

3. **Uz, M.,** I. Zorlu, S. Evlioglu, S. A. Altinkaya. **"Preparation of Lysozyme Loaded Chitosan Nanoparticles and Test of Their Antimicrobial Activity".** 6th Nanoscience and Nanotechnology Conference, Izmir, Turkey. June 2010.